Dissertation

submitted to the

Combined Faculty of Natural Sciences and Mathematics

of the Ruperto Carola University of Heidelberg, Germany

for the degree of

Doctor of Natural Sciences

Presented by

Felicitas Martha Boßler, M.Sc.

born in Freiburg im Breisgau, Germany

Oral examination:

AKT-dependent Repression of Human Papillomavirus E6/E7 Oncogene Expression under Hypoxia

Referees: Prof. Dr. Walter Nickel

Prof. Dr. Felix Hoppe-Seyler

Table of contents

Summary

Human papillomaviruses (HPVs) cause cervical cancer and are also closely linked to other malignancies in the anogenital and oropharyngeal regions. It is widely assumed that HPV-positive cancer cells are ‘oncogene addicted’ in that they depend on the continuous expression of the two viral oncogenes, E6 and E7, to maintain their malignant phenotype and to avoid tumor-suppressive senescence induction. However, recently it was shown that hypoxic HPV-positive cancer cells efficiently shut down E6/E7 expression and enter a growth arrest without inducing senescence. This process is reversible upon reoxygenation and can be counteracted by high glucose concentrations. These surprising findings shed new light on the crosstalk between the viral oncogenes and the host cell, particularly under hypoxia, a condition frequently found in cervical cancer that is associated with poor patient prognosis. The present work aimed to delineate the regulatory mechanisms underlying hypoxic E6/E7 repression. It was revealed that E6/E7 mRNA and protein expression is impaired in hypoxic HPV-positive cancer cells by a combination of transcriptional repression and reduction of mRNA and protein half-lives. Moreover, hypoxic repression of E6/E7 was shown to be not only glucose-sensitive, but also dependent on intracellular calcium. There was no indication for a role of HIF transcription factors, considered master orchestrators of the cellular response to hypoxia, or for involvement of transcription factors from the glucose-responsive Mlx network. However, the PI3K/AKT signaling pathway was identified as being crucial for the hypoxic repression of E6/E7. AKT is activated by hypoxia which can be counteracted by high glucose concentrations. Blocking of hypoxia-induced AKT activation by chemical inhibitors, including clinically applied drugs that target AKT or its upstream activators PI3K and mTORC2, counteracts repression of E6/E7 under hypoxia. Knockdown and overexpression experiments showed that the AKT1 and AKT2 isoforms act redundantly in hypoxic repression of E6/E7. Reactivation of E6/E7 expression under hypoxia upon inhibition of the PI3K/AKT pathway does not induce proliferation and can sensitize HPV-positive cells to therapeutic effects of chemotherapy in a cell line-dependent manner. Finally, comparison of the proteome composition of HPV-positive cancer cells under normoxia and hypoxia as well as proteome analyses of hypoxic cells treated with an AKT inhibitor or high glucose concentrations were performed. They identified several novel candidate proteins possibly linked to hypoxic repression of E6/E7 providing an experimental basis for future investigations. Collectively, these findings provide new insights into the regulation of the viral oncogenes in hypoxic HPV-positive tumor cells and have implications for the development of novel treatment strategies.

Zusammenfassung

Humane Papillomviren (HPVs) verursachen das Zervixkarzinom und sind eng assoziiert mit anderen Krebserkrankungen im Anogenitalbereich und im Oropharynx. Der maligne Phänotyp HPV-positiver Tumorzellen gilt als abhängig („oncogene addicted“) von der kontinuierlichen Expression der zwei viralen Onkogene, E6 und E7, die die Induktion von tumorsuppressiver Seneszenz verhindern. Kürzlich wurde jedoch gezeigt, dass hypoxische HPV-positive Tumorzellen die E6/E7-Expression effizient abschalten können und einen Wachstumsarrest eingehen ohne dabei Seneszenz zu induzieren. Dieser Vorgang ist umkehrbar durch Reoxygenierung und wird durch hohe Glukosekonzentrationen verhindert. Diese überraschenden Befunde führten zu neuen Einblicken in die Wechselwirkungen zwischen den viralen Onkogenen und der Wirtszelle, insbesondere unter Hypoxie, ein Zustand, der häufig in Subregionen von Zervixkarzinomen vorliegt und der mit einer schlechten Prognose assoziiert ist. Ziel dieser Arbeit war es regulatorische Mechanismen, die der hypoxischen E6/E7-Repression zugrunde liegen, zu entschlüsseln. Es wurde beobachtet, dass die Repression von E6/E7-mRNA und -Proteinen unter Hypoxie durch eine Kombination aus transkriptioneller Repression und Verkürzung der mRNA- und Protein-Halbwertszeiten erfolgt. Überdies wurde gezeigt, dass die hypoxische E6/E7-Repression nicht nur glukosesensitiv, sondern auch calciumabhängig ist. Die Ergebnisse ergaben keinen Hinweis auf eine Rolle für HIF-Transkriptionsfaktoren, die als Schlüsselfaktoren der zellulären Antwort auf Hypoxie gelten, oder für Transkriptionsfaktoren aus dem glukoseresponsiven Mlx-Netzwerk. Vielmehr wurde entdeckt, dass der PI3K/AKT-Signalweg entscheidend für die hypoxische Repression von E6/E7 ist. AKT wird durch Hypoxie aktiviert, was durch hohe Glukosekonzentrationen verhindert wird. Eine Inhibition der Hypoxie-induzierten AKT-Aktivierung durch (auch klinisch eingesetzte) Hemmstoffe, die gegen AKT oder vorgeschaltete Aktivatoren (PI3K und mTORC2) gerichtet sind, wirkt der hypoxischen Repression von E6/E7 entgegen. Sowohl ein gezieltes Ausschalten als auch eine ektopische Expression von AKT1 und AKT2 ergaben, dass diese AKT-Isoformen in der hypoxischen E6/E7-Repression funktionell redundant wirken. Die durch PI3K/AKT-Hemmung vermittelte Reaktivierung von E6/E7 unter Hypoxie induziert keine Proliferation und kann HPV-positive Zellen zellinienabhängig für Chemotherapeutika sensibilisieren. Schließlich wurden auch Proteomanalysen von HPV-positiven Zellen unter Hypoxie und Normoxie, sowie unter Hypoxie mit gleichzeitiger Behandlung mit einem AKT-Inhibitor oder hohen Glukosekonzentrationen durchgeführt. Als Grundlage für zukünftige Studien wurden dabei neue Kandidatenproteine identifiziert, die möglicherweise zur hypoxischen E6/E7-Repression beitragen. Zusammengefasst führen diese Resultate zu neuen Erkenntnissen über die Regulation der HPV-Onkogenexpression in hypoxischen Tumorzellen und haben Implikationen für die Entwicklung neuer Therapiestrategien.

Acknowledgements

This dissertation was conducted at the German Cancer Research Center in Heidelberg, Germany, in the research group ‘Molecular Therapy of Virus-Associated Cancers’ headed by Prof. Dr. Felix Hoppe-Seyler.

To begin with, I would like to express my gratitude to Prof. Dr. Felix Hoppe-Seyler for giving me the opportunity to work on this project and for constant guidance and support during my time in his lab. Also, I would like to thank Prof. Dr. Karin Hoppe-Seyler for many inspiring and productive discussions and for support concerning many aspects of (PhD-)life.

I would like to acknowledge to Prof. Dr. Walter Nickel (University of Heidelberg) for evaluating my thesis as first referee. I am also grateful to PD Dr. Karin Müller-Decker (German Cancer Research Center, DKFZ, Heidelberg) and Dr. Marco Binder (DKFZ) for being members of my Thesis Committee. Moreover, I would like to thank Prof. Dr. Thomas Hofmann (University of Mainz) for being a valuable member of my TAC meetings.

My gratitude also goes to my collaboration partners Bianca Kuhn and Prof. Dr. Jeroen Krijgsveld (DKFZ) for performing the mass spectrometry analyses. Furthermore, I would like to thank Dr. Thomas Günther and Prof. Dr. Adam Grundhoff (Heinrich-Pette Institute, Hamburg) for their contributions to MeDIP and ChIP experiments. I also want to thank Dr. Wilhelm Palm (DKFZ) for his input regarding mTOR and Dr. Joschka Willemsen (AG Binder, DKFZ) for providing plasmids and for help with the CRISPR protocol.

Importantly, I wish to express my gratitude to all former and present members of the F065-lab for creating a constantly supportive and enjoyable working atmosphere and also for the good times beyond the lab. I owe special thanks to Angela Holzer and Claudia Lohrey for a lot of excellent technical support in the lab. In addition, my gratitude goes to Svenja Adrian, Johanna Blase, Christina Boch, Julia Braun, Julia Bulkescher, Antonia Däschle, Anja Herrmann, Sofie Knoll, Bianca Kuhn, Julia Mändl and Tobias Strobel. I also thank Thomas Holz for support regarding any IT problems.

Many thanks go to my friends for lunches, talks and motivating messages.

Stephen, I am deeply grateful that you shared this time with me, that you always believe in me and that you are there for me.

Finally, I want to thank my family: My parents, Vanessa and Priska (with Annika and Matthias). Thank you for all your love and support!

Publications and Presentations

Publications

Bossler F, Kuhn B, Günther T, Krämer S, Khalkar P, Adrian S, Lohrey C, Holzer A, Dürst M, Rösl F, Grundhoff A, Krijgsveld J, Mayer A, Hoppe-Seyler K, Hoppe-Seyler F. Repression of human papillomavirus oncogene expression under hypoxia is mediated by AKT1/AKT2. Manuscript in preparation.

Hoppe-Seyler K, Bossler F, Lohrey C, Bulkescher J, Rösl F, Jansen L, Mayer A, Vaupel P, Dürst M, Hoppe-Seyler F. Induction of dormancy in hypoxic human papillomavirus-positive cancer cells. Proc. Natl. Acad. Sci. U. S. A., 2017. 114(6): p. E990-e998.

Hoppe-Seyler K, Bossler F, Braun JA, Herrmann AL, Hoppe-Seyler F. The HPV E6/E7 Oncogenes: Key Factors for Viral Carcinogenesis and Therapeutic Targets. Trends in Microbiology, 2018. 26(2): p. 158-168.

Hoppe-Seyler K, Honegger A, Bossler F, Sponagel J, Bulkescher J, Lohrey C, Hoppe-Seyler F. Viral *E6/E7* oncogene and cellular hexokinase 2 expression in HPV-positive cancer cell lines. Oncotarget, 2017. 8(63): p. 106342-106351.

Presentations

Bossler F, Lohrey C, Holzer A, Hoppe-Seyler K, Hoppe-Seyler F. AKT-dependent repression of HPV E6/E7 oncogene expression under hypoxia. Retreat of the DKFZ Research Program Infection, Inflammation and Cancer. 28-30. May 2018, Rastatt, Germany. Oral Presentation.

Bossler F, Lohrey C, Holzer A, Mayer A, Vaupel P, Hoppe-Seyler K, Hoppe-Seyler F. Repression of HPV E6/E7 oncogene expression under hypoxia. Helmholtz International Graduate School for Cancer Research 2017 PhD Poster Presentation. 24. November 2017. Heidelberg, Germany. Poster Presentation.

Hoppe-Seyler K, Bossler F, Lohrey C, Bulkescher J, Rösl F, Jansen L, Mayer A, Vaupel P, Dürst M, Hoppe-Seyler F. Induction of dormancy in hypoxic human papillomavirus-positive cancer cells. 27th Annual Meeting of the Society for Virology. 22-25. March 2017, Marburg, Germany. Oral Presentation.

Hoppe-Seyler K, Bossler F, Lohrey C, Bulkescher J, Rösl F, Jansen L, Mayer A, Vaupel P, Dürst M, Hoppe-Seyler F. Induction of dormancy in hypoxic human papillomavirus-positive cancer cells. 13th Charles Rodolphe Brupbacher Symposium. 01-03. February 2017, Zurich, Switzerland. Poster Presentation.

Bossler F, Lohrey C, Holzer A, Hoppe-Seyler K, Hoppe-Seyler F. Repression of HPV E6/E7 oncogene expression under hypoxia. Helmholtz International Graduate School for Cancer Research 2016 PhD Retreat. 13-15. July 2016, Weil der Stadt, Germany. Poster Presentation.

Bossler F, Lohrey C, Holzer A, Hoppe-Seyler K, Hoppe-Seyler F. Repression of HPV E6/E7 oncogene expression under hypoxia. Retreat of the DKFZ Research Program Infection, Inflammation and Cancer. 30. May - 01. June 2016, Schöntal, Germany. Oral Presentation.

Chapter 1

Introduction

1. Introduction

1.1 Cancer

Cancer is a significant global health burden accounting for an estimated 8.2 million deaths in 2012 worldwide that is expected to increase in the years to come, largely due to rising expectancy of life and changes in lifestyle behavior [1].

The development of cancer is a multistep process. During this process, cells accumulate several mutations and acquire an increasingly aberrant behavior [2]. Hence, the cause for malignant transformation from healthy cells into tumor cells is complex and encompasses many aspects of cellular biology. In a seminal paper Hanahan and Weinberg initially defined six common biological characteristics of tumor cells as the 'hallmarks of cancer'. These consist of sustained proliferative signaling, evasion from growth suppressors, tissue invasion and metastasis, limitless replicative potential, sustained angiogenesis and the resistance towards apoptosis. In an updated version, the authors later included deregulation of metabolism and immune evasion as additional emerging hallmarks and genomic instability and tumor-promoting inflammation as characteristics for tumor progression [3].

Due to the often time-consuming multistep nature of tumorigenesis, old age represents a strong cancer risk factor. However, additional factors exist that can significantly increase the risk for developing cancer. These include most prominently tobacco use, but also ultraviolet or ionizing radiation, alcohol, obesity, physical inactivity, chemical and biological toxins and infections [4, 5]. For the year 2012 it was estimated that approximately 15 % of all new cancer cases were attributable to infections with viruses, bacteria or parasites [6]. Human papillomaviruses (HPVs) are amongst the strongest contributors to infection-associated carcinogenesis with 4.5 % of all cancers worldwide being attributable to HPV [7].

1.2 Human papillomaviruses (HPVs) and cancer

HPVs are a diverse group of cutaneous and mucosal non-enveloped DNA viruses that belong to the family of *papillomaviridae*. More than 170 types of HPVs are classified today [8]. They are grouped into low-risk and high-risk types. While low-risk types are mainly characterized by their ability to cause benign lesions, skin and genital warts, high-risk HPVs represent major risk factors for the development of anogenital cancers such as cancer of the penis, vagina, vulva, anus and cervix, but also of oropharyngeal cancers at the tonsils, oropharynx and base of tongue [9].

1.2.1 Cervical cancer

Harald zur Hausen and colleagues first established a close connection between HPV and cervical cancer in 1983 [10]. The importance of his work was later recognized with the Nobel Prize in Physiology or Medicine in 2008.

Today, cervical cancer is well characterized for being in virtually all cases caused by sexually transmitted mucosa-infecting high-risk HPVs. Currently, twelve types are classified as carcinogenic: HPV-16, 18, 31, 33, 35, 45, 52, 58, 39, 51, 56 and 59. Several other types are classified as 'probably' or 'possibly carcinogenic' [11]. HPV16 is the most frequent type detected in cervical cancer cases, followed by HPV18 which together have a prevalence of approximately 70 % [12].

With more than 500,000 new cases and 250,000 deaths per year, cervical cancer is the fourth most common cancer in women worldwide. Although incidence rates are declining in many high-income industrialized countries, incidence and mortality remain especially high and are predicted to further increase in low-income developing countries where screening programs are scarce [1, 13, 14]. Consequently, development and implementation of effective treatment and prevention strategies are of great importance.

1.2.2 Prevention and therapy of cervical cancer

Currently recommended standard treatment for invasive cervical cancer consists of surgery often combined with radiotherapy or cisplatin-based chemoradiation. The development of aggressive cervical carcinomas can in many cases be prevented by screening that detects the presence of precancerous lesions. Available screening methods in industrialized countries are cytological evaluation of cells from cervical samples, HPV testing (detection of DNA or RNA) or cytology-HPV co-testing [15].

However, the most effective protection against any disease can be achieved by already preventing its initial establishment. In the case of cervical cancer, this can be accomplished by prophylactic vaccination. At present, three prophylactic vaccines have been licensed. The bivalent Cervarix (GlaxoSmithKline) contains antigens of HPV16 and 18, which are responsible for 70 % of all cervical cancer cases. The quadrivalent Gardasil (Merck) protects against HPV6, 11, 16 and 18 and thus, also protects against two low-risk HPV types causing roughly 90 % of genital warts. The most recently developed vaccine, the nonavalent Gardasil9 (Merck), comprises the four HPV types of the quadrivalent vaccine and protects against five additional carcinogenic types (31, 33, 45, 52, 58), thereby covering up to 90 % of HPV infections linked to cervical cancer. All vaccines show good safety profiles and high efficiency, especially in their main target group; young females prior to their first sexual encounter [16]. They are all based on virus-like particles (VLPs) of the HPV major coat

protein L1 and lead to a strong seroconversion with antibody titers much higher than obtained by natural infection [17].

However, despite the promising impact of HPV vaccination, there remain practical limitations. First, vaccination rates are disappointingly low, particularly in less developed countries where cervical cancer incidence is highest and where the recommended three-dose vaccination, now already discussed to be reduced to a two-dose vaccination, poses a considerable financial and logistic issue [18, 19]. Second, vaccination is directed against specific HPV types and is consequently not able to prevent 100 % of HPV-induced cervical cancer. In this regard, effort is currently put in the development of vaccines based on the minor capsid protein L2 that are expected to elicit an immune response comprising of broadly cross-type neutralizing antibodies [19]. Third, current vaccinations are only prophylactic and cannot prevent progression of the disease in already infected individuals. Since broad vaccination programs were implemented earliest in 2006 [16] and the time period between initial infection and progression to cancer often lasts decades [20], cervical cancer will remain a major health care problem for many years to come. Thus, development of novel therapeutic strategies for the management of HPV-associated cancers remains a significant challenge.

1.2.3 The biology of HPV infection and mechanisms of HPV-associated carcinogenesis

HPVs have a small circular double-stranded DNA genome of less than 8,000 base pairs (bp) that is divided into six early (E1, E2, E4, E5, E6, E7) and two late (L1 and L2) open reading frames (ORFs), termed ‘late’ and ‘early’ according to their expression during the viral life cycle. Additionally, there is a transcriptional regulatory region designated long control region (LCR) or upstream regulatory region (URR). Expression of different gene products is controlled by the early and late promoter (p97 and p670, respectively, for HPV16, see Fig. 1) and by mRNA splicing [21].

The late genes code for structural proteins, essential for virus assembly, with L1 representing the major and L2 representing a smaller capsid protein. E1 and E2 are proteins involved in viral replication and gene expression. The functions of E4-E7 are more diverse [15]. The E4 protein plays a role in genome amplification and may be involved in virus release and transmission [22]. E5 also contributes to genome amplification [23] and moreover, is suggested to exert transforming activities early in the transformation process [24]. E6 and E7 are the two viral oncoproteins that are essential for malignant transformation to cancer (see chapter 1.2.4).

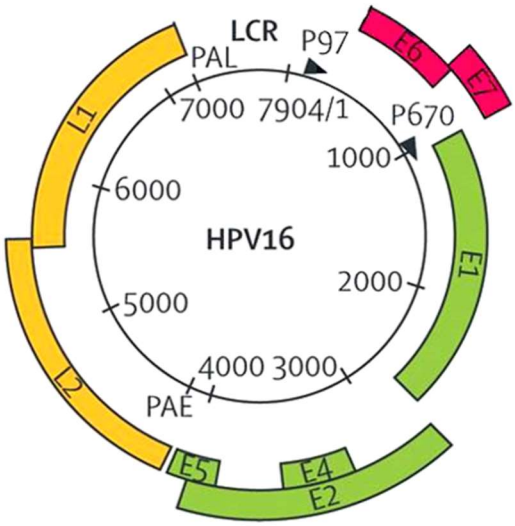

Fig. 1. Genome structure of HPV16. The eight ORFs of HPV16, encoded on one DNA strand, are depicted: L1, L2 (yellow), E1, E2, E4, E5 (green) and E6, E7 (red). Early (p97) and late (p670) promoters are indicated by arrows. LCR = long control region, also designated upstream regulatory region (URR), PAE = early polyadenylation site, PAL = late polyadenylation site. Modified from [21].

The peak of cervical cancer diagnosis lies at an age of 45 to 60 years, whereas HPV infection typically occurs in adolescent or young women demonstrating the decades are often required to develop invasive cervical cancer [25]. Initial infection is often rapidly cleared. However, HPV can modulate the immune response of their host cells facilitating immune evasion [26]. Long-term persistence of the virus can lead to the development of precancerous lesions that can regress over time or further progress to more critical precancer forms that can eventually result in invasive cancer. Several classifications have been established to stage cervical lesions according to their risk of developing into invasive carcinoma such as the histological staging from mild to severe dysplasia classified as cervical intraepithelial neoplasia (CIN) 1-3. Notably, only a small minority of HPV infected women develop cervical carcinomas during their life-time indicating that HPV infection is required but not sufficient to induce cancer of the cervix [25].

During HPV infection, the virus enters cells of the epithelial basal layer, usually via microwounds. As the basal cells divide and cells begin to migrate to the mid and upper epithelial layers, they start a differentiation program. The differentiation-associated changes of the host cell support the differential expression of viral gene products at various stages. Expression of E6 and E7 is tightly regulated and mainly involved in genome amplification in mid-epithelial layers, whereas strong expression of L1, L2 and E4 can be detected primarily in the mid to upper epithelial layers. Assembly and release of virus particles eventually occurs in layers close to the epithelial surface [15, 27] (Fig. 2).

HPV-associated neoplasias and ultimately cancerous lesions occur when this productive viral life-cycle is impaired, which is characterized by increased cell proliferation up into the mid epithelial layers. This is mainly driven by enhanced activity of E6 and E7 that promote cell cycle progression and inhibit differentiation. Elevated levels of E6 and E7 go along with more and more restricted expression of late viral genes, thereby no longer allowing virion production [15, 28] (Fig. 2). Continuously elevated expression of E6/E7 generates chromosomal instability that facilitates integration of HPV DNA into the host cell genome. Thus, many invasive cervical carcinomas do no longer contain viral episomes and are instead characterized by integrated viral DNA with disruption of the E1/E2 ORF, but with an intact E6/E7 ORF [29, 30].

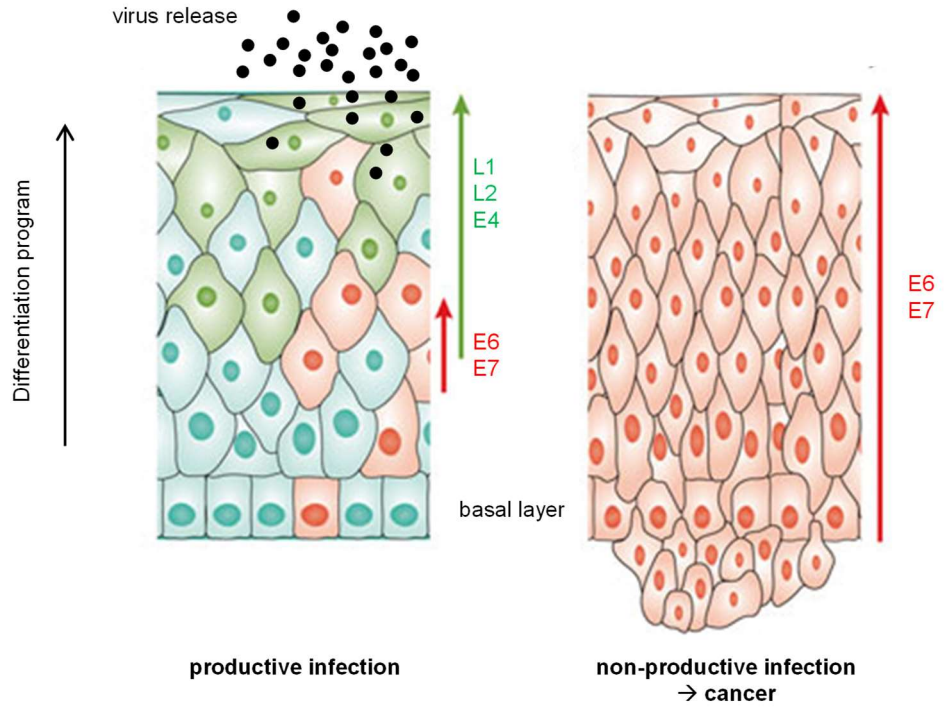

Fig. 2. HPV life cycle and cancer development. During the productive viral life cycle (left) viral gene expression is regulated during epithelial differentiation and virus is released from the epithelial surface. In cancerous tissue (right) late gene expression is retarded and E6 and E7 expression is elevated no longer allowing virion production. Protein expression of L1, L2, E4 (green) and of E6, E7 (red) is indicated. Figure modified from [15].

The majority of cervical cancers develop at the transformation zone or the endocervix (cervical canal) and rarely at the ectocervix. The ectocervix, the vaginal portion of the cervix, consists of stratified squamous epithelium and is maintained by epithelial stem cells. HPV infection of these conventional epithelial stem cells is suggested to result primarily in a productive viral life cycle. Persistent lesions are thought to be caused by infection of cervical reserve cells that maintain the transformation zone between ecto- and endocervix or of reserve cells of the endocervix itself, which consists of a simple columnar epithelium that

occasionally undergoes metaplasia [15, 28]. Noteworthy, a second cell type has recently been proposed as cell of origin for persistent HPV infections; a stem-like cell at the squamocolumnar (SC) junction, where columnar epithelium of the endocervix meets squamous epithelium [31].

1.2.4 E6 and E7 – the viral oncoproteins

The transforming abilities of high-risk HPVs are attributed to two rather small proteins: E6 and E7 with a length of approximately 150 and 100 amino acids, respectively. In contrast to other HPV encoded proteins, expression of E6 and E7 is always retained in cervical cancer cells. HPV-associated cancer cells are even considered to be 'oncogene addicted' meaning that they depend on sustained expression of E6/E7 to maintain their malignant phenotype [32]. This is demonstrated by findings revealing that silencing of E6/E7 rapidly induces senescence, an irreversible growth arrest [33-35].

E6 and E7 are transcribed as polycistronic transcripts from a common early promoter under the control of the transcriptional control region URR (Fig. 1) that encompasses a 5' terminal region, a central enhancer element and a promoter proximal region (PPR) at the 3' part of the URR [36, 37]. In principle, the viral E2 protein can act as transcriptional repressor for E6/E7. However, E2-mediated repression of E6/E7 is commonly abolished in HPV-positive tumor cells, largely by disruption of the E2 ORF upon integration of viral DNA into host cell chromosomes or by methylation of E2 binding sites in the URR [38]. Functional binding sites for several host transcription factors in the URR that regulate expression of *E6/E7* have been characterized. This includes most prominently AP1 and SP1, which are important cellular activators of E6 and E7 expression [39, 40].

The molecular mechanisms employed by E6 and E7 to contribute to cellular transformation are diverse and include modulation of various cellular proteins.

One major critical target of E6 is the tumor suppressor p53, which is bound by E6 and subsequently degraded [41]. More precisely, E6 forms a trimeric complex with p53 and E6-associated protein (E6-AP), which results in the ubiquitination and subsequent proteasomal degradation of p53 with E6-AP functioning as ubiquitin ligase [42, 43].

A key target for E7 is the pRb family, which encompasses important regulators of the cell cycle. In non-dividing cells, pRb is unphosphorylated and binds to and inactivates E2F transcription factors. Upon mitogenic signals, pRB is phosphorylated and E2Fs are released, which then activate transcription of a variety of genes driving cell cycle progression [44]. E7 can bind pRb, disrupt its interaction with E2F and even induce its degradation [45-47]. As a consequence, E2F transcription factors are released leading to unscheduled cell cycle progression.

Protective cellular mechanisms against uncontrolled cell growth include the induction of apoptosis or senescence via p53. Indeed, stabilization of p53 can be observed in cells expressing E7, but no E6 [48]. However, in HPV-positive cancer cells E6 and E7 are expressed together and thus, E6 mediated degradation of p53 prevents apoptosis (Fig. 3) or senescence otherwise induced by uncontrolled pRb-driven proliferation. In line with this model, it has been shown that transforming abilities of E6 and E7 are strongest when both are expressed [49] indicating how E6 and E7 cooperate in cellular transformation.

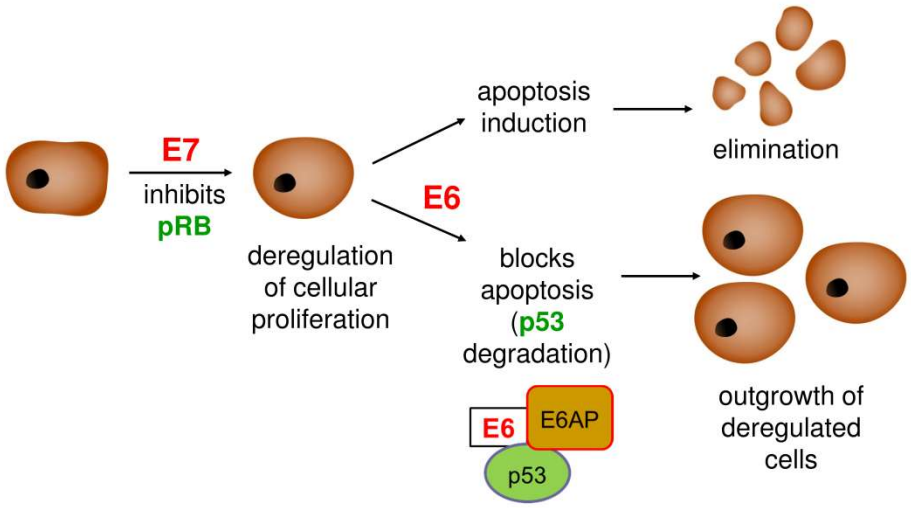

Fig. 3. Cooperation of E6 and E7 in cellular transformation. E7 induces inactivation of pRb and subsequent deregulation of proliferation, which leads to p53-dependent apoptosis. Concomitant expression of E6 counteracts this by the formation of a trimeric E6/E6-AP/p53 complex followed by degradation of p53. Blockade of apoptosis results in the outgrowth of deregulated cells. Figure from [32].

Apart from their best characterized targets, p53 and pRB, E6 and E7 interact with many additional cellular factors. The E6 protein, for instance, contains a PDZ (post synaptic density protein, drosophila disc large tumor suppressor, zonula occludens-1 protein) ligand motif and can bind to numerous PDZ domain containing cellular proteins leading to their degradation. Since many of the PDZ domain containing targets of E6 are tumor suppressors and play roles in regulation of cell polarity (e.g. DLG, MAG1-3, Scribble), this poses an important tumorigenic feature of E6 [50].

Moreover, E6 can induce telomerase activity [51] by upregulating transcription of human telomerase reverse transcriptase (hTERT), a component of telomerase [52]. The absence of telomerase activity in healthy cells leads to telomere erosion during mitosis eventually resulting in cellular senescence. Hence, via activation of telomerase E6 can prevent replicative senescence. Increased expression of hTERT was suggested to be achieved via the c-Myc oncoprotein, which was reported to be stabilized by E6 [53, 54] and whose mRNA and protein expression is downregulated upon silencing of E6 in HPV18-positive HeLa cells

[55, 56]. However, there are also reports suggesting a c-Myc independent mechanism of E6-induced telomerase activity [57].

While E7 mainly drives cell cycle progression via inactivation of pRb, E7 can also directly bind to E2F1 and increase expression of pro-proliferative genes [58] or promote cell growth by modulating activity of histone-modifying enzymes such as class I histone deacetylases (HDACs) [59].

Expression of E6 and E7 is a requirement for HPV-associated tumorigenesis, but additional oncogenic events are necessary for the formation of invasive cancer indicated by the long latency between HPV infection and cancer development (see chapter 1.2.3). For instance, full transformation of keratinocytes immortalized by expression of E6 and E7 only occurs after many passages in cell culture [60]. Likely, E6 and E7 generate a predisposition for the accumulation of mutagenic events by facilitating genomic instability. Hence, chromosomal aberrations are frequently found in E6/E7-immortalized keratinocytes and HPV-positive tumor cells [61, 62].

Many of the described transforming characteristics of E6 and E7 are exclusively found in high-risk but not in low-risk types further emphasizing the oncogenic potential of high-risk HPV types. E6 of low-risk types, for instance, lacks the PDZ ligand motif and only weakly interacts with p53, if at all, without mediating its degradation. Likewise, only high-risk E7 has the potential to induce degradation of pRb [63].

The dependency of HPV-positive tumor cells on continuous expression of E6 and E7 makes the viral oncoproteins interesting highly tumor-specific therapeutic targets. Particularly the targeting of E6 should be a promising strategy since its inhibition leads to apoptosis in HPV-positive cancer cells (Fig. 3). Thus, numerous studies were performed using siRNAs, small molecule inhibitors, small peptides, peptide aptamers, intrabodies or immunotherapeutic approaches directed against E6 and E7. However, despite the promising potential of these strategies, no E6 or E7 targeted therapy has reached the clinic yet [32].

1.3 Tumor hypoxia

The level of tissue oxygenation is an important biological and clinical aspect with a strong impact on the cellular phenotype [64-66]. Typically, solid tumors are heterogeneously oxygenized and frequently characterized by the presence of areas with oxygen (O_2) concentrations significantly below the physiological level ('hypoxia'). Tissue hypoxia is usually defined as O_2 concentrations below 1.5-2 %. This *in vivo* situation forms a tremendous contrast to many *in vitro* studies, which are usually performed under standard cell culture conditions at 20-21 % O_2, hereafter defined as 'normoxia'. Even O_2 concentrations of normal healthy tissue ('physoxia', for most tissues in the range between 3.5-7 % O_2) are only poorly represented under standard experimental conditions [64, 65].

Inadequate supply of tumor cells with O_2 can be caused by large distances from blood vessels (> 70 µm) that do not allow sufficient diffusion of O_2. This diffusion-limited hypoxia is described as chronic hypoxia. A state of chronic hypoxia can also be the result of anemia or low O_2 levels in the blood (hypoxemia). Intermittent, or also termed acute hypoxia, is often a consequence of perfusion-limited O_2 delivery, for example due to structural and functional defects of tumor microvessels [66].

Hypoxic tumors are usually associated with poor patient prognosis and high resistance towards therapy. Hypoxia contributes to malignant tumor progression since hypoxic tumor cells undergo extensive adaptations to survive under low oxygen conditions. These include alterations in gene expression mainly regulated by hypoxia-inducible factors (HIFs, see chapter 1.4.2), genetic changes and clonal selection of especially resistant cells [64, 66]. An important aspect of hypoxia-mediated therapy resistance is the radioprotective effect of hypoxia. Ionizing radiation produces free radicals, for instance in DNA, that can react with O_2 to generate fixed peroxy radicals. This DNA damage leads to the desired therapeutic effect. However, if O_2 is missing during radiation, the generated radicals can be reduced to their original composition. Apart from radiotherapy, hypoxic tumor cells are also more resistant towards many chemotherapeutic or other anticancer drugs. This is partly caused by insufficient drug delivery to the hypoxic cells due to inadequate tumor vascularization. Moreover, chemotherapeutics often target highly proliferative cells and hypoxic tumor cells commonly show lower proliferation rates than non-hypoxic tumor cells. Additionally, the aforementioned selection for extremely malignant cells that often downregulate conventional apoptosis pathways, contributes to hypoxic therapy resistance [67].

Moreover, hypoxia contributes to immune evasion of tumor cells by enhancing immunosuppressive pathways and by inhibiting the activity of immunocompetent cells. Thus, hypoxia also poses a major obstacle for immunotherapeutic approaches [68].

Consequently, in recent years research efforts have been put in anticancer drugs that are effective under hypoxic conditions such as hypoxia-activated prodrugs (HAPs) that get activated under hypoxia or small molecule inhibitors directed against essential hypoxia-induced molecular targets [69, 70].

1.3.1 Hypoxia and HPVs

The median O_2 concentration of cervical cancer lies at 1.2 %. Hence, hypoxia is frequently detected in cervical cancer patients and importantly, has a negative impact on patient prognosis [65, 66]. Nevertheless, functional investigations of HPV-positive cancer cells under hypoxia are rare, as is true for many tumor diseases. Intriguingly however, work of the Hoppe-Seyler lab recently revealed that the viral oncogenes E6 and E7 are strongly, but reversibly, downregulated at protein and mRNA level in hypoxic cervical cancer cells. E6 and

E7 level slightly decreased at 3 % O_2 when compared to normoxic cells, but significantly dropped when cells were cultured at 1 % O_2 [71] (Fig. 4). Notably, this downregulation was counteracted by unphysiologically high glucose concentrations [71].

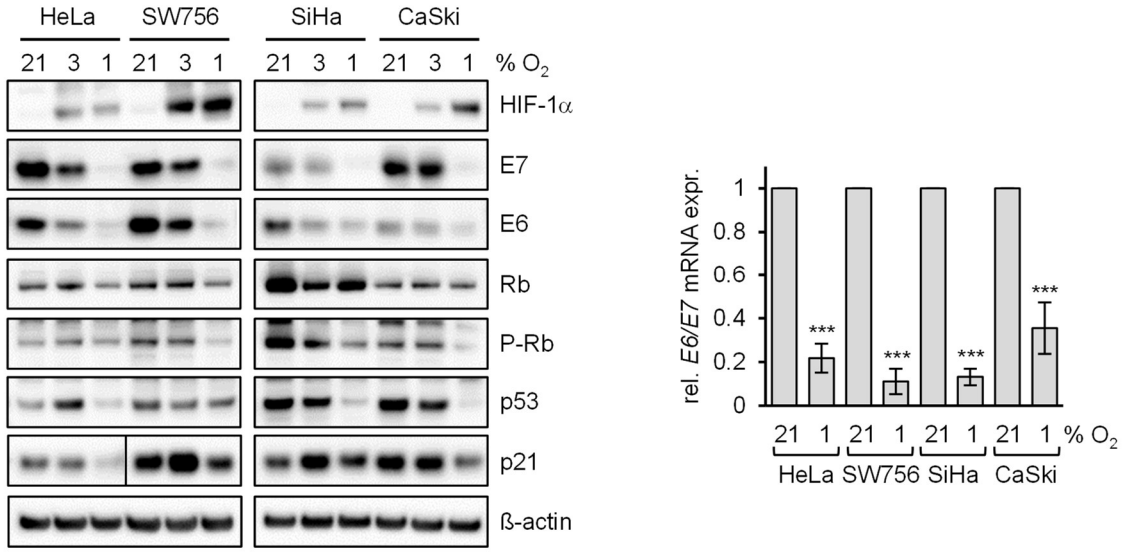

Fig. 4. E6 and E7 expression is downregulated in hypoxic cervical cancer cells. HPV16- and HPV18-positive cervical cancer cell lines were cultured at the indicated O_2 concentrations. Left panel: Immunoblot analyses show expression of HIF-1α (hypoxia-linked marker), HPV16/18 E6 and E7, Rb, phosphorylated Rb (P-Rb), p53 and p21. β-actin = loading control. Right panel: qRT-PCR analyses of relative E6/E7 mRNA expression (all three transcript classes). Standard deviations are depicted. Asterisks indicate statistically significant differences to normoxia (21 % O_2), ***$p < 0.001$. Figure from [71].

Silencing of E6 and E7 expression in HPV-positive cancer cells under normoxia has well established consequences. First, cells undergo an irreversible growth arrest by entering senescence and second, they restore p53 level otherwise degraded via E6 and E6-AP (see also chapter 1.2.4). Surprisingly these conceptions are not valid under hypoxic conditions where cells only undergo a reversible growth arrest that can be overcome by reoxygenation and where p53 levels remain low despite efficient downregulation of E6 and E7. Mechanistically, it was shown that hypoxic HPV-positive cancer cells evade efficient induction of senescence by downregulation of mechanistic target of rapamycin (mTOR) signaling that plays a crucial role in senescence induction under various conditions [72]. In line with this, reactivation of mTOR signaling under hypoxia by silencing of protein regulated in development and DNA damage response 1 (REDD1) or tuberous sclerosis complex 2 (TSC2), both negative regulators of mTOR complex 1 (mTORC1), counteracted the evasion of hypoxic cervical cancer cells from chemotherapy-induced senescence [71].

Hence, hypoxia causes significant alterations in HPV-positive tumor cells that provide resistance towards conventional therapies. Moreover, the inhibition of viral oncogene

expression may render hypoxic HPV-positive tumor cells less vulnerable to E6/E7-targeted therapeutic approaches and may contribute to immune evasion mechanisms due to reduced presentation of viral antigens on the cell surface in combination with the overall immunosuppressive effects of hypoxia [68]. Importantly, since hypoxic HPV-positive cancer cells only enter a reversible dormant state, they may form a reservoir for recurring tumors that can develop after reoxygenation [71]. Deciphering the molecular mechanism underlying hypoxia-induced repression of E6/E7 expression should therefore yield important insights to increase our current understanding of HPV-associated tumorigenesis and to provide a foundation for future design of therapeutic approaches.

1.4 Regulatory mechanisms and cellular pathways under hypoxia

Limited oxygen supply poses a fundamental challenge on the survival of cells. Thus, to successfully adapt to hypoxia, cells have to undergo a series of regulatory alterations.

1.4.1 Metabolic adaptations

Under conditions of sufficient oxygen supply, normal cells gain the majority of energy through ATP production via mitochondrial oxidative phosphorylation (OXPHOS). Many cancer cells, however, shift their metabolism towards enhanced glycolysis with accompanying lactate production, even under aerobic conditions. This aerobic glycolysis (also termed 'Warburg effect') provides a fast supply of ATP, although with a lower yield per molecule of glucose compared to energy production via OXPHOS, and allows the production of many cellular building blocks. Under hypoxia, cells are even more dependent on glycolysis since OXPHOS is downregulated to reduce the amount of O_2 molecules that are consumed. This metabolic reprogramming is mediated in part by increased expression of glycolytic enzymes and glucose transporters [73]. Moreover, transporters that excrete lactate from the cell are upregulated to prevent intracellular acidification by enhanced lactate production from glycolysis [74].

Another noteworthy key feature of hypoxic cells is an increase in the intracellular cytosolic calcium (Ca^{2+}) concentration that is involved in the regulation of the cellular adaptation to hypoxia [75].

Apart from regulation of Ca^{2+} homeostasis and glucose metabolism, cellular modifications concerning, amongst others, fatty acid metabolism, glutamine metabolism and maintenance of adequate redox balance are carried out in hypoxic cells to cope with the demanding nature of O_2 deprivation [76].

1.4.2 Hypoxia-inducible factors (HIFs)

Hypoxia-inducible factors (HIFs) are transcription factors that are considered master orchestrators of the cellular adaptation to hypoxia. If O_2 levels are high, prolyl hydroxylases (PHDs) hydroxylate proline residues on the HIF-α subunits (HIF-1α and HIF-2α) in an O_2- and α-ketoglutarate-dependent manner. Hydroxylated HIF-α is recognized by the von Hippel-Lindau (pVHL) protein that functions as E3 ubiquitin ligase and targets HIF-α for proteasomal degradation. Upon hypoxia, PHDs are less active and HIF-α is stabilized. The HIF-α subunits each form an obligatory heterodimer with the stably expressed HIF-1β, also termed ARNT. The HIF heterodimer then regulates gene expression by binding to DNA sequences termed hypoxia-responsive elements (HREs) with the consensus sequence G/ACGTG. Another mechanism of O_2-dependent regulation of HIF is mediated by factor-inhibiting HIF-1α (FIH1), an asparaginyl hydroxylase. FIH1 hydroxylates HIF-α and thereby inhibits recruitment of HIF transcriptional coactivators p300 and CREB-binding protein (CBP) [77]. Additionally, it has been proposed that increased production of reactive oxygen species (ROS) by the mitochondrial electron transport chain under hypoxia are required for stabilization of HIF-α [78]. However, HIF-α can also be regulated independently of O_2, for instance by oncogenic signaling [77].

HIFs are critically involved in regulating most of the aforementioned metabolic adaptations to hypoxia (see chapter 1.4.1). Despite having some overlapping functions, HIF-1α and HIF-2α can also regulate unique target genes. HIF-1α is ubiquitously expressed, whereas expression of HIF-2α is more restricted, but can still be detected in many cell types [79]. Expression of glycolytic genes is largely regulated via HIF-1α, which for instance activates hexokinase 1 and 2 (HK1, HK2), phosphofructokinase (PFK) or lactate dehydrogenase A (LDHA). While HIF-1α and HIF-2α have both been reported to induce expression of glucose transporters, several enzymes involved in redox homeostasis are uniquely regulated by HIF-2α such as heme oxygenase 1 (HMOX1) or superoxide dismutase 1 (SOD1) [77, 79]. HIFs also regulate the activity of various oncogenes or tumor suppressors. Activity of the pro-proliferative oncogenic transcription factor MYC and the pro-growth kinase complex mTORC1 are negatively regulated by HIF-1α and positively by HIF-2α. Such an opposing regulation has also been described for the p53 pathway with an activating effect of HIF-1α and a repressive function of HIF-2α. Thus, HIF-1α and HIF-2α often function in a balancing manner to regulate the cellular response to hypoxia [77, 79].

Apart from HIF-1α and HIF-2α, a third O_2-labile HIF-α subunit is described: HIF-3α. Several variants of HIF-3α with putatively varying functions exist, generated by alternative splicing or usage of different transcription start sites. Studies addressing HIF-3α are limited, but there are indications for a role of HIF-3α in hypoxia-induced transcriptional regulation [80].

1.4.3 Epigenetic alterations

While HIF transcription factors are key drivers of hypoxia-induced alterations in gene expression, they are supported by many epigenetic modifications induced under hypoxia [81]. These can occur independently of HIF and contribute to global transcriptional repression, but also to activation of specific genes [82].

DNA hypermethylation to silence tumor suppressor genes is commonly found in hypoxic tumor cells. This was proposed to be largely caused by reduced activity of O_2-dependent ten-eleven translocation (TET) enzymes that are required for DNA demethylation [83].

Hypoxia has a significant impact not only on the methylation of DNA, but also on methylation of histones. Interestingly, many histone demethylases are described as O_2-dependent, resulting in overall enhanced levels of trimethylation at lysine 4 of histone 3 (H3K4me3) and at lysine 27 of histone 3 (H3K27me3) under hypoxia [84, 85]. Since H3K4me3 and H3K27me27 are opposing histone marks being associated with active and silenced gene expression, respectively, consequences of hypoxia-induced histone methylation are complex, but lead to significant alterations in gene expression depending on the cellular and genetic context [84-86].

1.4.4 The PI3K/AKT signaling pathway

Activation of the serine/threonine kinase AKT, also known as protein kinase B (PKB), is typically induced by growth factors, cytokines or hormones such as insulin that is secreted upon high blood glucose [87]. Interestingly, AKT can also be activated by glucose deprivation [88-90]. Moreover, there is emerging evidence that AKT is frequently activated under hypoxia [91-93]. In this context, there are also reports connecting the AKT pathway to HIF, insofar as PI3K/AKT activity has been described to contribute to increased levels of HIF-1α [91, 94].

The AKT1-3 proteins are the three distinct isoforms of AKT. They are highly homologous, but are each encoded by a separate gene [95]. Belonging to the AGC group of kinases they share some structural similarities with protein kinase A, G and C. AKT kinases all consist of an N-terminal pleckstrin homology (PH) domain, a central kinase domain and a C-terminal hydrophobic regulatory domain. The C-terminal segment is thereby characteristic also for other AGC kinases. The three AKT isoforms share approximately 80 % amino acid sequence homology with the kinase domain being especially conserved [96, 97]. AKT is fully activated when phosphorylated at two specific sites; at T308, T309 or T305 in the kinase domain and at S473, S474 or S472 in the C-terminal domain for AKT1, AKT2 or AKT3, respectively [97, 98]. Hereafter only the phosphorylation sites for AKT1 will be named when referring to all AKT isoforms in general. An additional phosphorylation site at a highly conserved threonine (T450 in AKT1), phosphorylated by the mTOR complex 2 (mTORC2), was reported to contribute to AKT protein stability [99].

AKT is activated downstream of class I phosphoinositide 3-kinases (PI3Ks, see Fig. 5). In detail, upon receiving extracellular stimuli, for instance via growth factors or cytokines, receptor tyrosine kinases (RTKs) or G protein-coupled receptors (GPCRs) are activated leading to recruitment and activation of PI3K, a process that often involves Ras GTPases. PI3K phosphorylates the membrane lipid phosphatidylinositol-4,5-bisphosphate ($PI4,5P_2$) to generate phosphatidylinositol-3,4,5-trisphosphate (PIP_3) that can be further converted to phosphatidylinositol-3,4-bisphosphate ($PI3,4P_2$). This can be counteracted by the phosphatase PTEN [100]. PIP_3 and $PI3,4P_2$ recruit AKT to the membrane by binding to the PH domain of AKT. In its inactive state AKT is mainly localized in the cytosol and its PH domain closely interacts with its kinase domain. In this conformation, T308 in the kinase domain of AKT is inaccessible for phosphorylation. Upon interaction of the PH domain of AKT with PIP_3 or $PI3,4P_2$, the T308 residue becomes accessible and is phosphorylated by phosphoinositide-dependent kinase-1 (PDK1) that is itself recruited to the membrane by interaction of its PH domain with phosphoinositides [101]. In a recent report it was proposed that translocation of AKT to the plasma membrane is facilitated by calmodulin (CaM) [102]. CaM is a Ca^{2+}-sensing protein that can bind to the PH domain of AKT and has been shown to colocalize with AKT at the plasma membrane upon growth factor stimulation [103].

AKT phosphorylated at T308 alone has some enzymatic activity but additional phosphorylation at S473 is required for full activation [98].

The responsible kinase for AKT S473 phosphorylation is mTORC2 [104]. mTORC2 has been reported to be activated in a PI3K-dependent manner by being recruited to the membrane via PIP_3. However, PI3K-independent activity of mTORC2 has been described as well [95]. On a side note, AKT S473 phosphorylation has also been described to be carried out by DNA-dependent protein kinase (DNA-PK) in the context of DNA damage [105]. mTORC2-mediated phosphorylation at S473 is reported to facilitate T308 phosphorylation and suggested to occur prior to T308 phosphorylation [104].

AKT signaling is negatively regulated by the phosphoinositide phosphatase PTEN, but also by protein phosphatase 2A (PP2A) that dephosphorylates AKT at T308 and by PH domain leucine-rich repeat protein phosphatases 1 and 2 (PHLPP1, PHLPP2) that dephosphorylate AKT at S473 [95].

Once phosphorylated at T308 and S473, active AKT dissociates from the membrane and can phosphorylate its substrates in the cytoplasm or nucleus [101]. However, it has also been reported that AKT activity is dependent on binding to PIP_3 or $PI3,4P_2$ and is therefore restricted to cellular membranes. Furthermore, activation of AKT has not only been reported at the plasma membrane, but also at endomembranes [95].

The exact mechanism of how AKT is activated under hypoxia is unclear so far. However, hypoxia-induced ligand-independent activation of growth factor receptors or modulation of

ligand expression resulting in increased AKT activity has been reported for specific conditions and cell types [106, 107]. Moreover, in a recent publication it has been suggested that AKT is regulated via hydroxylation by the prolyl hydroxylase EgIN1 in an O_2-dependent manner. Hydroxylated AKT interacts with and is dephosphorylated by PP2A associated with pVHL. Since activity of EgIN1 is dependent on O_2, hypoxia leads to reduced hydroxylation and reduced dephosphorylation of AKT resulting in enhanced AKT activation [108].

Taken together, despite considerable progress and substantial amounts of data already existing in the PI3K/AKT research field, there remain many aspects to be clarified to get a more complete picture of AKT signaling.

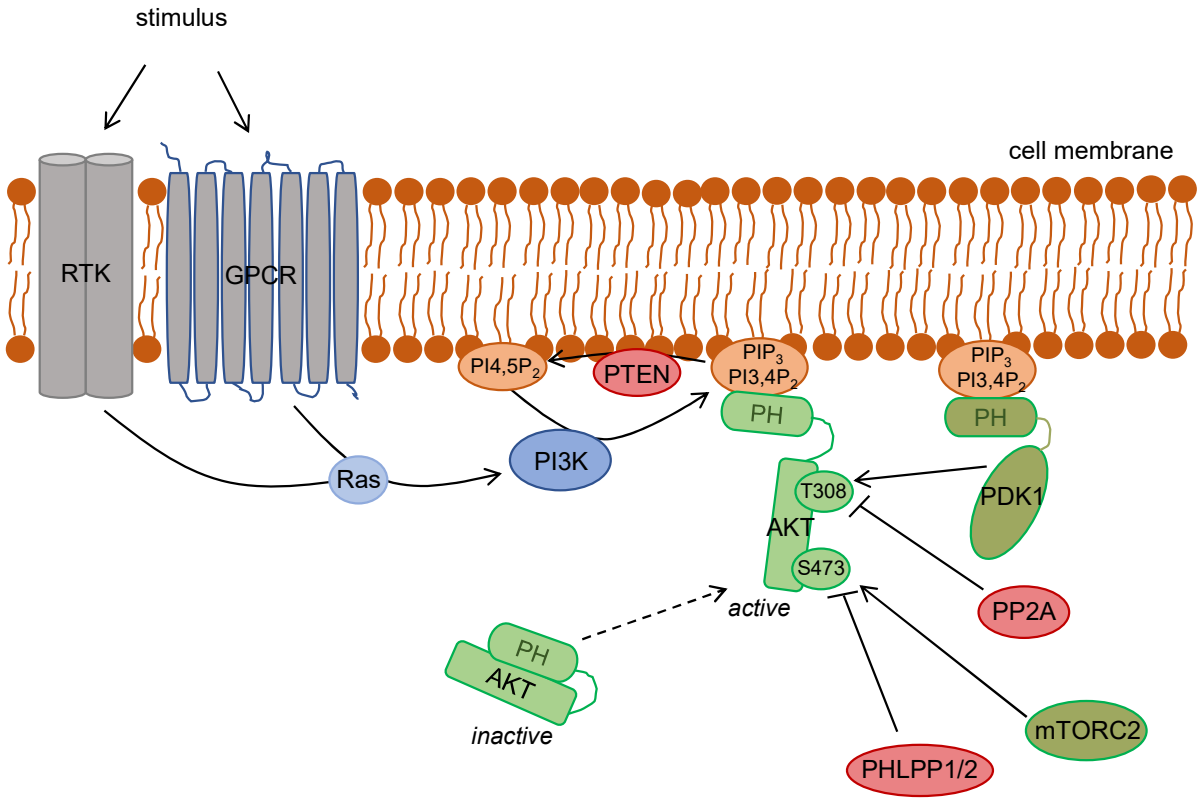

Fig. 5. PI3K-dependent AKT activation. PI3K is activated by RTKs or GPCRS and phosphorylates phosphoinositides. AKT and PDK1 are recruited to the membrane via their PH domains. AKT is positively regulated by mTORC2 and PDK1. PTEN, PP2A and PHLPP1 and 2 are negative regulators. Simplified schematic, for details refer to text.

AKT kinases influence many essential aspects of cell biology by modulating energy metabolism and promoting cell survival, growth, proliferation, migration and angiogenesis. In line with this, more than 100 proteins have been suggested as AKT substrates [109].

Amongst the earliest established AKT targets are the two glycogen synthase kinase 3 isoforms GSK3-α and GSK3-β [110]. AKT phosphorylates GSK3-α at S21 and GSK3-β at S9.

This phosphorylation acts inhibitory by preventing association of GSK3-α/β with their substrates. GSK3 has a multitude of targets that are mainly inhibited by GSK3-induced phosphorylation. Many of these targets are involved in cell survival and metabolism such as c-Myc, HIF-1α or glycogen synthase [95].

Another important downstream target of AKT is mTORC1. A major function of mTORC1 is the promotion of anabolic processes such as protein, lipid and nucleotide synthesis. AKT phosphorylates and inhibits TSC2 thereby releasing TSC2-mediated inhibition of mTORC1. Additionally, AKT phosphorylates PRAS40, another inhibitor of mTORC1, and induces its dissociation from mTORC1 [111, 112]. Moreover, it has been proposed that AKT directly phosphorylates and activates mTOR [113]. Hence, via activation of mTORC1, AKT contributes to cell growth and survival. AKT-mediated mTORC1 activation is particularly interesting considering the induced negative feedback regulation. mTORC1 activation leads to enhanced degradation of insulin receptor substrates 1 and 2 (IRS) and consequently reduces PI3K activation by insulin and insulin-like growth factor 1 (IGF1) receptors. Furthermore, mTORC1 activates p70 S6 kinase (p70S6K), which in turn phosphorylates components of the second mTOR-containing complex; mTORC2, resulting in inhibition thereof. As a consequence, mTORC2-mediated phosphorylation of AKT at S473 is impaired. mTORC1-dependent negative feedback regulation of PI3K/AKT signaling includes further mechanisms and is complemented by additional distinct downstream effectors [95].

Major outputs of AKT signaling can also be observed at the level of cellular energy metabolism. Importantly, AKT stimulates glucose uptake, mainly in response to insulin, by inducing translocation of glucose transporters to the plasma membrane [87]. Moreover, AKT promotes (aerobic) glycolysis and thus, may be a strong contributor to shifting cellular energy metabolism in the context of the Warburg effect (see chapter 1.4.1) [114].

Taken together, only a few AKT targets have now been mentioned exemplarily, however, those already illustrate how activation of PI3K/AKT can expand to a broad signaling network with a multitude of effectors and regulatory mechanisms. This network becomes even more complex considering that there exist three distinct isoforms of AKT.

AKT1 is ubiquitously expressed and AKT2 expression is also found in most tissues, but with particularly high levels in insulin-sensitive tissues. Expression of AKT3 is more restricted and primarily found in neuronal tissues [95]. Moreover, AKT3 is frequently upregulated in melanoma cells [115]. The three AKT isoforms have many overlapping, but also some distinct functions. This is clearly demonstrated by comparing phenotypes of isoform-specific knockout mice. AKT1-knockout mice have severe growth defects [116], whereas AKT2-knockout mice show strongly impaired glucose homeostasis with type 2 diabetes-like symptoms [117]. Knockout of AKT3 results in impaired brain development in mice [118]. These data, together with many other functional studies, indicate that AKT1 is essential for

proliferation and cell growth, AKT2 is primarily involved in regulating glucose metabolism and AKT3 is crucial for neuronal development. However, combined AKT knockout mice also reveal some compensating effects between the isoforms [119, 120]. How isoform-specific functions of AKT are regulated is only incompletely understood. Although distinct tissue distribution certainly plays a role in isoform-specific effects, expression of more than one AKT isoform is frequently found in many tissues. Additionally, subcellular localization, relative expression levels, differential activation by diverse stimuli and differences in substrate specificity based on molecular distinctions between the individual isoforms may account for isoform specificity [95].

The PI3K/AKT pathway is aberrantly activated in many cancers and contributes significantly to the malignant phenotype of tumor cells and to their resistance towards conventional therapies. The most commonly detected alteration in this pathway is an activating mutation in the *PIK3CA* gene, coding for a subunit of class I PI3K. However, alterations in other pathway members can also contribute to enhanced AKT activity such as loss of function of the negative regulator PTEN or amplifications or activating mutations of RTKs, further PI3K subunits or other downstream effectors including AKT isoforms themselves [121]. Thus, the PI3K/AKT pathway is subject to intensive investigations as putatively promising therapeutic target in cancer therapy. Various small molecule inhibitors targeting PI3K, mTOR or AKT are currently tested in the clinic. This includes single-agent studies, but also combinations with chemo- and radiotherapy or combination therapies with other targeted drugs [122].

Cervical cancer belongs to the tumor types frequently associated with aberrant PI3K/AKT activation. Mutations in *PIK3CA* are linked to shorter survival of cervical cancer patients and high levels of phosphorylated AKT have been shown to correlate with poor outcome after chemoradiation [123, 124]. Hence, the clinical application of PI3K/AKT inhibitors for the treatment of cervical cancer is intensely studied [125].

1.5 Research objectives

Continuous expression of the viral oncogenes E6 and E7 has generally been considered a prerequisite for the maintenance of the malignant phenotype of HPV-positive tumor cells since silencing of E6 and E7 rapidly induces senescence in these cells. Intriguingly, it was recently found that this widely accepted dogma is not valid under hypoxia, a condition that is frequently detected in HPV-positive cancers. In specific, hypoxic HPV-positive cancer cells, can efficiently and reversibly shut down viral oncogene expression, but evade senescence. These surprising findings shed new light on the crosstalk between the viral oncogenes and the host cell, which could be of high relevance for both basic research and clinical aspects of HPV-linked cancers. To gain mechanistic insights into the underlying regulatory phenomena, the following major questions will be addressed:

(i) At which molecular level are the viral oncogenes downregulated under hypoxia? Is the effect linked to changes in E6/E7 promoter activity, to epigenetic modifications of the viral transcriptional control region or to alterations in E6/E7 mRNA or protein stability?

(ii) Is HPV oncogene repression linked to the activity of transcription factors which are known key regulators for the cellular response towards hypoxia? Analyses will include the examination of HIF proteins, considered the master orchestrators of hypoxia-induced alterations in gene expression. In addition, glucose-responsive factors will be investigated since E6/E7 repression under hypoxia is sensitive to glucose.

(iii) Which signaling cascade is responsible for hypoxic E6/E7 repression? Here, a special focus will be put on a detailed analysis of the PI3K/AKT pathway that is activated by hypoxia and emerged as a particularly promising candidate. Questions that will be addressed include: Is AKT activation required for repression of E6 and E7 under hypoxia? Is there a connection to the cellular calcium and energy metabolism? Can hypoxic regulation of E6 and E7 be affected by inhibitors targeting different factors in the PI3K/AKT signaling cascade, including clinically used PI3K/AKT inhibitors, and what are the phenotypic consequences of PI3K/AKT inhibitor treatment on hypoxic HPV-positive cells? What is the functional role of the individual AKT isoforms? Finally, hypoxia-linked alterations in the protein composition of HPV-positive cancer cells will be analyzed by proteomic studies and the effects of a concomitant application of an AKT inhibitor or high glucose supply will be assessed.

It is the overall aim of the present work to gain a better understanding of the mechanism by which HPV-positive cancer cells are able to repress viral oncogene expression under hypoxia. The elucidation of the underlying pathway(s) will provide important new insights into the host/virus interaction in HPV-positive cancer cells and should be relevant for prospective therapeutic approaches which aim to target E6/E7.

Chapter 2

Results

2. Results

2.1 Transcriptional regulation of HPV E6/E7 expression under hypoxia

The expression of HPV E6/E7 is strongly downregulated in cervical cancer cells under hypoxic conditions [71]. This repression of E6/E7 is detectable at protein and mRNA level raising the question whether transcription of the polycistronic E6/E7 mRNA is impaired under hypoxia.

2.1.1 HPV transcriptional activity is reduced under hypoxia

To investigate the transcriptional regulation of E6/E7 under hypoxia, the transcriptional control region of HPV18 E6/E7 (HPV18 URR), was investigated using luciferase reporter assays. More precisely, the HPV18 URR fused to a luciferase gene was transfected into HPV18-positive HeLa cells and luciferase activity, representing the transcriptional activity of the E6/E7 promoter in the physiological context of the complete HPV18 URR, was determined under hypoxia (1 % O_2) and normoxia (21 % O_2). Activity of the full length reporter construct (p18URRL) was significantly impaired under hypoxia with a mean log2 fold change of -0.97, which represents a reduction in activity of approximately 50 % (Fig. 6A). A similar effect was observed for a 5′-deletion construct that still contains the HPV enhancer and the promoter proximal region PPR (p436/L). A further truncated reporter, only consisting of the PPR (p232/18L) was no longer repressed by hypoxia indicating a critical role for the HPV enhancer region.

To further investigate whether the PPR is dispensable for hypoxia-mediated repression, additional luciferase assays were performed with reporter constructs containing the 230 bp HPV18 enhancer region fused to the heterologous HSV TK promoter. Activity of this reporter was equally impaired under hypoxia when compared to reporter constructs with the homologous HPV E6/E7 promoter indicating that the 230 bp enhancer is sufficient to mediate repression of transcriptional activity under hypoxia (Fig. 6B). Likewise, a further 5′-deletion construct of the HPV enhancer (p157s/tk*L) still showed significantly reduced activity under hypoxia. Contrarily, the activity of a 3′-deletion construct encompassing only 116 bp of the 5′-enhancer region (p116s/tk*L) was not altered under hypoxia. The activity of the GAPDH promoter was measured in parallel as a positive control and showed the expected stimulation under hypoxia [126].

Taken together, the activity of the HPV18 URR under hypoxia was reduced by about 50 % with a 157 bp enhancer fragment being sufficient to mediate the repression indicating that transcriptional regulation is, at least partially, involved in hypoxic repression of E6/E7.

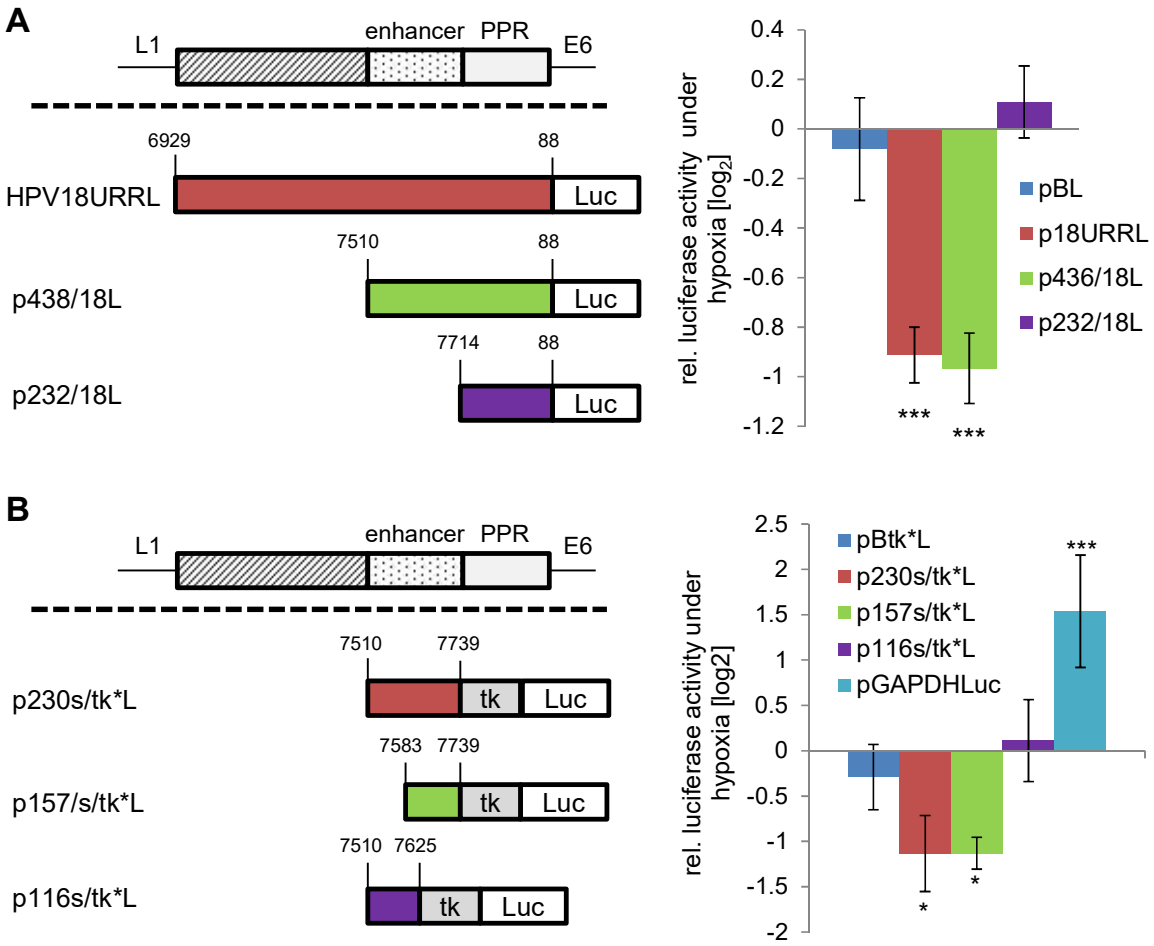

Fig. 6. Reduced activity of the HPV18 URR under hypoxia. Luciferase reporter assays of HeLa cells incubated for 24 h under hypoxia (1 % O_2) or normoxia (21 % O_2). Left panels show a schematic representation of the investigated reporter constructs. The full length construct encompasses the 5′ terminal region, the central enhancer and the promoter proximal region (PPR). Nucleotide positions according to reference [127]. **(A)** Reporter assay with constructs containing the firefly luciferase gene under the control of the complete HPV18 URR (p18URRL) or deletion constructs thereof (p436/18L, p232/18L), pBL = basic vector. **(B)** Reporter assay with the firefly luciferase gene under the control of the HSV TK promoter fused to the HPV18 enhancer (p230s/tk*L) or deletion constructs thereof (p157s/tk*L, p116s/tk*L). pBtk*L = basic vector, pGAPDHLuc = positive control. **(A+B)** Shown is the log2 of the relative luciferase activity under hypoxia. Standard deviations are depicted (n = 4 (A), n = 5 (B)). Asterisks above columns show statistically significant differences from the basic vector control as determined by one-way ANOVA (*p<0.05, ***p < 0.001).

2.1.2 The role of YY1, Brd4 and the BET inhibitor JQ-1 in repression of E6/E7 under hypoxia

Jha and colleagues previously published that the transcription factor YY1 facilitates binding of the histone acetyltransferase TIP60 to the HPV URR, which leads to the recruitment of the BET family member Brd4 and eventually results in repression of HPV E6/E7 transcription [128]. Since the reported binding sites for TIP60 and YY1 overlap with the 157 bp enhancer element identified as crucial for the repression of the HPV URR activity under hypoxia (see

chapter 2.1.1), it was tested whether YY1 and Brd4 are negative regulators of E6/E7 expression under hypoxia. However, silencing of YY1 or Brd4 by shRNAs or siRNAs, respectively, did not prevent the downregulation of E7 expression under hypoxia as was shown by immunoblot analyses (Fig. 7A and B). Moreover, YY1 and Brd4 proteins showed no increased expression under hypoxia. In addition to that, ectopic overexpression of YY1 did not alter E7 expression levels under hypoxia or normoxia (Fig. 7A), all in all arguing against a repressive function of YY1 and Brd4 on E6/E7 expression under the investigated conditions. Interestingly though, unlike to the shRNA-mediated knockdown of Brd4, treatment with the BET inhibitor JQ-1 restored E7, but not E6 expression under hypoxia in HeLa cells (Fig. 7C). Noteworthy, treatment with JQ-1 under normoxia slightly decreased E7 expression in HeLa cells. However, this latter observation was subject to great variation, thus, two representative experiments out of six are shown in this case. By extending the investigations to further cell lines, it was revealed that JQ-1-mediated reactivation of E7 expression under hypoxia was not observed in HPV18-positive SW756 and HPV16-positive SiHa cells (Fig. 7D). Downregulation of E6 and E7 expression after JQ-1 treatment under normoxia was on the other hand clearly detectable in SW756 and SiHa cells.

Altogether, YY1 and Brd4 were not confirmed as repressors of HPV E6/E7 expression under hypoxia. However, the BET inhibitor JQ-1 was shown to influence E6/E7 expression under hypoxia and normoxia in a cell line-dependent manner.

2.1.3 Trimethylation at H3K4 and H3K27 increases under hypoxia

Results obtained with luciferase reporter assays indicate that transcriptional regulation plays a role in repression of E6/E7 expression under hypoxia. Since epigenetic changes can mediate hypoxia-induced alterations in gene expression [81], the epigenetic status of the HPV URR was studied next. These investigations were focused on SiHa cells since they contain only 1 to 2 HPV16 integrates in contrast to many other cervical cancer cell lines, such as HeLa, that harbor a multitude of viral integrates [129].

The abundancy of H3K4me3 and H3K27me3 at the HPV16 URR in SiHa cells was investigated by chromatin immunoprecipitation (ChIP). H3K4me3 is primarily associated with active transcription, whereas H3K27me3 is closely linked to inactive genes [130].

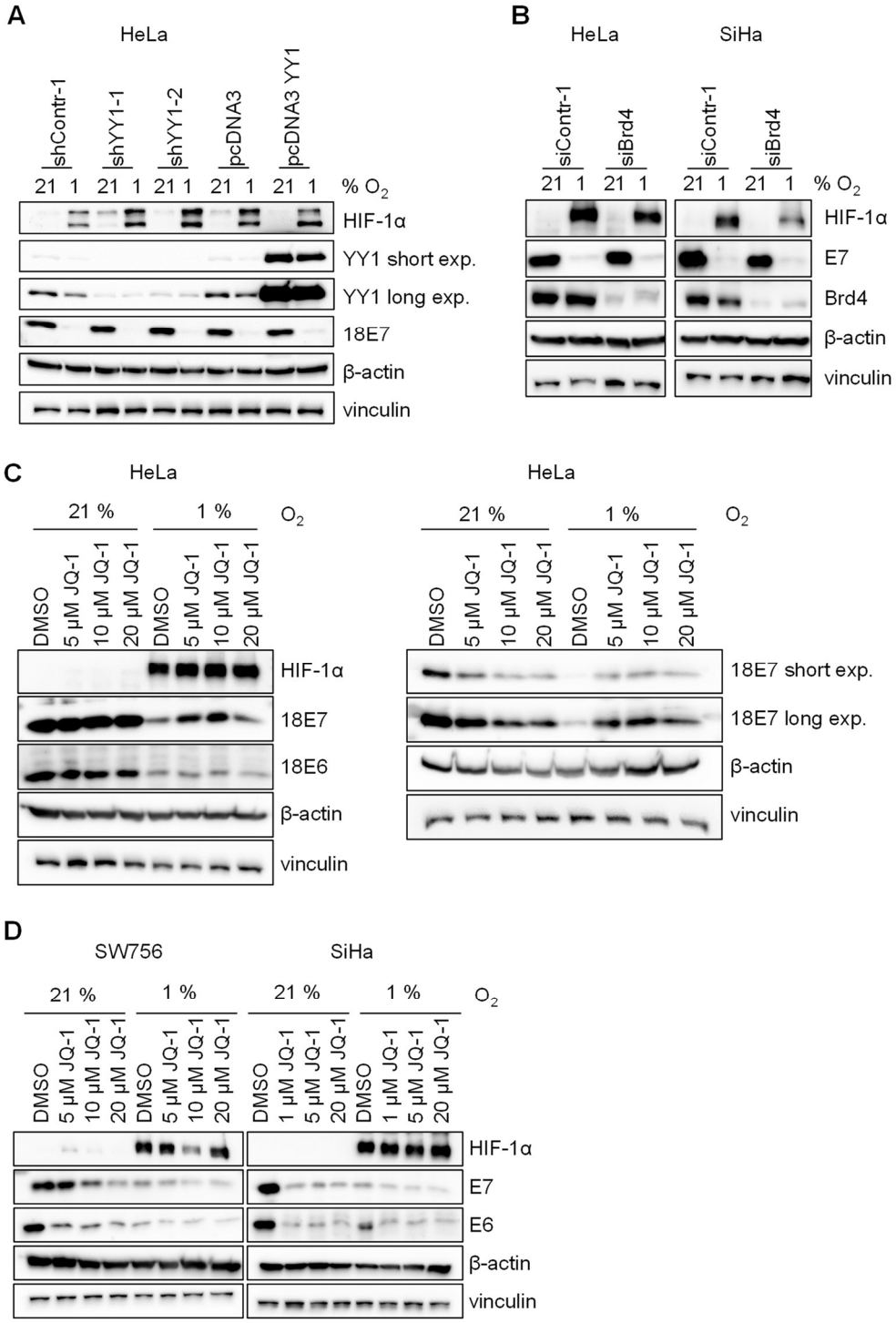

Fig. 7. Role of YY1 and Brd4 in regulation of E6/E7 under hypoxia. (A) HeLa cells expressing shRNAs against YY1 (shYY1-1, shYY1-2) or ectopically expressing YY1 (pcDNA3YY1) were cultured for 24 h under hypoxia or normoxia. shContr-1 = control shRNA, pcDNA3 = vector control. **(B)** HeLa and SiHa cells transfected with a Brd4 targeting siRNA were cultured for 24 h under hypoxia or normoxia. **(C)** HeLa cells were treated with the indicated concentrations of JQ-1 or DMSO as solvent control and cultured for 24 h under hypoxia or normoxia. Shown are two representative experiments out of six. **(D)** SW756 and SiHa cells were treated and cultured as in (C). **(A-D)** Immunoblot analyses of HIF-1α (hypoxia-linked marker), YY1, HPV16/18 E6 and E7 and Brd4. Vinculin, β-actin = loading control. Short exp. = short exposure, long exp. = long exposure.

By qPCR analyses of H3K27me3 ChIPs, an increase of H3K27me3 under hypoxia was detected at the HPV16 URR (Fig. 8A). However, an increase of H3K27me3 was also detected at all other analyzed regions including regulatory regions of VEGF and Glut1, both hypoxia-induced proteins [131, 132]. The viral L1 and L2 genes generally exhibited a slightly higher occupancy of H3K27me3 compared to the HPV URR and the hypoxia-induced genes. qPCR analyses of H3K4me3 ChIPs revealed that the marker for active genes was also enriched under hypoxia at all analyzed regions (Fig. 8B). Notably, H3K4me3 signals at the L1 and L2 gene were very low under both conditions.

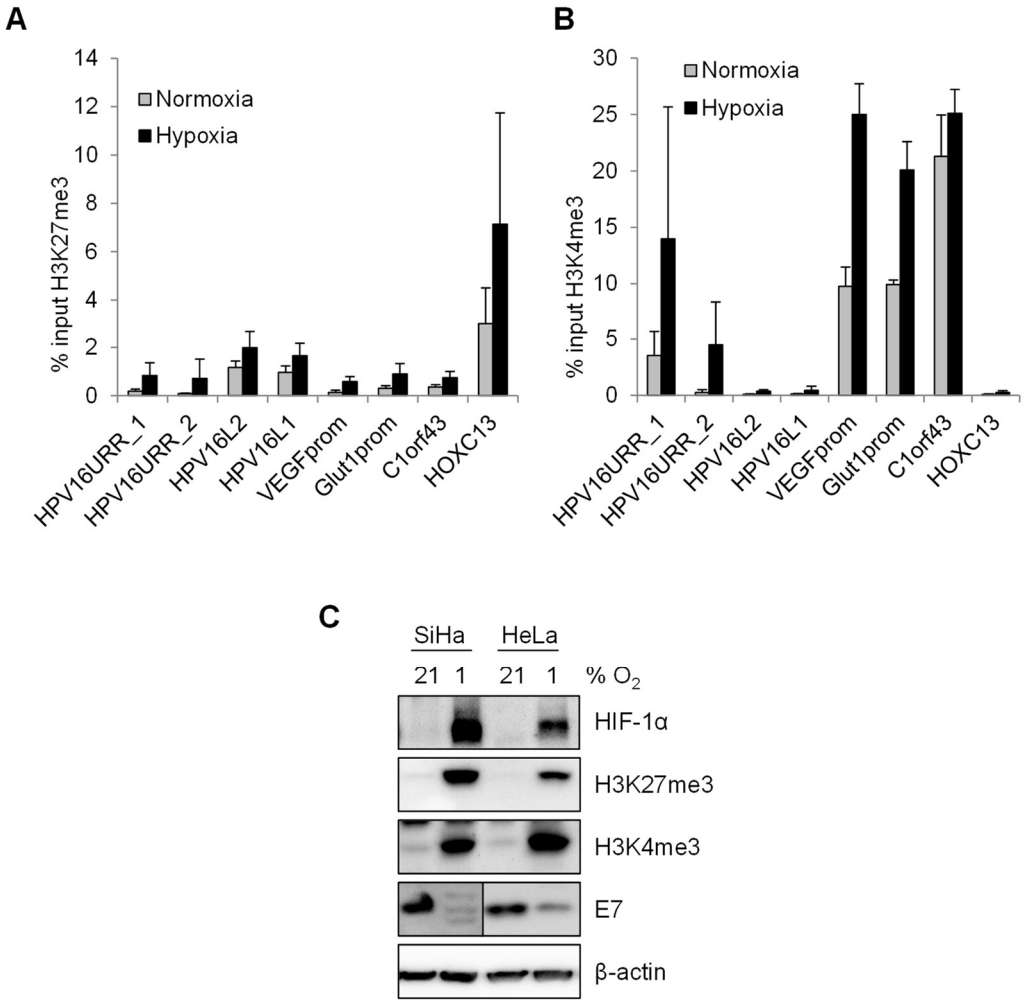

Fig. 8. H3K4 and H3K27 trimethylation under hypoxia. (A+B) SiHa cells were cultured for 24 h under hypoxia or normoxia, ChIP against H3K27me3 **(A)** or H3K4me3 **(B)** was performed and qRT-PCR analyses were carried out using primers located in the HPV16 URR (HPV16URR_1, HPV16_URR2), in the L1 and L2 gene (HPV16L2, HPV16L1) and in regulatory regions for VEGF and Glut1 (VEGFprom, Glut1prom). C1orf43 and HOXC13 served as control regions. Depicted is the mean percentage of input of 3 independent experiments. Error bars indicate standard deviations. ChIP was performed in collaboration with T. Günther and A. Grundhoff (Heinrich-Pette-Institute, Hamburg). **(C)** Immunoblot analyses of HeLa and SiHa cells cultured for 24 h under hypoxia or normoxia show protein expression of HIF-1α (hypoxia-linked marker), H3K27me3, H3K4me3 and HPV16/18 E7. β-actin = loading control.

C1orf43 served as control for an actively transcribed region and showed the expected enrichment of H3K4me3. The HOXC13 gene served as reference for a transcriptionally silenced region and was enriched in H3K27me3. Under hypoxic conditions, a general increase of H3K4me3 and H3K27me3 was detected at both control regions (Fig. 8A and B).
Since the HPV URR was enriched in both, active and repressive histone marks, an effect that was mirrored at all other tested genomic regions, global H3K27me3 and H3K4me3 level were monitored under hypoxia. In fact, total cell lysates of HeLa and SiHa cells showed increased levels of H3K27me3 and H3K4me3 under hypoxia as determined by immunoblot (Fig. 8C). Thus, the detected enrichments of the investigated histone marks in ChIP experiments go in line with a general increase in cellular H3K27me3 and H3K4me3 level under hypoxia.

2.1.4 DNA methylation is likely not involved in repression of E6/E7 under hypoxia

Apart from histone modifications, DNA methylation is another epigenetic mechanism that can be linked to hypoxic gene silencing [83]. To investigate if DNA methylation is crucial for repression of E6/E7 under hypoxia, cells were treated with the global DNA methylation inhibitor 5-aza-2'-deoxycytidine (5-Aza) which is a cytidine analog that is incorporated into DNA strands during replication. Upon engaging DNA methyltransferases, the enzymes become irreversibly bound to DNA resulting in loss of methyltransferase activity [133]. However, despite pre-treatment with 5-Aza, E7 expression was still effectively downregulated in HeLa and SiHa cells under hypoxia (Fig. 9A) indicating that DNA methylation is not required for repression of E6/E7. On a side note, in normoxic SiHa cells, E7 expression was slightly reduced upon treatment with 5-Aza when compared to DMSO treated control cells. Expression of DNA methyltransferase 1 (Dnmt1) was monitored as a positive control for 5-Aza treatment since 5-Aza-induced the degradation of Dnmt1 [134]. Indeed, downregulation of Dnmt1 expression was observed upon 5-Aza treatment. Noteworthy however, under hypoxic conditions, Dnmt1 expression was also strongly impaired.
In parallel, the DNA methylation status of the HPV16 URR in SiHa cells was investigated via qPCR of methylated DNA immunoprecipitation (MeDIP) samples. Methylation levels at the analyzed regions in the HPV16 URR were not induced by hypoxia (Fig. 9B) confirming that DNA methylation is likely not involved in repression of E6/E7 under hypoxia. In line with previous reports [135], the transcriptionally silenced HPV L1 and L2 genes generally exhibited higher DNA methylation levels compared to the URR. Interestingly, methylation at L1 and L2 slightly decreased under hypoxia. As expected, the hypoxia-induced genes VEGF and Glut1 showed low methylation levels that were comparable to the negative control region in the human tubulin alpha-1c chain (Tuba1C). A methylated CpG island in the gene SHANK1 (CpG 4) served as positive control (Fig. 9B).

In conclusion, there were no indications for a role of DNA methylation in repression of E6/E7 expression under hypoxia since an inhibitor of DNA methylation was not able to alter hypoxic E6/E7 expression and, moreover, DNA methylation levels at the HPV16 URR remained low under hypoxia.

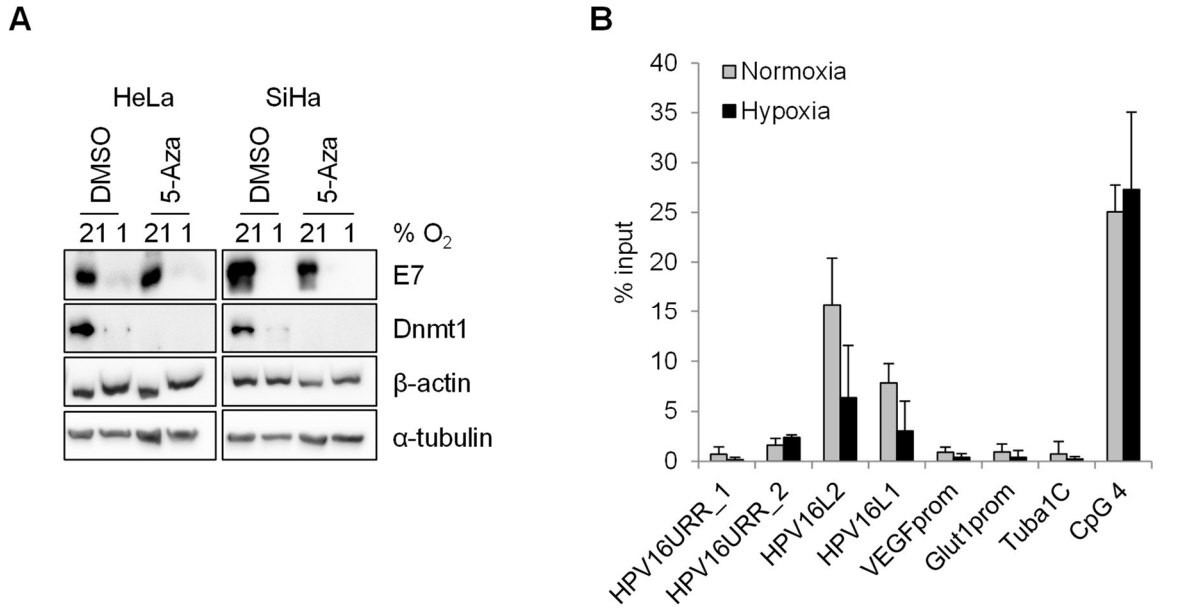

Fig. 9. Role of DNA methylation in regulation of E6/E7 under hypoxia. (A) HeLa and SiHa cells were treated with DMSO as solvent control or with 10 µM 5-aza-2'-deoxycytidine (5-Aza) for 3 days. Prior to harvesting, cells were cultured for 24 h under hypoxia or normoxia as indicated. Medium with fresh inhibitor was replaced every 24 h. Immunoblots of HPV18/16 E7 and Dnmt1 are shown. β-actin, α-tubulin = loading control. **(B)** SiHa cells were cultured for 24 h under hypoxia or normoxia, MeDIP was performed and qRT-PCR analyses were carried out using primers located in the HPV16 URR (HPV16URR_1, HPV16_URR2), in the L1 and L2 gene (HPV16L2, HPV16L1) and in regulatory regions of VEGF and Glut1 (VEGFprom, Glut1prom). Tuba1C = negative control region, CpG 4 = positive control region. Depicted is the mean percentage of input of 3 independent experiments. Error bars show standard deviations. MeDIP was performed in collaboration with T. Günther and A. Grundhoff (Heinrich-Pette-Institute, Hamburg).

2.2 Protein and mRNA stability of HPV E6/E7 under hypoxia

The activity of the E6/E7 transcriptional promoter was reduced under hypoxia, by approximately 50 % (Fig. 6). Since hypoxia-induced downregulation of E6/E7 mRNA and protein is more pronounced (80 % mRNA reduction in HeLa cells, see [71]), the question emerged whether reduced protein or mRNA stability may also contribute to this effect.

2.2.1 E6 and E7 protein stability is reduced under hypoxia

To determine E6 and E7 protein stability, HeLa cells were pre-incubated for 4 h under hypoxia, thereby ensuring that E6 and E7 protein levels were still detectable under hypoxia. Hypoxic and normoxic HeLa cells were then treated with the protein translation inhibitor

cycloheximide (CHX) and E6 and E7 protein expression was compared over 6 h under hypoxia and normoxia.

Calculation of E6 and E7 protein half-life in Hela cells based on quantification of immunoblots and assuming exponential protein decay resulted in the mean half-lives indicated in Tab. 1.

Tab. 1. Mean protein half-lives of E6 & E7 in HeLa cells.

	HeLa	
	Hypoxia	**Normoxia**
E7	1.94 ± 0.22 h	1.58 ± 0.19 h
E6	1.99 ± 0.17 h	1.75 ± 0.82 h

In HeLa cells, the half-lives of HPV18 E6 and E7 were slightly reduced under hypoxia as can be seen in Fig. 10 showing one representative immunoblot with the corresponding quantification. Notably, variations between the individual experiments were detected leading to high standard deviations, particularly for E6 expression under normoxia (Tab. 1). However, the tendency towards a reduced protein half-life was consistently identified in all experiments, suggesting that this effect may contribute to some extent to the downregulation of E6 and E7 protein level under hypoxia.

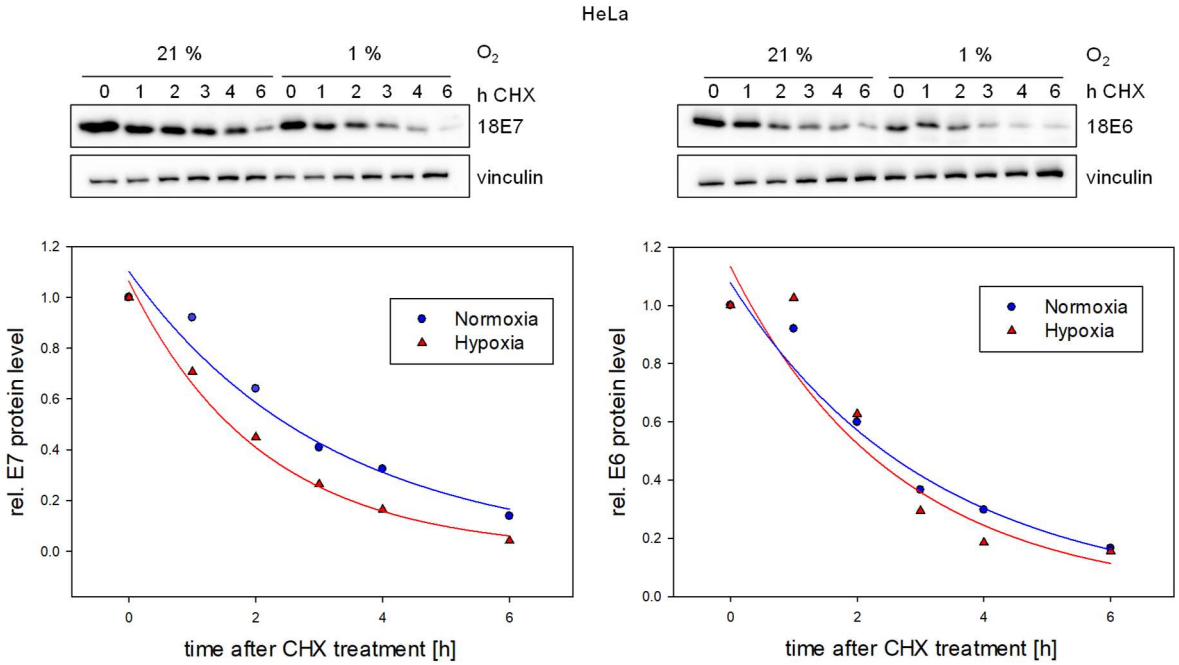

Fig. 10. E6 and E7 protein stability under hypoxia and normoxia. HeLa cells were pre-incubated for 4 h under hypoxia or normoxia, treated with 10 µg/ml cycloheximide (CHX) and harvested at the indicated time-points after treatment. Upper panels show immunoblot analyses of HPV18 E7 and E6. Vinculin = loading control. Lower panels depict quantification of the respective immunoblot relative to vinculin with an exponential decay curve determined by non-linear regression. The time point 0 h after CHX treatment was set as 1 under hypoxia and normoxia, respectively.

2.2.2 E6/E7 mRNA stability is reduced under hypoxia

The half-life of the *E6/E7*-encoding mRNAs was assessed by treating normoxic and hypoxic HeLa cells with the transcriptional inhibitor actinomycin D (ActD) and *E6/E7* mRNA levels were measured over 4 h by qRT-PCR. The applied primers recognize all three different transcript classes coding for HPV18 E6/E7. Half-life calculation using 5 independent experiments and assuming exponential mRNA decay, revealed a half-life of 3.08 h under normoxia and 2.48 h under hypoxia (Fig. 11). Notably, half-life measurements were subject to strong fluctuations (see discussion, chapter 3.1.2). Nevertheless, the trend consistently points towards a reduced *E6/E7* mRNA stability under hypoxia, which likely contributes to downregulation of E6/E7 expression under hypoxia.

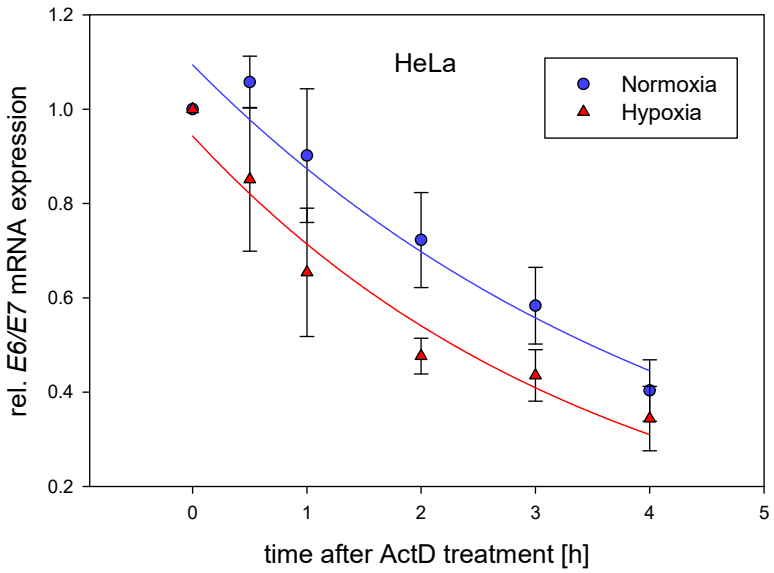

Fig. 11. *E6/E7* mRNA stability under hypoxia and normoxia. HeLa cells were pre-incubated for 4.5 h under hypoxia or normoxia, treated with 0.5 µg/ml actinomycin D (ActD) and harvested at the indicated time-points after treatment. The mean relative HPV18 *E6/E7* mRNA expression (all three transcript classes) of 5 independent experiments is depicted. The time point 0 h after ActD treatment was set as 1 under hypoxia and normoxia, respectively. Error bars indicate standard deviations. An exponential decay curve was generated by non-linear regression.

2.3 Candidate transcription factors in regulation of hypoxic E6/E7 expression

To gain insights into the underlying mechanism of E6/E7 repression under hypoxia, key transcriptional regulators mediating the cellular response towards hypoxia were investigated.

2.3.1 HIF transcription factors in regulation of E6/E7 expression under hypoxia

HIF transcription factors (HIF-1α and HIF-2α) are major orchestrators of the cellular transcriptional response to hypoxia [136]. Thus, it was investigated if hypoxia-induced stabilization of HIF-1α or HIF-2α is required to repress E6/E7 under hypoxia. To that end, HeLa cells expressing shRNAs targeting HIF-1α or HIF-2α were cultured under hypoxia. Immunoblot analyses show that induction of HIF-1α and HIF-2α mediated by hypoxia was efficiently blocked by shRNAs (Fig. 12). However, hypoxic repression of E6 and E7 was not impaired by silencing HIF-1α and HIF-2α, alone or in combination.
Hence, regulation of E6/E7 expression under hypoxia appears to occur independently of HIF.

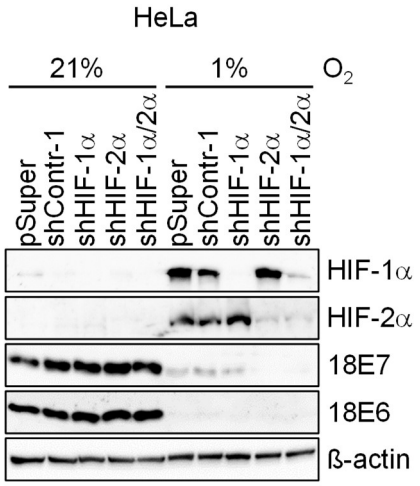

Fig. 12. HIF transcription factors in repression of E6/E7 under hypoxia. HeLa cells expressing shRNAs against HIF-1α and HIF-2α, alone or in combination, were cultured for 24 h under hypoxia or normoxia. Immunoblot shows protein expression of HIF-1α, HIF-2α, HPV18 E6 and E7. β-actin = loading control. pSuper = basic vector, shContr-1 = control shRNA. Figure is published in reference [71].

2.3.2 The Mlx transcription factor network in regulation of E6/E7 expression under hypoxia

Previously, work of our group showed that downregulation of E6/E7 under hypoxia is glucose-sensitive and can be counteracted by an excess of glucose [71]. One major orchestrator of glucose-induced gene regulation is the Mlx network of transcription factors. In short, high glucose activates transcription factor heterodimers composed of Mlx on the one hand and MondoA or ChREBP on the other hand. These dimers then localize to the nucleus and bind to carbohydrate response elements to regulate gene expression [137]. Their activity has been shown to be inhibited by hypoxia independently of HIF [138]. This raised the question whether hypoxia-induced abrogation of Mlx heterodimer activity - which is counteracted by artificially high glucose supply - may be linked to hypoxic E6/E7 regulation.

As demonstrated by immunoblots, repression of E6/E7 protein expression under hypoxia was still efficient in HeLa cells expressing Mlx targeting shRNAs (Fig. 13A). Reactivation of hypoxic E6/E7 expression induced by high glucose (25 mM) was also not affected by silencing Mlx. Knockdown of Mlx was verified by detecting Mlx mRNA expression level (Fig. 13B) and additionally by measuring mRNA expression of TXNIP (Fig. 13C), which was previously reported to be induced by high glucose via the Mlx:MondoA complex [139]. In fact, a strong upregulation of *TXNIP* mRNA expression was observed in HeLa cells cultured with high glucose concentrations. This was still detectable, but significantly impaired in Mlx-silenced cells indicating that Mlx knockdown was successful albeit there may be some residual Mlx activity. In contrast to *TXNIP*, *E6/E7* mRNA expression was not affected in Mlx-silenced cells (Fig. 13C), but followed in line with the pattern observed at protein level.

On a side note, *TXNIP* mRNA expression was generally downregulated in hypoxic cells cultured under physiological glucose conditions (5.5 mM, Fig. 13C), which is in agreement with previous reports [138]. Moreover, this effect was slightly enhanced in Mlx-silenced cells.

The two possible interaction partners of Mlx are MondoA and ChREBP. Expression of *ChREBP* mRNA in HeLa cells was approaching the detection level and could not be further reduced by expression of shRNAs. Thus, further studies were focusing on the second potential Mlx interaction partner; MondoA.

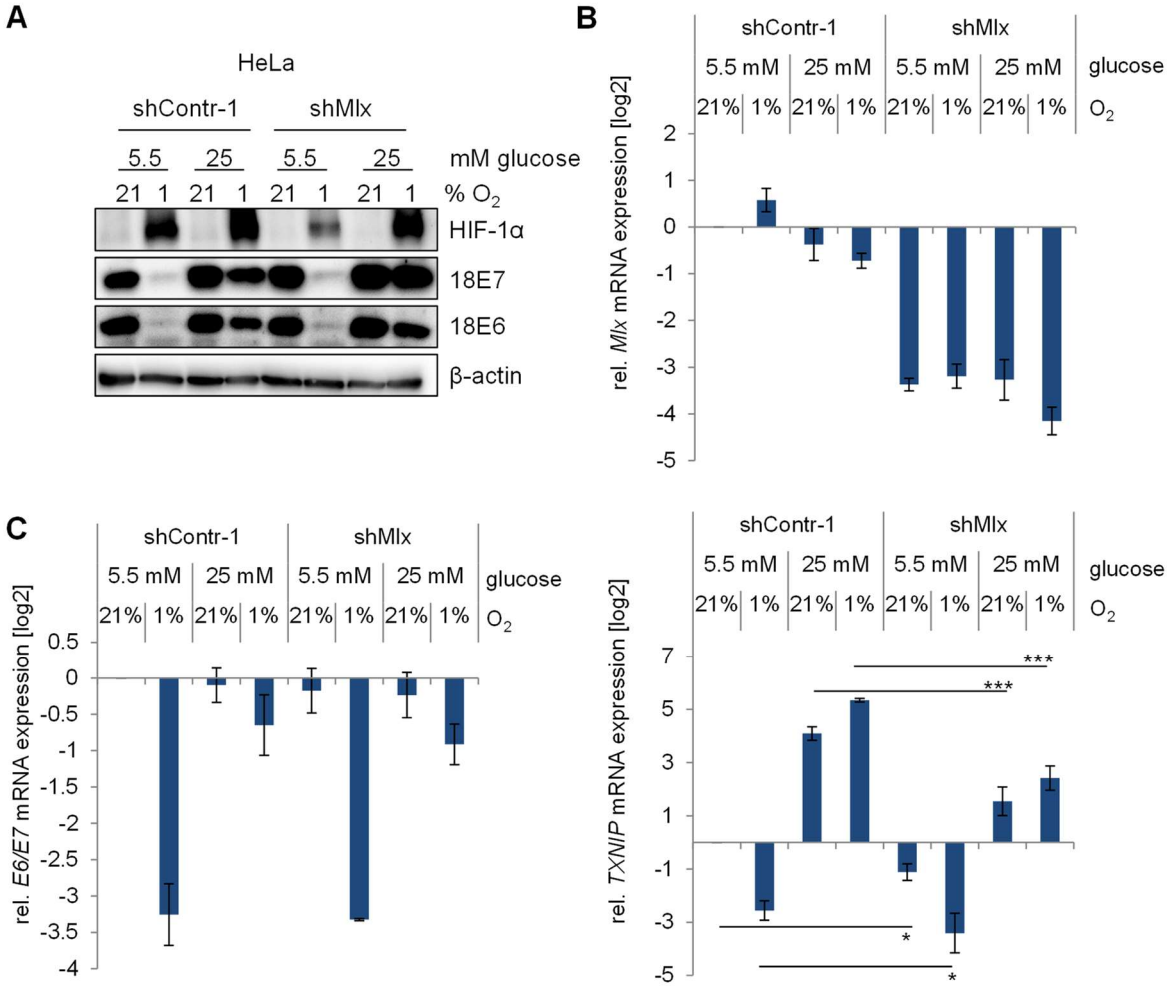

Fig. 13. The Mlx transcription factor in repression of E6/E7 under hypoxia. HeLa cells expressing shRNAs against Mlx were cultured for 24 h under hypoxia or normoxia with medium containing 5.5 or 25 mM glucose. shContr-1 = control shRNA **(A)** Immunoblots detecting protein expression of HIF-1α, HPV18 E6 and E7. β-actin = loading control. **(B)** qRT-PCR analyses of *Mlx* mRNA expression showing knockdown efficiency. **(C)** qRT-PCR analyses of *E6/E7* and *TXNIP* mRNA expression. **(B+C)** Depicted is the log2 of the mean expression relative to shContr-1 under normoxia with standard deviations of 3 individual experiments. Asterisks indicate statistically significant differences to the respective shContr-1 as determined by one-way ANOVA. (***p < 0.001, *p < 0.05).

Results obtained upon shRNA-mediated silencing of MondoA mirrored the effects following Mlx silencing. Protein and mRNA expression of E6/E7 were unaffected by MondoA knockdown under all experimental conditions including hypoxia and high glucose concentrations (Fig. 14A and C). High glucose-induced upregulation of *TXNIP* mRNA expression on the other hand, was severely impaired in cells expressing MondoA targeting shRNAs, although a MondoA-knockdown induced enhanced downregulation of *TXNIP* under hypoxia was not detected (Fig. 14C).

Taken together, the obtained data indicates that hypoxic and glucose-sensitive repression of E6/E7 expression occurs in a manner independent of Mlx heterodimers.

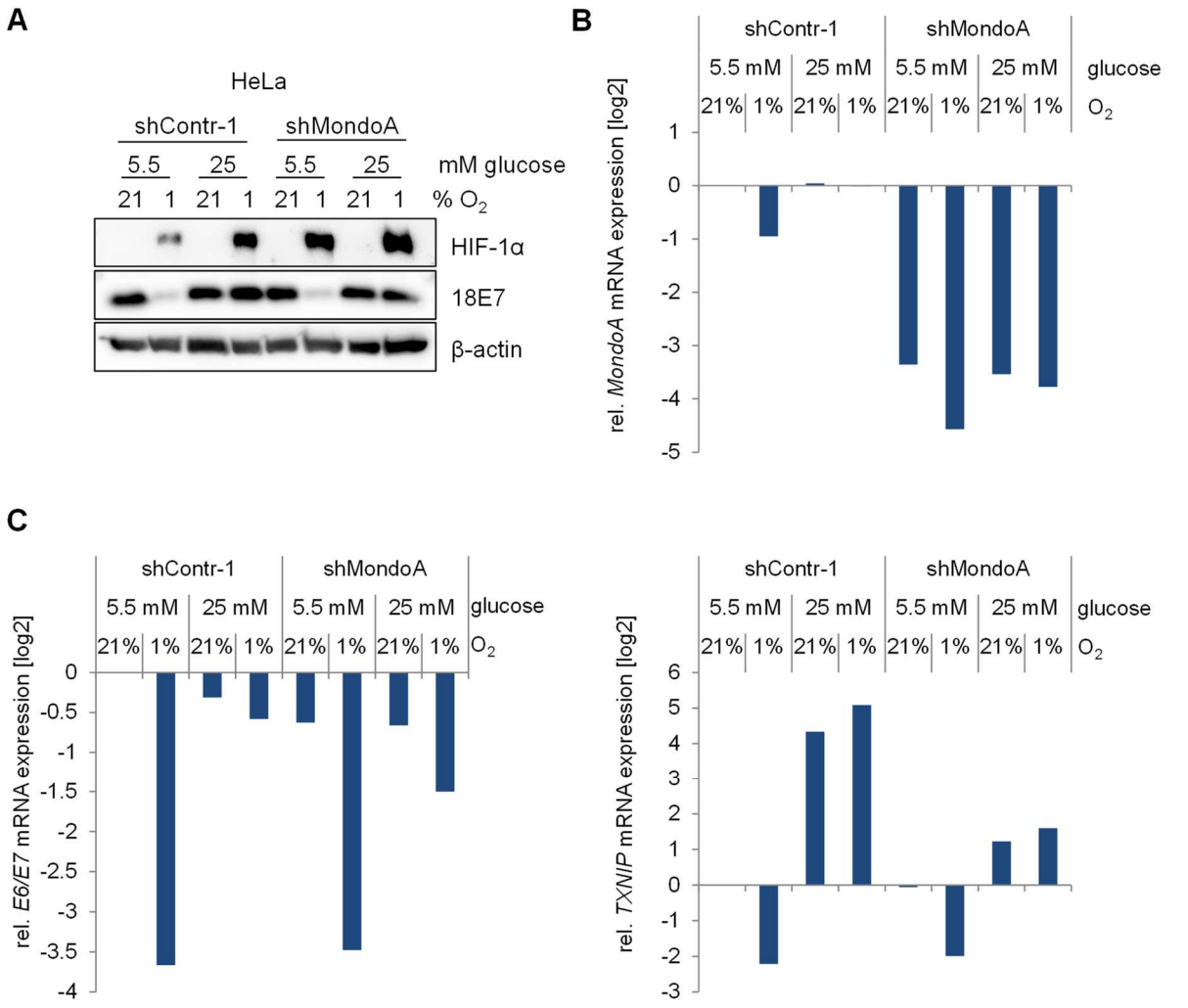

Fig. 14. The MondoA transcription factor in repression of E6/E7 under hypoxia. HeLa cells expressing shRNAs against MondoA were cultured for 24 h under hypoxia or normoxia with medium containing 5.5 or 25 mM glucose. shContr-1 = control shRNA. **(A)** Immunoblots of HIF-1α and HPV18 E7 are shown. β-actin = loading control. **(B)** Corresponding qRT-PCR analyses of *Mlx* mRNA expression showing knockdown efficiency. **(C)** Corresponding qRT-PCR analyses of *E6/E7* and *TXNIP* mRNA expression. **(B+C)** Depicted is the log2 of the expression relative to shContr-1 under normoxia. One representative experiment of two is shown.

2.3.3 c-Myc in regulation of E6/E7 expression under hypoxia

The Mlx transcription factor network closely resembles the better characterized Myc network. The c-Myc transcription factor is a proto-oncoprotein that dimerizes with its obligatory interaction partner Max to regulate gene expression and is known to be a major regulator of cellular metabolism as its activity can depend on the cellular nutrient status [140]. Since c-Myc was described to be destabilized under hypoxia and glucose-deprived conditions [141, 142], it was investigated whether c-Myc is involved in glucose-sensitive hypoxia-induced downregulation of E6/E7.

Immunoblot analyses of HeLa cells cultured under hypoxia and normoxia with different glucose concentrations revealed that c-Myc protein levels were slightly downregulated under hypoxia with physiological glucose concentrations (5.5 mM, Fig. 15). High glucose levels (25 mM) counteracted this effect and led to an upregulation of c-Myc protein levels under hypoxia. In cells expressing shRNAs targeting c-Myc, c-Myc protein could no longer be detected by immunoblot. However, E7 protein expression remained unaltered in c-Myc-silenced cells and showed the previously described pattern of oxygen- and glucose-dependent downregulation. In summary, hypoxia-induced downregulation of c-Myc expression that can be counteracted by high glucose does likely not affect the regulation of E7 under hypoxia.

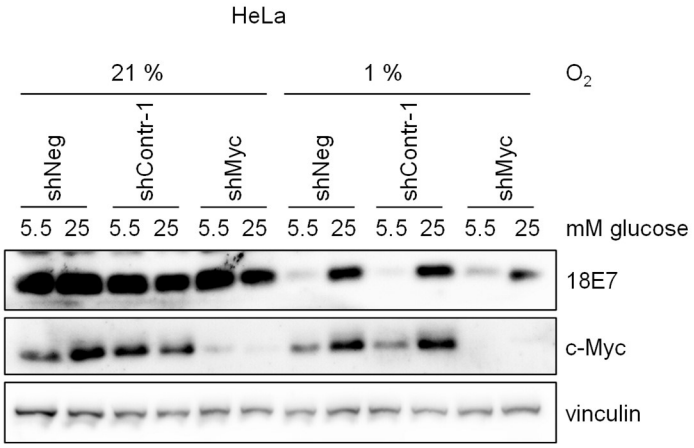

Fig. 15. The c-Myc transcription factor in repression of E6/E7 under hypoxia. HeLa cells expressing an shRNA targeting c-Myc were cultured under hypoxia or normoxia for 24 h in medium containing 5.5 or 25 mM glucose. shNeg, shContr-1 = control shRNAs. Immunoblot shows protein expression of HPV18 E7 and c-Myc. Vinculin = loading control.

2.4 A functional role for the PI3K/AKT pathway in repression of E6/E7 under hypoxia

2.4.1 Inverse correlation between activation of AKT and repression of E6/E7 under hypoxia

An important coordinator of cellular signaling that is closely associated with glucose metabolism [95] and reported to be activated by hypoxia [92, 93] is the AKT pathway. Therefore, the AKT kinase emerged as a putative candidate for hypoxic regulation of E6/E7. Indeed, the following experiments revealed an inverse correlation between the activation of AKT and the repression of E6/E7 under hypoxia.

Time-course experiments of HeLa and SiHa cells showed that phosphorylation of AKT was induced by hypoxia at both residues required for full kinase activation [98]. The applied Phospho-AKT (P-AKT) specific antibodies detect all three isoforms of AKT phosphorylated at T308 (AKT1), T309 (AKT2), T305 (AKT3) or at S473 (AKT1), S474 (AKT2), S472 (AKT3) (see also chapter 1.4.3). For simplification, only the residues for AKT1 will be named in the following text and figures. The antibody against P-AKT T308 occasionally recognized a band of slightly lower molecular weight. By using P-AKT inhibitors and by performing knockdown experiments it was shown that only the upper 60 kDa band was specific for P-AKT.

Increased phosphorylation of AKT at T308 was detectable in HeLa cells after 1 h of hypoxia, increased phosphorylation at S473 already after 10 min (Fig. 16A). In Siha cells, induction of AKT phosphorylation at both residues was detected after 30 min of hypoxia. Downregulation of E6 and E7 protein expression started after 3 h of hypoxia in HeLa cells and after 6-9 h in SiHa cells, therefore hypoxia-mediated AKT induction preceded the repression of E6/E7.

Hypoxic cells that regain access to oxygen start to upregulate E6/E7 expression again after several hours ([71], Fig. 16B). Hypoxia-induced upregulation of P-AKT was abolished already 10 min after reoxygenation as was shown by immunoblot of SiHa cells (Fig. 16B). Hence, like repression of E6/E7, activation of AKT by hypoxia was reversible and, furthermore, occurred chronologically before reactivation of E6/E7 expression.

Notably, hypoxia-induced phosphorylation of AKT was only observed in cells cultured in medium containing physiological glucose concentrations (5.5 mM) but was abolished when cells were cultured under high glucose conditions (25 mM, Fig. 16C). This inversely correlated with E6 and E7 expression, which was reactivated under hypoxia by high glucose supply. Despite an increase in P-AKT, the expression levels of total AKT protein after 24 h hypoxia under physiological glucose conditions were slightly reduced when compared to normoxia (Fig. 16C). Since no decline in total AKT protein was detected in the hypoxia time kinetic (Fig. 16A), this may be attributed to an increase of AKT over time under normoxia.

Taken together, hypoxia-mediated activation of AKT was closely connected to repression of E6/E7, thereby pointing at AKT as a promising candidate for regulating the repression of E6/E7 under hypoxia.

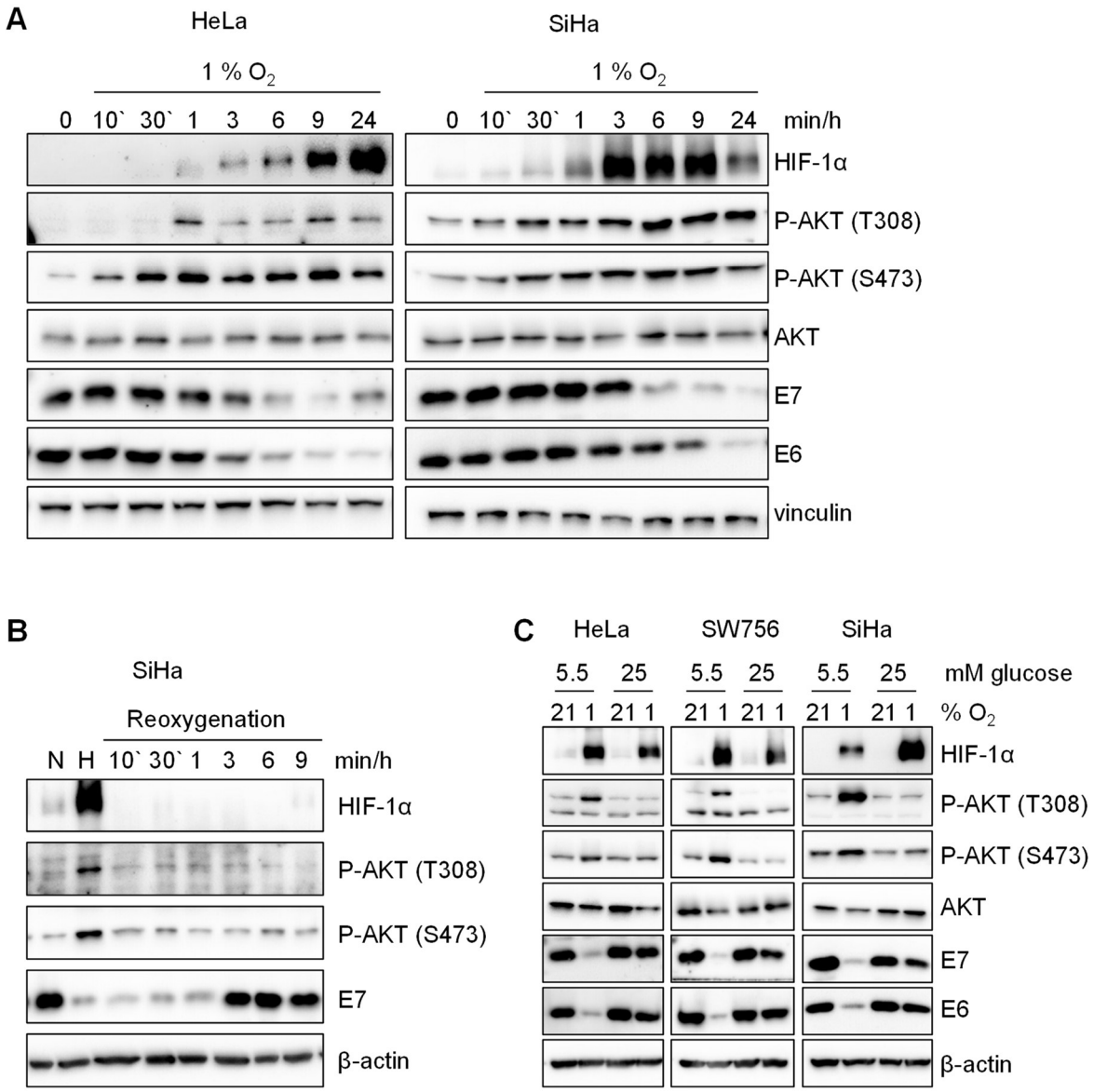

Fig. 16. AKT phosphorylation is induced under hypoxia in a glucose-dependent manner. (A) Time course of HeLa and SiHa cells subjected to hypoxia. Immunoblot shows protein levels of HIF-1α, AKT phosphorylated at T308 and S473 (P-AKT T308, P-AKT S473), pan-AKT (AKT), HPV16/18 E6 and E7. Vinculin = loading control. **(B)** Immunoblot of SiHa cells cultured for 24 h under normoxia (N, 21 % O_2) or hypoxia (H, 1 % O_2) and subsequent reoxygenation of hypoxic cells for the indicated time periods. Protein expression of P-AKT T308 and S473 and HPV16 E7 was measured. β-actin = loading control. **(C)** HeLa, SW756 and SiHa cells were cultured for 24 h under hypoxia or normoxia with medium containing 5.5 or 25 mM glucose. Protein expression was analyzed by immunoblot of HIF-1α, P-AKT T308 and S473, pan-AKT, HPV16/18 E6 and E7. β-actin = loading control.

2.4.2 Inhibitors of the PI3K/AKT pathway counteract repression of E6/E7 under hypoxia

The activation status of AKT under hypoxia correlates with repression of E6/E7 providing circumstantial evidence for a crosstalk between AKT signaling and the hypoxic repression of E6/E7 expression. Consequently, further experiments aimed to elucidate the possible role of

the PI3K/AKT pathway in regulation of E6/E7 under hypoxic conditions by functional analyses.

To investigate if hypoxia-induced activation of AKT is required for repression of E6/E7 under hypoxia, HeLa, SW756, SiHa and MRI-H-186 cells were treated with the allosteric AKT inhibitor AKTi VIII [143] or the PI3K inhibitor LY294002 [144] and cultured under hypoxia. Immunoblot analyses showed that phosphorylation of AKT at T308 and S473 was efficiently blocked by both inhibitors under normoxia and hypoxia (Fig. 17A). Intriguingly, treatment with the PI3K/AKT pathway inhibitors counteracted repression of E7 under hypoxia as was shown by immunoblot. E6 expression was also effectively reactivated in HeLa and SW756 cells but results were less coherent for E6 in the HPV16-positive SiHa and MRI-H-186 cells where E6 repression was not or only weakly counteracted by PI3K/AKT inhibitor treatment under hypoxia. Notably, protein expression of E6 and E7 was not significantly affected by inhibitor treatment in normoxic cells, albeit some minor increases in protein level were detected in SW756 and MRI-H-186 cells.

Based on the fact that PI3K and AKT inhibitors are intensely investigated as anti-cancer drugs [121], two agents currently tested in the clinic were included in further studies, namely the AKT inhibitor MK-2206 [145] and the PI3K inhibitor PX-866 [146]. Treatment with MK-2206 and PX-866 also counteracted repression of E6/E7 protein expression under hypoxia in a dose-dependent manner (Fig. 17B).

qRT-PCR analyses in HeLa cells revealed that this regulation was already detectable at the transcript level since all tested inhibitors significantly counteracted hypoxic repression of *E6/E7* mRNA expression under hypoxia, although *E6/E7* mRNA levels did not completely return to basal expression levels (Fig. 17C). *E6/E7* mRNA expression after inhibitor treatment under normoxia showed a small tendency towards an increased expression but no major induction was detected.

These results strongly argue that hypoxia-induced activation of PI3K/AKT signaling is necessary for inhibition of E6/E7 expression under hypoxia.

LY294002, although widely applied to study PI3K signaling, can also inhibit the autokinase activity of mTOR [147] and has various other molecular targets [148, 149]. PX-866 is more specific but still shows relevant activity towards other kinases such as mTOR [150]. Hence, to further corroborate the results above, the highly selective class I PI3K inhibitor GDC-0941 was also analyzed and showed similar effects on E6 and E7 expression under hypoxia to those observed with the other inhibitors (Fig. 17D). Collectively, these findings indicate that activation of AKT under hypoxia, mediated via PI3K, is required for the hypoxic repression of E6/E7.

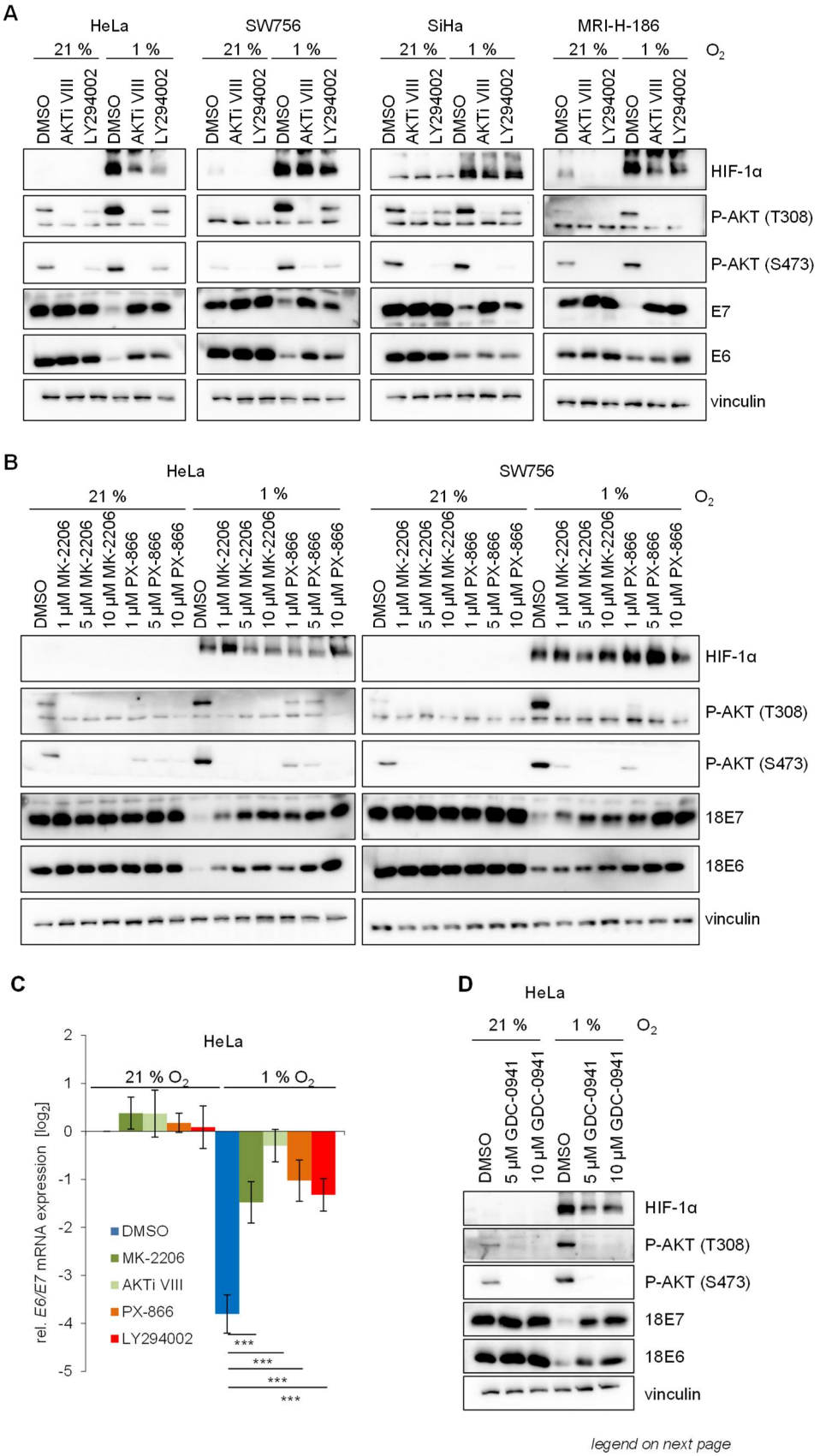

legend on next page

Fig. 17 (*see previous page*). Inhibitors of PI3K and AKT counteract repression of E6/E7 under hypoxia. (A) HeLa, SW756, SiHa and MRI-H-186 cells were treated with 10 µM AKTi VIII, 20 µM LY294002 or DMSO (solvent control) and cultured for 24 h under hypoxia or normoxia. Immunoblot analyses show protein expression of HIF-1α, P-AKT T308 and S473, HPV18/16 E6 and E7. Vinculin = loading control. **(B)** HeLa and SW756 cells were treated with the indicated concentrations of MK-2206 and PX-866 and cultured for 24 h under hypoxia or normoxia. Immunoblot of HIF-1α, P-AKT T308 and S473, HPV18 E6 and E7 is shown. Vinculin = loading control. **(C)** qRT-PCR analyses of HeLa cells treated with 3 µM MK-2206, 10 µM AKTi VIII, 3 µM PX-866 or 20 µM LY294002 and cultured for 24 h under hypoxia or normoxia. Depicted is the log2 of the mean mRNA expression of *E6/E7* relative to the DMSO-treated normoxic control. Standard deviations are indicated (n = 3). Asterisks indicate statistically significant differences to DMSO treated cells under hypoxia as determined by one-way ANOVA (***p < 0.001). **(D)** HeLa cells treated for 24 h with GDC-0941 and cultured under hypoxia or normoxia. Immunoblot of HIF-1α, P-AKT T308 and S473, HPV18 E6 and E7 is shown. Vinculin = loading control.

The PI3K/AKT pathway is closely connected to mTOR signaling in that mTORC2 phosphorylates AKT at S473 and therefore contributes to activating AKT [151]. To gain a deeper understanding of the AKT regulatory pathway under hypoxia, different mTOR inhibitors were applied. The inhibitor KU-0063794 inhibits mTORC1 and mTORC2 [152], whereas rapamycin almost selectively targets mTORC1, at least during short-term treatment [153]. Treatment of HeLa cells with rapamycin only weakly counteracted E7 protein repression under hypoxia. However, treatment with KU-0063794 led to a clear reactivation of E6 and E7 protein expression under hypoxia (Fig. 18A). This goes in line with effects observed for AKT phosphorylation. More precisely, KU-0063794 prevented phosphorylation of AKT at S473 under normoxia and hypoxia as was expected due to inhibition of mTORC2. Hypoxia-induced phosphorylation of AKT at T308 was only abolished when high concentrations (5 µM) of KU-0063794 were applied. As expected, treatment with rapamycin, which only targets mTORC1, had no inhibitory effect on hypoxia-induced AKT phosphorylation. Hence, reactivation of E6/E7 expression under hypoxia strongly correlated with a blockade of AKT S473 phosphorylation via mTORC2. Notably, rapamycin induced phosphorylation of AKT at S473 and T308 under normoxia, indicating a feedback mechanism on mTORC2 triggered by inhibition of mTORC1.

In parallel to immunoblot analyses, *E6/E7* mRNA expression was measured by qRT-PCR. KU-0063794 treatment induced *E6/E7* mRNA expression under normoxia and hypoxia (Fig. 18B). Treatment with rapamycin also induced *E6/E7* mRNA expression under normoxia, although to a lesser extent than observed for KU-0063794. Under hypoxia, rapamycin weakly counteracted repression of *E6/E7*, albeit much less efficient than KU-0063794.

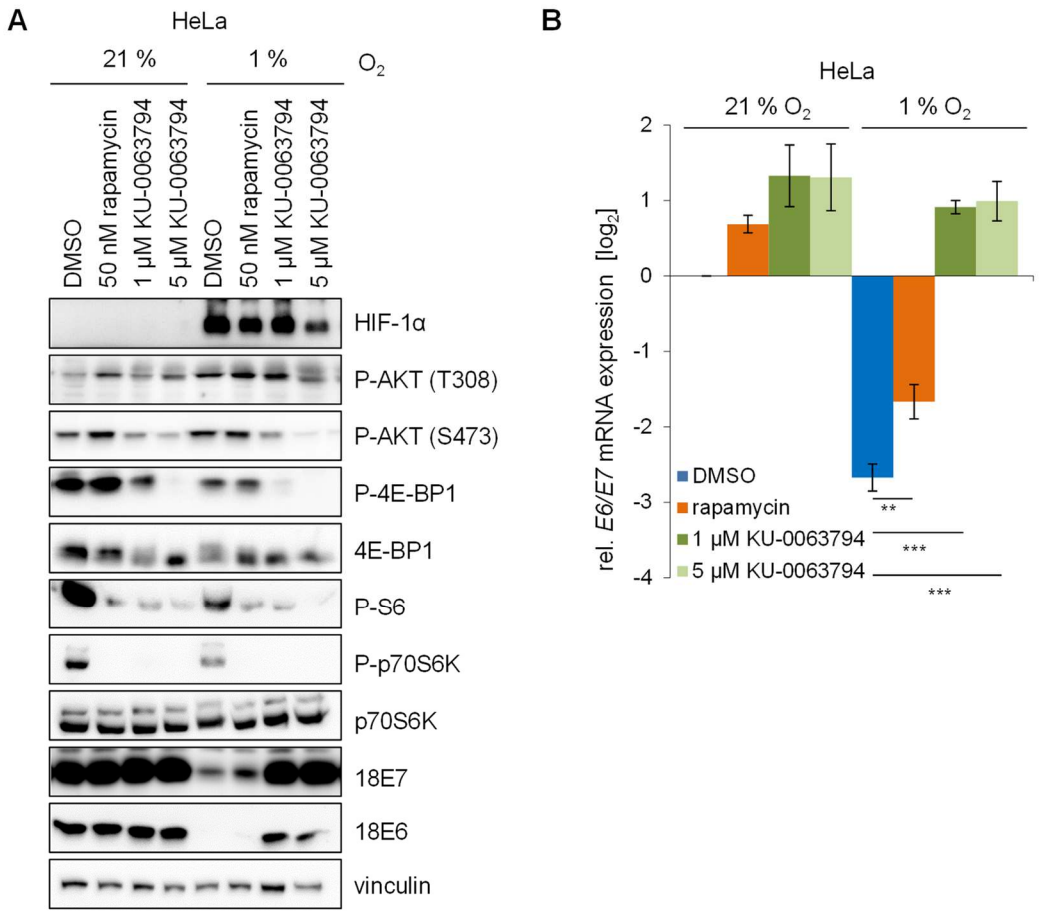

Fig. 18. mTOR inhibitors counteract repression of E6/E7 under hypoxia. (A) HeLa cells were treated with the indicated concentrations of rapamycin and KU-0063794 or DMSO as solvent control and cultured for 24 h under hypoxia or normoxia. Immunoblot analyses of HIF-1α, P-AKT T308 and S473, phosphorylated 4E-BP1 (P-4E-BP1, S65), 4-E-BP1, phosphorylated S6 (P-S6, S235/236), phosphorylated p70S6K (P-p70S6K, T389), p70S6K, HPV18 E6 and E7 are shown. Vinculin = loading control. **(B)** *E6/E7* mRNA expression of HeLa cells treated as in (A) was determined by qRT-PCR. The log2 of the mean expression relative to DMSO treated normoxic control cells is shown. Standard deviations are indicated (n = 3). Asterisks indicate statistically significant differences to DMSO treated cells under hypoxia as determined by one-way ANOVA (***p < 0.001, **p < 0.01).

To ensure functionality of the mTOR inhibitors, the phosphorylation status of the mTOR targets 4E-BP1, S6 and p70S6K was monitored by immunoblot. A general downregulation of mTOR target phosphorylation under hypoxia was observed as was reported previously [71]. Upon inhibitor treatment they showed the expected effects with a strong downregulation of Phospho-S6 and Phospho-p70S6K by both inhibitors (Fig. 18A). Pospho-4E-BP1 was only reduced by treatment with KU-0063794 and was insensitive to rapamycin under the applied experimental conditions, as expected [154].

In conclusion, experiments with small molecule inhibitors revealed that hypoxia-induced activation of AKT, mediated via the upstream regulators PI3K and mTORC2, is responsible for the HPV E6/E7 repression under hypoxia.

2.5 Repression of E6/E7 under hypoxia in the context of AKT, calcium and energy metabolism

The observed glucose responsiveness of hypoxic activation of AKT and repression of E6/E7 suggest a close connection to the cellular metabolism and energy status. Under hypoxia, cells are forced to carry out major alterations in their energy metabolism to survive since they can no longer rely on mitochondrial oxidative phosphorylation (OXPHOS) as their main source of ATP production [73]. Furthermore, oxygen deprivation causes an increase in intracellular Ca^{2+} concentrations. Noteworthy, Ca^{2+} signaling is important for the regulation of mitochondrial energy metabolism [75, 155]. Thus, a potential connection between Ca^{2+} signaling, OXPHOS and E6/E7 repression was investigated, also focusing on AKT which has previously been associated with both Ca^{2+} signaling [102] and metabolic reprogramming under hypoxia [156].

2.5.1 Calmodulins (CaMs) in regulation of E6/E7 expression under hypoxia

The ubiquitously expressed Ca^{2+}-binding protein calmodulin (CaM) has been shown to co-localize with AKT at the plasma membrane and it has been proposed that CaM facilitates translocation of AKT to the plasma membrane for activation [102]. Since CaM is dependent on Ca^{2+}, it was investigated whether CaM is responsible for increased activation of AKT under hypoxia and for a subsequent repression of E6/E7.

However, HeLa and SiHa cells treated with the CaM antagonist W-7 [157] showed no alterations in AKT phosphorylation under hypoxia and normoxia as demonstrated by immunoblotting (Fig. 19A). Only SiHa cells treated with a high concentration of W-7 that was already lethal for HeLa cells reduced AKT phosphorylation under hypoxia and E7 expression levels under normoxia. This may, however, be attributed to high toxicity accompanied by extensive side effects.

HeLa cells expressing shRNAs targeting the three CaM isoforms CaM1, CaM2 and CaM3 were also not showing any significant alterations in phosphorylation of AKT at T308 (Fig. 19B). E7 protein and mRNA expression under normoxia and hypoxia was also not affected. Knockdown of CaM was assessed by measuring mRNA expression of the three isoforms (Fig. 19C).

Taken together, there were no indications for a connection between the Ca^{2+}-sensing CaM on the one hand and repression of E6/E7 or activation of AKT under hypoxia on the other hand.

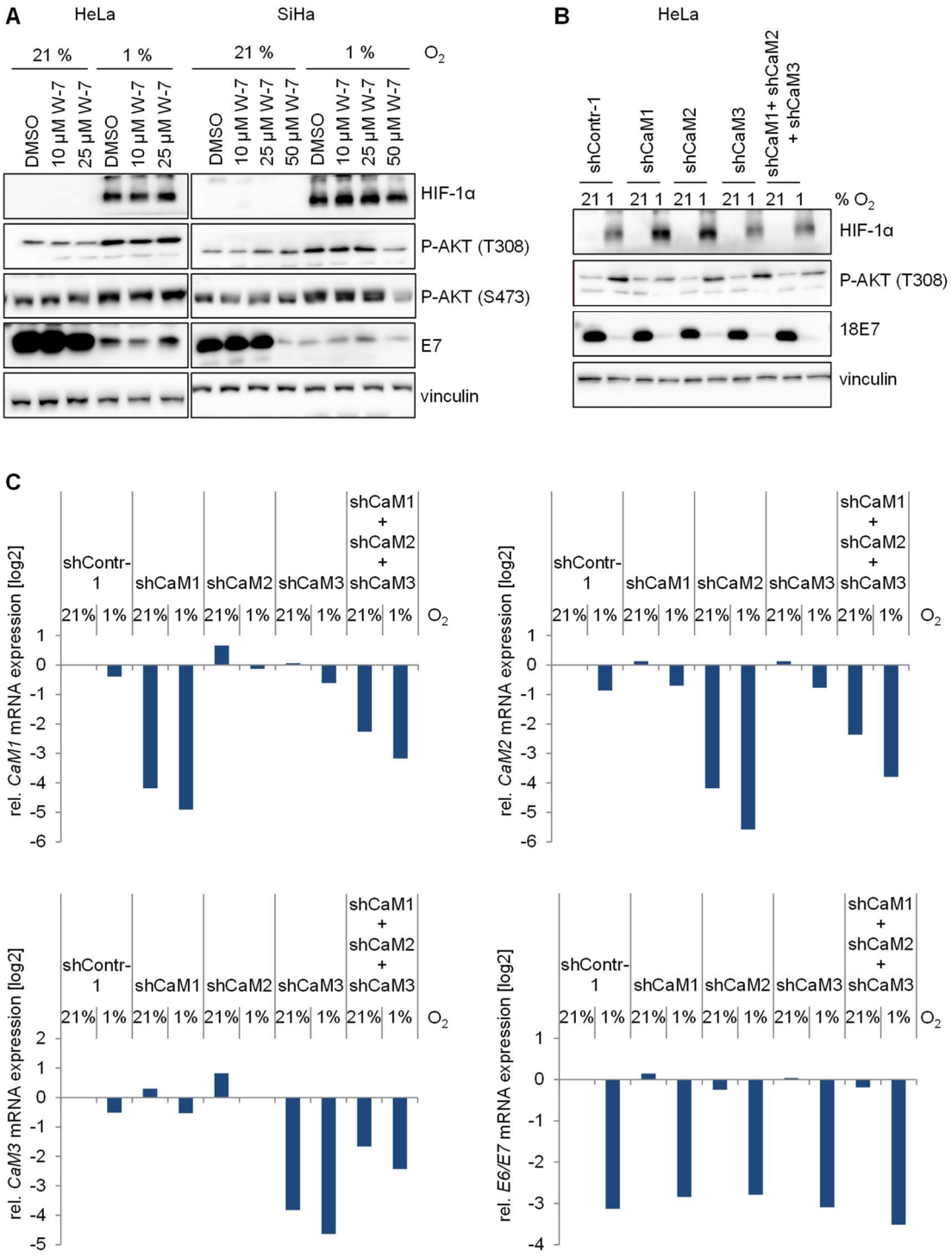

Fig. 19. Role of CaMs in hypoxic regulation of E6/E7. (A) Immunoblot analyses of hypoxic and normoxic HeLa and SiHa cells treated for 24 h with the indicated concentrations of W-7. DMSO = solvent control. Protein expression of HIF-1α, P-AKT T308 and S473 and HPV16/18 E7 is shown. Vinculin = loading control. **(B)** HeLa cells expressing shRNAs against CaM1, CaM2 and CaM3, alone or in combination, were cultured for 24 h under hypoxia or normoxia. shContr-1 = control shRNA. Immunoblot of HIF-1α, P-AKT T308 and HPV18 E7. Vinculin = loading control. **(C)** qRT-PCR analyses of CaM1, CaM2, CaM3 and HPV18 E6/E7 mRNA expression accompanying to experiment in B. Depicted is the log2 of the mRNA expression relative to shContr-1 under normoxia. One representative experiment out of two is shown.

2.5.2 Calcium chelation can block repression of E6/E7 under hypoxia

To gain general insight in whether Ca^{2+} signaling is required for repression of E6/E7 under hypoxia, cells were treated with the Ca^{2+} chelator BAPTA-AM [158].

In fact, concomitant treatment with BAPTA-AM during hypoxia counteracted downregulation of E6/E7 as was shown by immunoblots of HeLa and SiHa cells (Fig. 20). Notably, HeLa cells were more sensitive to BAPTA-AM treatment showing effects already at lower concentrations. Hypoxia-induced phosphorylation of AKT was not prevented by treatment with BAPTA-AM in HeLa cells, but phosphorylation of S473 was even induced under normoxia. Contrarily, in SiHa cells, high concentrations of BAPTA-AM were able to repress AKT phosphorylation at both residues under hypoxia and, in case of S473 phosphorylation, also under normoxia. Furthermore, treatment with the ionophore A23187 [159], which increases membrane permeability for Ca^{2+}, reduced basal E6 expression and inhibited AKT S473 phosphorylation in SiHa cells. In HeLa cells, A23187 reduced E6 and E7 level and AKT S473 and T308 phosphorylation under normoxia (Fig. 20).

Hence, results support the notion that Ca^{2+} plays a crucial role in regulation of E6/E7 expression. However, a general correlation between Ca^{2+}-dependent E6/E7 regulation and AKT activation status was not detected.

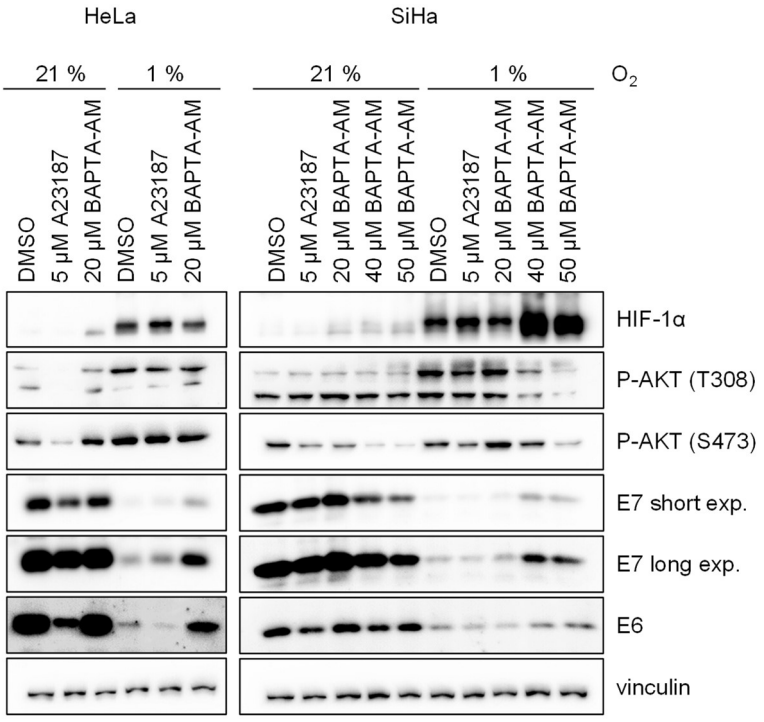

Fig. 20. Ca^{2+} chelation counteracts repression of E6/E7 under hypoxia. HeLa and SiHa cells were treated with the indicated concentrations of A23187 and BAPTA-AM and cultured for 24 h under hypoxia or normoxia. DMSO = solvent control. Immunoblot shows protein expression of HIF-1α, P-AKT T308 and S473 and HPV16/18 E6 and E7. Vinculin = loading control. Short exp. = short exposure, long exp. = long exposure.

2.5.3 Inhibitors of oxidative phosphorylation repress expression of E6/E7

To investigate whether hypoxic downregulation of E6/E7 can be linked to alterations in mitochondrial activity, cells were treated with OXPHOS inhibitors, namely rotenone, an inhibitor of complex I of the mitochondrial electron transport chain or antimycin A, an inhibitor of complex III [160].

Indeed, after treatment with rotenone or antimycin A, repression of E6 and E7 protein expression was observed in HeLa and SiHa cells that was counteracted when cells were cultured with high concentrations of glucose (Fig. 21A). The phosphorylation status of AKT was also affected, however, this was cell line- and inhibitor-dependent. In SiHa cells, both inhibitors blocked AKT phosphorylation in a glucose-dependent manner. In HeLa cells, treatment with rotenone induced P-AKT, which was counteracted by high glucose. Antimycin A rather reduced P-AKT S473, which was reinduced again by high glucose. On a side note, phosphorylation of AKT at T308 was not detectable in untreated or Antimycin A-treated HeLa cells.

To assess if repression of E6/E7 expression induced by OXPHOS inhibitors is, like hypoxic repression of E6/E7, dependent on Ca^{2+}, HeLa cells were treated additionally with BAPTA-AM. Interestingly, treatment with BAPTA-AM efficiently counteracted repression of E6/E7 otherwise caused by rotenone or antimycin A (Fig. 21B).

Previous work of our group showed that the anti-diabetes drug metformin, which is also known to, amongst other mechanisms of action, inhibit mitochondrial complex I [161] represses E6/E7 expression (A. Däschle, unpublished data). In this context, it was observed here that metformin-mediated repression of E6/E7 is not only glucose- but also Ca^{2+}-dependent (Fig. 21C).

In conclusion, these results indicate that E6/E7 repression induced by both, hypoxia and inhibitors of the mitochondrial electron transport chain, is orchestrated by a glucose-linked and Ca^{2+}-dependent mechanism. However, a clear correlation between activation of AKT and repression of E6/E7 was not observed in this context.

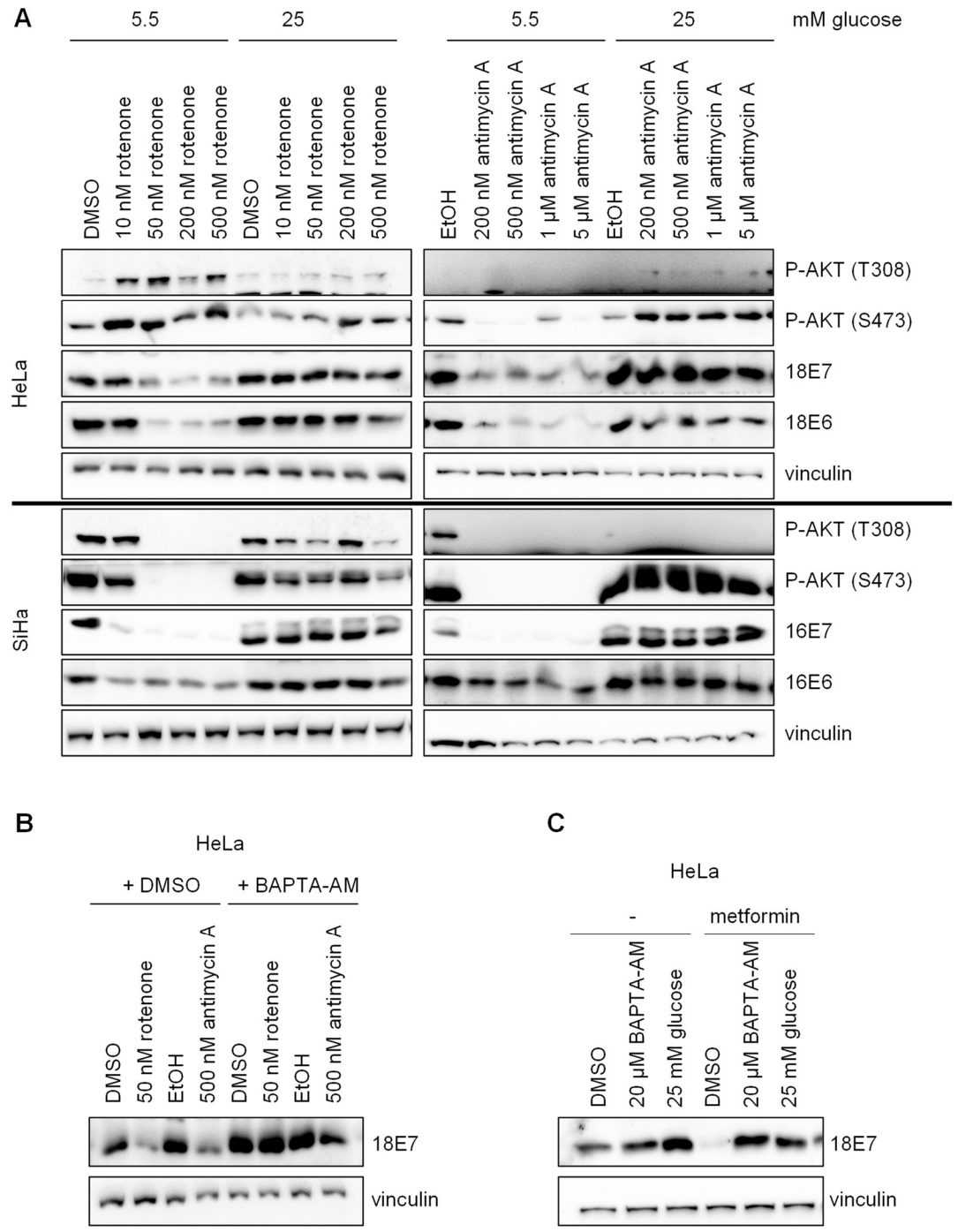

Fig. 21. OXPHOS inhibitors downregulate E6/E7 expression in a glucose- and Ca^{2+}-dependent manner. (A) HeLa and SiHa cells were treated with the indicated concentrations of rotenone and antimycin A and cultured for 24 h in medium containing 5.5 or 25 mM glucose. Immunoblot analyses of P-AKT T308 and S473, HPV16/18 E6 and E7. Vinculin = loading control. DMSO and ethanol (EtOH) are the respective solvent controls. **(B)** HeLa cells were treated with 25 µM BAPTA-AM, 50 nM rotenone and 500 nM antimycin A in the indicated combinations and cultured for 24 h before immunoblot analyses of HPV18 E7. Vinculin = loading control. **(C)** HeLa cells treated with 2.5 mM metformin were kept in medium containing physiological glucose concentrations (5.5 mM) and treated with BAPTA-AM or DMSO (solvent control) or were kept in medium containing 25 mM glucose for 24 h. Immunoblot shows expression of HPV18 E7. Vinculin = loading control.

2.6 AKT1 and AKT2 mediate repression of E6/E7 under hypoxia

In the studies described above, a key role of the PI3K/AKT pathway in repression of E6/E7 under hypoxia was demonstrated by using various small molecule inhibitors targeting this pathway. Next, it was aimed at identifying which AKT isoforms are involved in this process. AKT1 is ubiquitously expressed and AKT2 expression is also found in most tissues with particular high levels in insulin-sensitive tissues [95]. Expression of AKT3, however, is described to be more restricted and for instance important in neuronal tissues or frequently found to be activated in melanoma cells [115, 162]. The AKT-specific inhibitors applied in the present study (AKTi VIII, MK-2206) can target all three AKT isoforms (AKT1, AKT2, AKT3), with the highest affinity towards AKT1 and the lowest towards AKT3.

2.6.1 AKT3 expression in cervical cancer cells

To investigate whether AKT3 is present in cervical cancer cell lines, immunoblot analyses using a polyclonal AKT3-specific antibody (Cell Signaling Technologies, CST) were performed. This antibody detected a 60 kDa band that was strongly upregulated in hypoxic HeLa, SW756 and SiHa cells (Fig. 22A). Based on this finding, a putative role of AKT3 in repression of E6/E7 was assessed by silencing AKT3 via the CRISPR/Cas9 technique in HeLa cells. However, no reduction of the hypoxia-induced AKT3 band detected by the CST antibody was observed upon application of four different AKT3 targeting guideRNAs (gRNAs, Fig. 22B) raising the question of antibody specificity. In contrast to the CST antibody, a monoclonal AKT3-specific antibody (Upstate) directed against an N-terminal epitope of AKT3 revealed no detectable signal for AKT3 in HeLa cells under all investigated conditions. Since melanoma cells frequently express increased levels of AKT3, AKT3 knockdown was performed in the melanoma cell line MeWo with AKT3 targeting gRNAs. The band detected with the monoclonal Upstate antibody was significantly decreased, whereas the signals derived from the polyclonal CST antibody remained unaffected (Fig. 22C). This indicates that hypoxia-induced immunoblot signals observed with the CST antibody in cervical cancer cell lines were most likely not AKT3-specific whereas the Upstate antibody detected AKT3. Furthermore, and in stark contrast to melanoma cells, AKT3 is undetectable in HeLa cervical carcinoma cells. Thus, further studies were focusing on the two ubiquitously expressed isoforms AKT1 and AKT2.

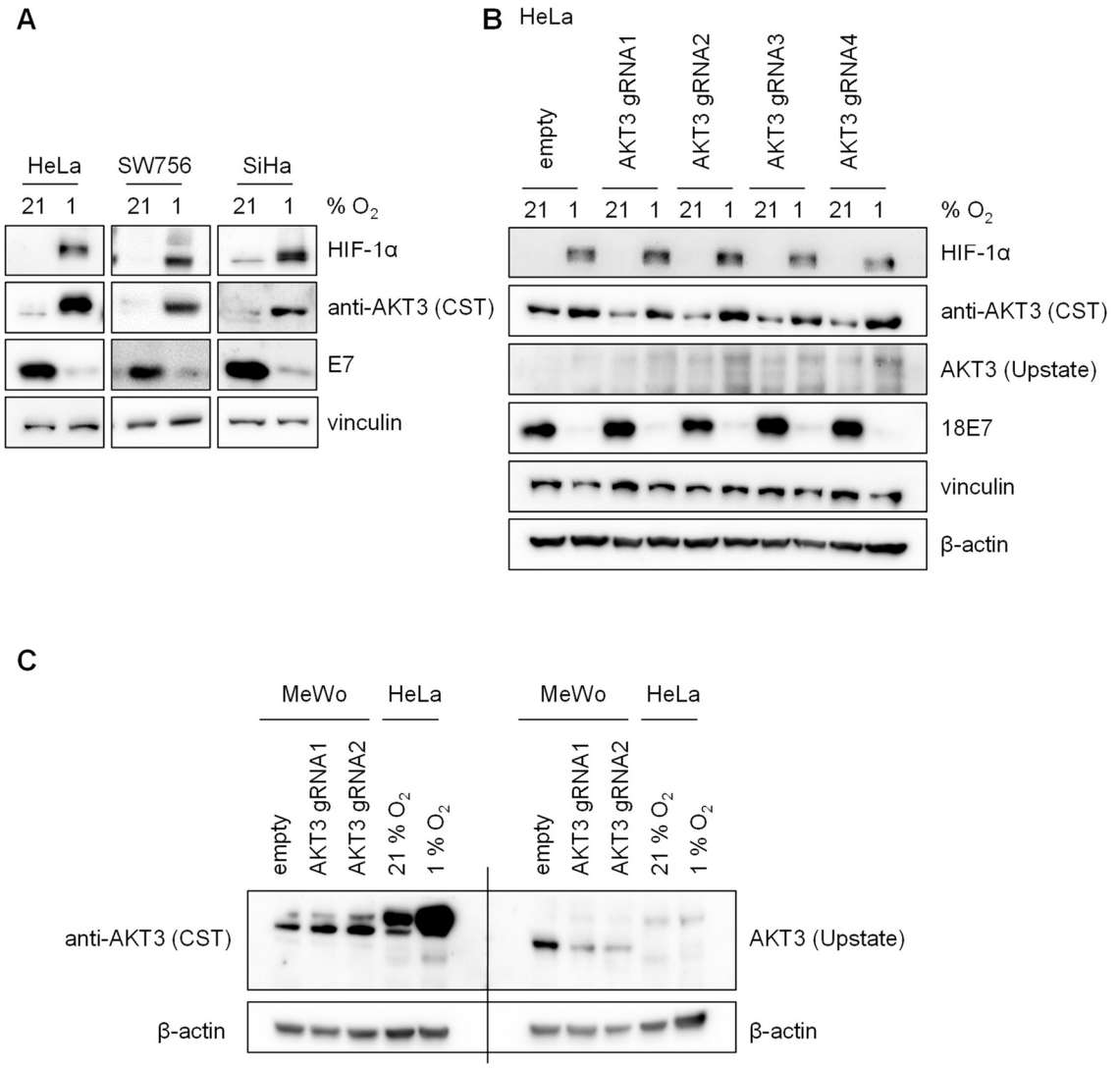

Fig. 22. AKT3 expression in cervical cancer cell lines. (A) Analyses of AKT3 protein expression in HeLa, SW756 and SiHa cells cultured for 24 h under hypoxia or normoxia. Immunoblot analyses of HIF-1α, an unspecified band detected by an anti-AKT3 antibody (anti-AKT3 (CST)) and HPV16/18 E7. Vinculin = loading control. **(B)** HeLa cells were transfected with AKT3 targeting gRNAs (AKT3 gRNA1-4) and cultured for 24 h under hypoxia or normoxia. Empty = empty basic vector. Immunoblot analyses of HIF-1α, anti-AKT3 (CST), AKT3 Upstate antibody) and HPV18 E7. Vinculin, β-actin = loading control. **(C)** Immunoblot analyses compares AKT3 expression in MeWo cells that were silenced for AKT3 expression with the CRISPR/Cas9 method using two gRNAs (AKT3 gRNA1 and 2), and HeLa cells, incubated for 24 h under hypoxia or normoxia. Empty = empty basic vector. Protein expression of AKT3 (Upstate antibody) and unspecified protein detected by anti-AKT3 (CST antibody) is shown. β-actin = loading control.

2.6.2 Effect of AKT1 and AKT2 modulation on E6/E7 expression under hypoxia

As illustrated above, AKT inhibitors reactivate expression of E6/E7 under hypoxia. In a next step, the question was addressed whether this effect could be counteracted by enhancing the activities of AKT1 and AKT2.

To that end, constitutively-active myristoylated forms of AKT1 and AKT2 were overexpressed in HeLa cells. Due to myristoylation, AKT is recruited to the plasma membrane and becomes constitutively activated [163]. Transfected Hela cells were treated with different concentrations of AKTi VIII and cultured under hypoxia or normoxia before protein expression was assessed by immunoblot analyses. Successful overexpression of constitutively-active AKT was confirmed by detecting P-AKT T308 (Fig. 23). Since ectopically expressed AKT has a lower molecular weight due to deletion of its PH-domain, which is normally required for regulation of PI3K-dependent membrane recruitment and activation [101], it can be distinguished from the much weaker expressed endogenous form. Functionality of constitutively-active AKT1 and AKT2 was confirmed by detecting an induction of phosphorylation of the well-defined AKT substrate glycogen synthase kinase 3-α/β (GSK3-α/β) [110]. Overexpression of either AKT isoform did not affect E6/E7 expression under normoxia. However, the reactivation of E6/E7 protein expression under hypoxia that was observed when cells were treated with AKTi VIII was counteracted by the concomitant overexpression of constitutively-active AKT1 or AKT2, alone or in combination. Concomitant overexpression of both isoforms together did not further enhance the effect observed on E6/E7 expression by the individual isoforms (Fig. 23).

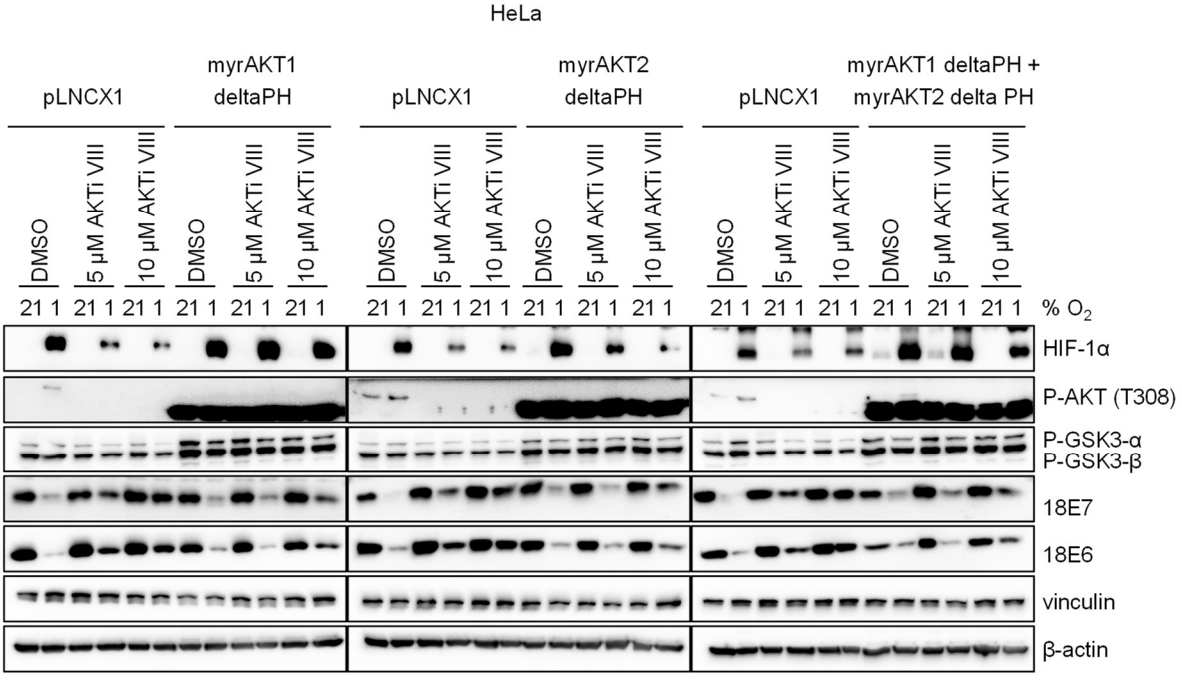

Fig. 23. Overexpression of constitutively-active AKT1 and AKT2 counteracts reactivation of hypoxic E6/E7 expression induced by AKTi VIII. HeLa cells were transfected with expression vectors for myristoylated AKT1 (myrAKT1deltaPH) and AKT2 (myrAKT2deltaPH), alone or in combination, treated with 5 and 10 µM AKTi VIII and cultured for 24 h under hypoxia or normoxia. Immunoblot of HIF-1α, P-AKT (T308), phosphorylated GSK3-α and GSK3-β (P-GSK3-α (S21)/P-GSK3-β (S9)) HPV18 E6 and E7 is shown. Vinculin, β-actin = loading control.

Whereas these experiments indicate that AKT activation does not induce repression of E6/E7 under normoxia, they further confirmed an involvement of AKT, more precisely AKT1 and AKT2, in the repression of E6/E7 under hypoxia. Moreover, they suggest a functional redundancy of both isoforms in this process.

2.6.3 Concomitant silencing of AKT1 and AKT2 counteracts repression of E6/E7 under hypoxia

The results obtained after increasing AKT activity via ectopic expression of constitutively-active isoforms indicate an important role for AKT1 and AKT2 in the hypoxic repression of HPV oncogene expression. In this case, silencing of endogenous AKT1 and/or AKT2 expression should block hypoxia-induced repression of E6/E7.

To test this hypothesis, HeLa cells were transfected with siRNAs targeting AKT1 and AKT2, alone or in combination and cultured under hypoxia or normoxia. Knockdown efficiency was monitored by immunoblotting of pan-AKT that showed a significant decrease upon treatment with AKT1 targeting siRNAs (Fig. 24A). Upon knockdown of AKT2, expression levels of pan-AKT were not detectably altered indicating that AKT1 is the predominantly expressed isoform. Hence, immunoblot analyses of AKT2 were performed revealing that AKT2 was expressed in HeLa cells and that its levels were reduced upon transfection with siRNAs. Moreover, it was observed that AKT2 levels remained unaffected by silencing of AKT1 and were downregulated under hypoxia similar to what was already observed for general protein expression of AKT (Fig. 16C, Fig. 24). Interestingly, hypoxia-induced phosphorylation of AKT was not altered upon silencing of AKT2 and diminished, but still detectable, upon silencing of AKT1. However, a concomitant silencing of both isoforms very efficiently blocked AKT phosphorylation at both investigated residues. Accordingly, repression of E7 was counteracted in AKT1 and in AKT1/2 silenced cells with the effect being slightly more pronounced upon concomitant knockdown of AKT1 and AKT2. However, reactivation of E6 expression under hypoxia was not observed upon effective blockade of AKT1/2 expression by RNAi (Fig. 24A).

To obtain more efficient AKT knockdown cells, AKT1 knockdown single cell clones were generated by the CRISPR/Cas9 method and subsequently transfected with AKT2 targeting siRNAs. AKT1 knockdown clones still showed hypoxia-induced phosphorylation of AKT at T308 that was only blocked by additional silencing of AKT2 (Fig. 24B). Phosphorylation of AKT at S473 was still detectable in AKT1 knockdown cells, but no induction by hypoxia was observed. Importantly, complete disappearance of the P-AKT signal was only observed in AKT1 knockdown cell clones in which AKT2 expression was additionally silenced. Correspondingly, the reactivation of E7 expression under hypoxia in AKT1 knockdown cells

was significantly enhanced when AKT2 was concomitantly blocked. Weak reactivation of E6 expression under hypoxia was also detectable in the double knockdown cells (Fig. 24B).

In conclusion, the reactivation of E6/E7 expression under hypoxia that was observed upon treatment with PI3K/AKT/mTORC2 inhibitors could be reproduced by silencing AKT1 and AKT2 expression. Although the results suggest a predominant role of AKT1, combined blockade of AKT1 and AKT2 showed the most efficient effects, indicating functional redundancy of the two isoforms in hypoxic regulation of E6/E7 expression.

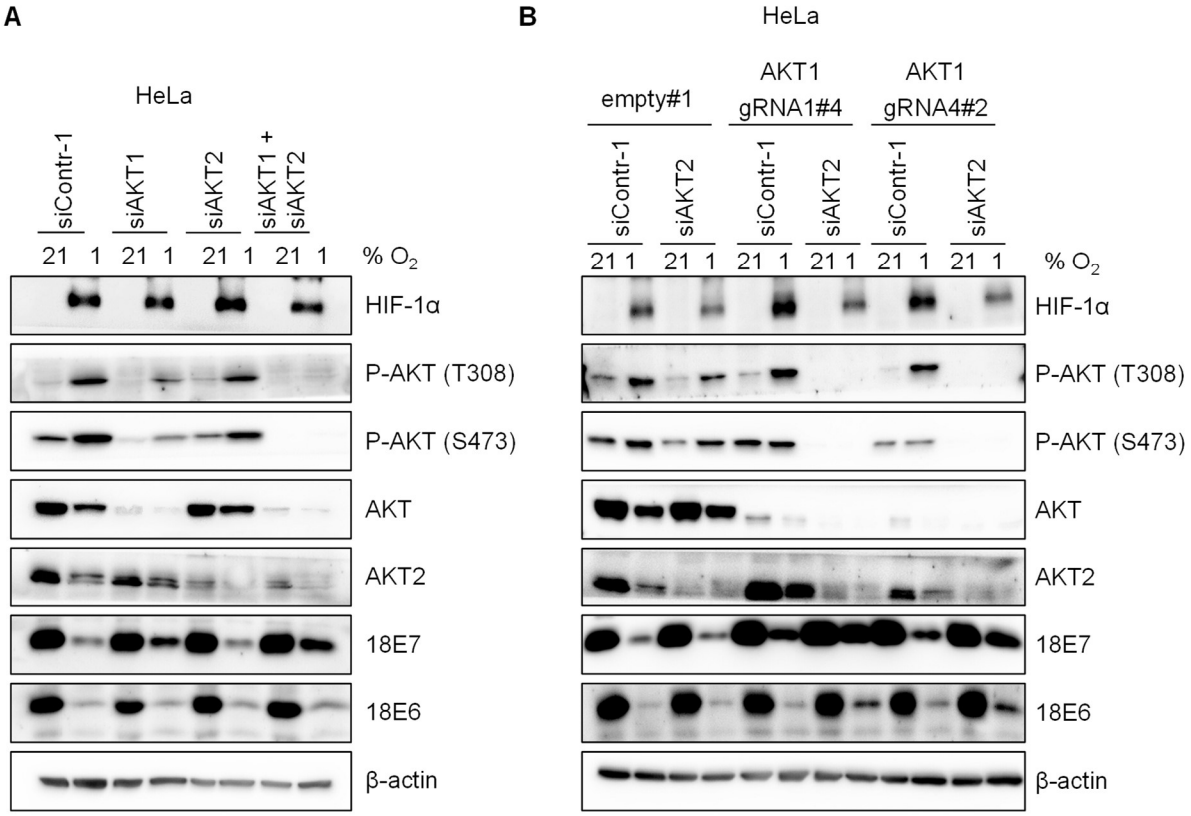

Fig. 24. Combined silencing of AKT1 and AKT2 counteracts repression of E6/E7 expression under hypoxia. (A) HeLa cells were transfected with siRNAs targeting AKT1 (siAKT1) and AKT2 (siAKT2), alone or in combination, and incubated for 24 h under hypoxia or normoxia. siContr-1 = control siRNA. **(B)** AKT1 was silenced in HeLa cells using the CRISPR/Cas9 technique. Two single cell clones generated with different gRNAs are shown (AKT1 gRNA1#1, AKT1 gRNA4#2). Control cell clone was transfected with the empty basic vector (empty#1). Single cell clones were transfected with siRNAs targeting AKT2 (siAKT2) or a control siRNA (siContr-1) and cultured for 24 h under hypoxia or normoxia. **(A+B)** Immunoblot analyses show protein expression of HIF-1α, P-AKT T308 and S473, pan-AKT (AKT), AKT2 and HPV18 E6 and E7. β-actin = loading control.

2.7 Phenotypic consequences of AKT inhibition on hypoxic cervical cancer cells

2.7.1 PI3K/AKT inhibitors do not induce proliferation in hypoxic cervical cancer cells

The observation that clinically tested PI3K/AKT inhibitors can reactivate viral oncogene expression under hypoxia (Fig. 17) is intriguing and may have clinical consequences, since E6/E7 can act pro-proliferative. Thus, the effects of PI3K/AKT inhibitor treatment on the proliferation of hypoxic cervical cancer cells were investigated.

Analysis of cell proliferation by quantification of crystal-violet stained cells revealed that treatment with AKTi VIII over a period of 3 days did not reinduce cell growth under hypoxia but that cell numbers were slightly lower or remained constant when compared to DMSO treated control cells as was shown for HeLa and SiHa cells (Fig. 25A). On a side note, treatment of normoxic cells with AKTi VIII led to the expected growth inhibition (Fig. 25B) corroborating the well characterized pro-proliferative function of AKT [95]. Moreover, comparison of hypoxic and normoxic growth curves of control cells showed the previously reported growth inhibition under hypoxia [71].

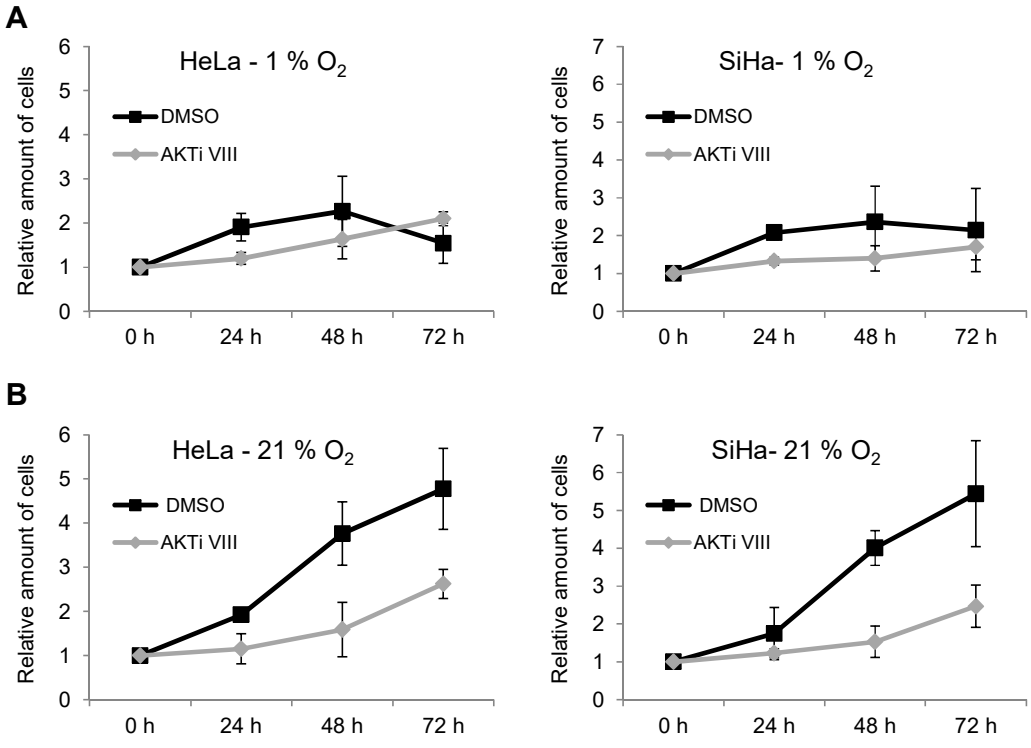

Fig. 25. AKTi VIII does not induce proliferation under hypoxia. (A+B) Time course of HeLa and SiHa cells treated with 10 µM AKTi VIII and cultured under hypoxia **(A)** or normoxia **(B)** for 3 days. Crystal violet staining of cells was performed every 24 h. Depicted is the relative amount of cells determined by quantification of cell-bound crystal violet. The time point 0 h was set as 1 for each condition. Shown is the mean of 3 independent experiments with standard deviations.

A more detailed analysis was carried out by live cell imaging with acquisition of images every 2-4 h and subsequent computerized cell quantification. For this purpose, nuclei-labelled (H2B-mCherry) cells were used. The resulting growth curves again depicted the anti-proliferative effects of AKTi VIII on normoxic Hela and SiHa cells (Fig. 26B). Under hypoxia, there was no proliferative activity detectable for SiHa cells, with and without AKTi VIII. In hypoxic HeLa cells, AKTi VIII further inhibited the already reduced, but still measurable, cell growth (Fig. 26B). Moreover, treatment with MK-2206 and PX-866 caused similar effects in HeLa cells (Fig. 26C). Appreciable increases in cell death were not observed under any described treatment conditions.

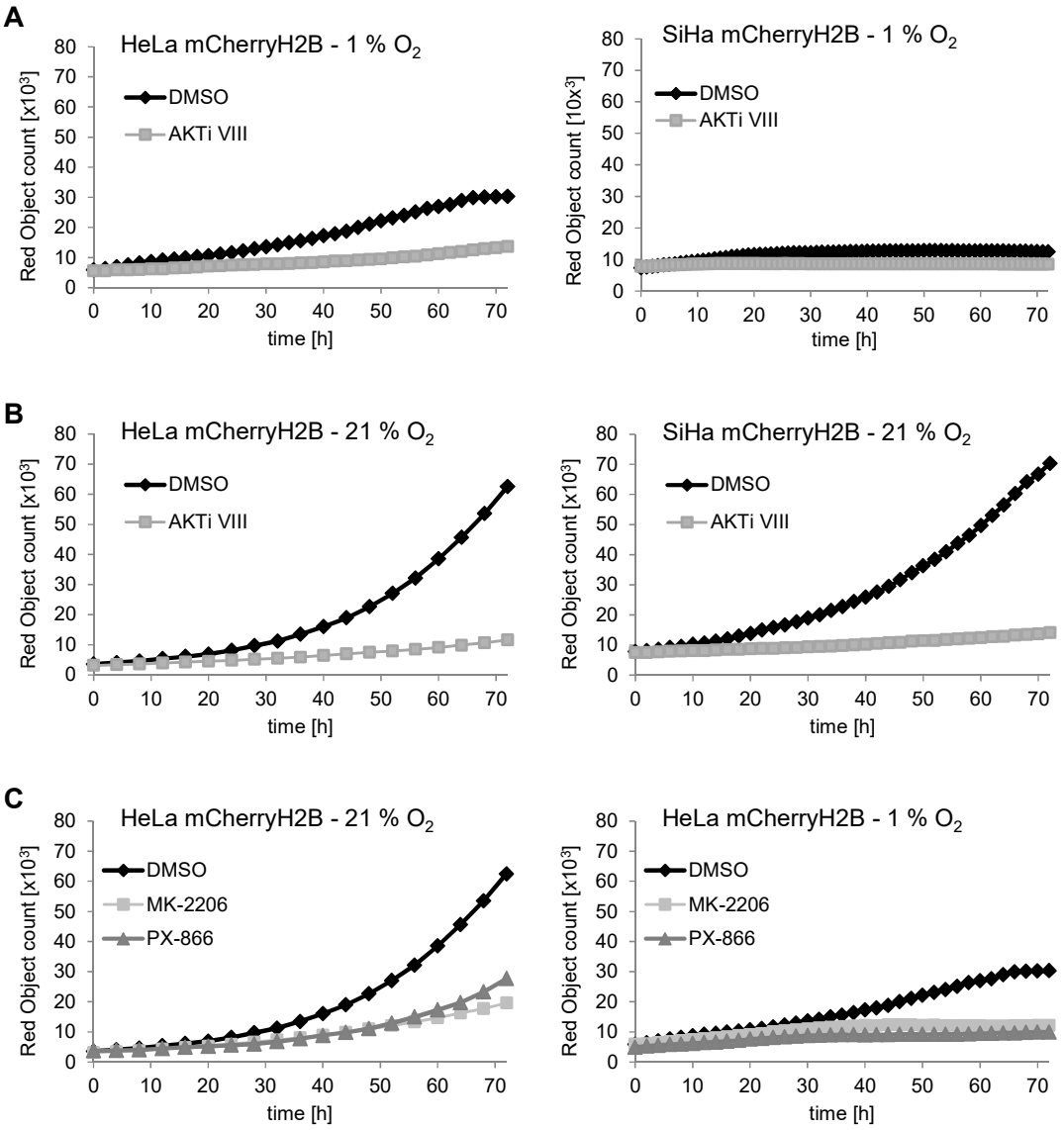

Fig. 26. AKTi VIII, MK-2206 and PX-866 do not induce proliferation under hypoxia as determined by live cell imaging. (A-C) HeLa and SiHa mCherryH2B cells were seeded in 96 well plates. 2 days after seeding cells were treated with 10 µM AKTi VIII **(A)** or 5 µM MK-2206 and 5 µM PX-866 **(C)** and monitored for the following 72 h. DMSO served as solvent control. Images were acquired every 2-4 h using an IncuCyte® system and red object count (representing cell number) was determined. Shown is the mean of technical triplicates of one representative experiment.

Collectively, these results indicate that hypoxic cervical cancer cell lines remain growth-arrested even upon PI3K/AKT inhibitor-induced reactivation of viral oncogene expression indicating that the suppression of cell proliferation via inhibition of PI3K/AKT signaling acts dominantly over the pro-proliferative stimulus derived from E6/E7 expression.

2.7.2 PI3K/AKT inhibitors modulate the response of hypoxic HeLa cells to etoposide

Hypoxic tumors are generally associated with poor patient prognosis that can largely be attributed to their high resistance towards radio- and chemotherapy [64]. Since PI3K/AKT inhibitors are tested in the clinic not only as single agents, but also to complement conventional therapies [121], the effects of such inhibitors on hypoxic cervical cancer cells in combination with chemotherapy were investigated. In particular the induction of senescence and the clonogenic capacity of treated cells were assessed.

For this purpose, cells were pre-treated with AKTi VIII, MK-2206 or PX-866, cultured under hypoxia or normoxia and 24 hours later treated with the chemotherapeutic drug etoposide. Cells were kept under hypoxia for two additional days, then split and cultured further under normoxia for colony formation and senescence assays according to the schematic depicted in Fig. 27. In normoxic cells, treatment with etoposide led to the induction of senescence, as was shown by staining for senescence associated β-galactosidase (SA-β-Gal) activity and by the typical morphological signs of senescence that were observed, such as long cytoplasmic projections, cell enlargement and flattening (Fig. 27). In contrast, hypoxic cells were better able to evade senescence induction resulting in an increased outgrowth of cells after subsequent cultivation under normoxia. This was also verified by colony formation assays showing a reduced number of outgrowing clones under normoxia (Fig. 28). Interestingly, in HeLa cells concomitant treatment with AKTi VIII, MK-2206 or PX-866 abrogated the protective effect of hypoxia in that hypoxic cells were no longer able to evade the etoposide-induced senescence resulting in a significantly diminished number of outgrowing clones (Fig. 27, Fig. 28). However, in hypoxic SiHa and SW756 cells, senescence induction and number of clones was not affected by PI3K/AKT inhibitor treatment. On a side note, in SiHa and SW756 cells an increase in the number of clones outgrowing after etoposide treatment was observed in normoxic cells that were treated with AKTi VIII (Fig. 27, Fig. 28).

In conclusion, it was observed that PI3K/AKT inhibitors can modulate the behavior of hypoxic cervical cancer cells towards chemotherapy in that they can sensitize cells to etoposide-induced senescence induction in certain cell lines.

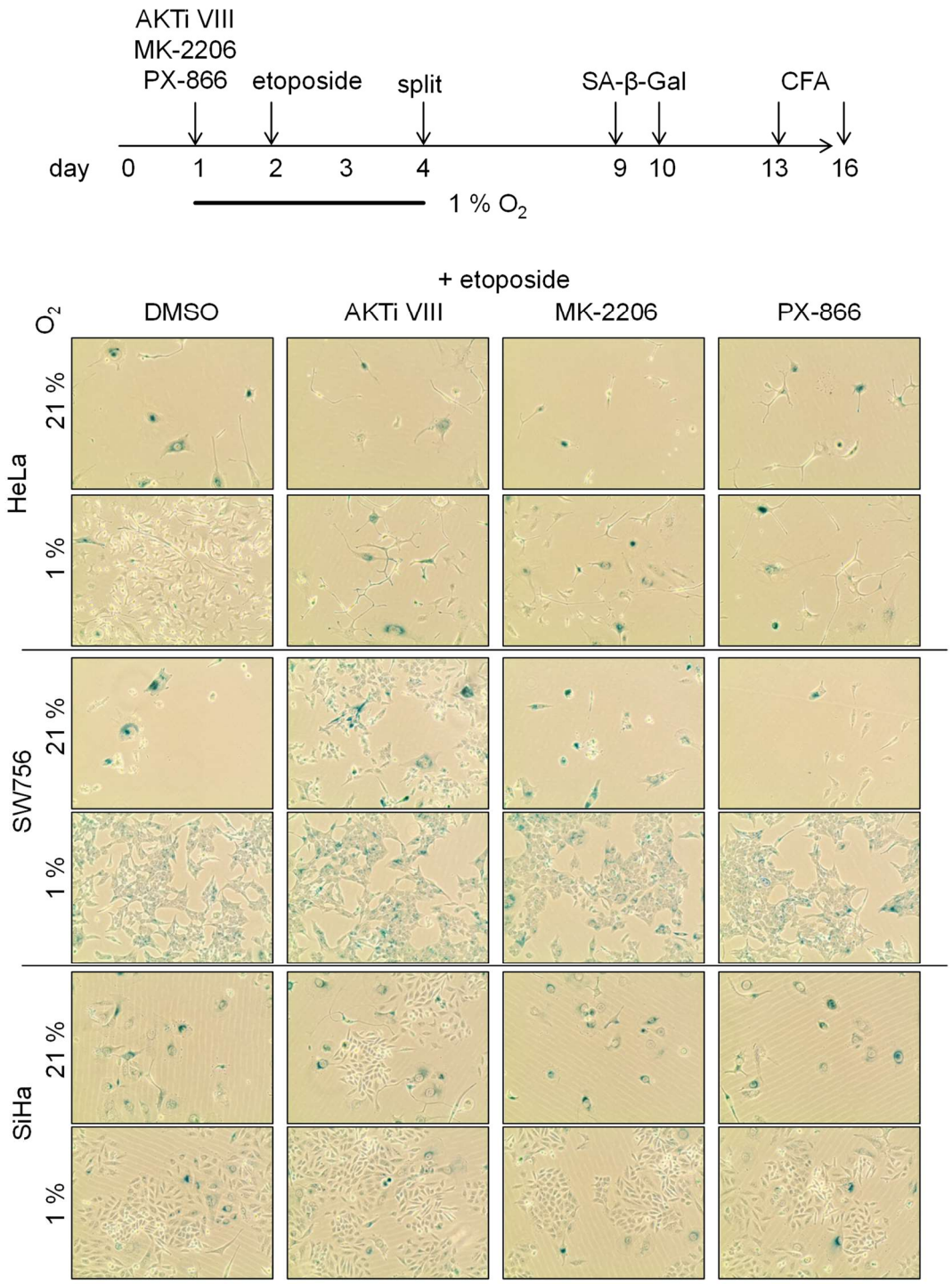

Fig. 27. PI3K/AKT inhibitors modulate etoposide-induced senescence under hypoxia in a cell line-dependent manner. Senescence assay after etoposide (10 µM) treatment of normoxic or hypoxic HeLa, SiHa and SW756 cells treated with 10 µM AKTi VIII, 5 µM MK-2206 or 5 µM PX-866. DMSO = solvent control. Scheme on top: Treatment protocol, further specified in the text. SA-β-Gal = senescence associated β-galactosidase assay. CFA = colony formation assay.

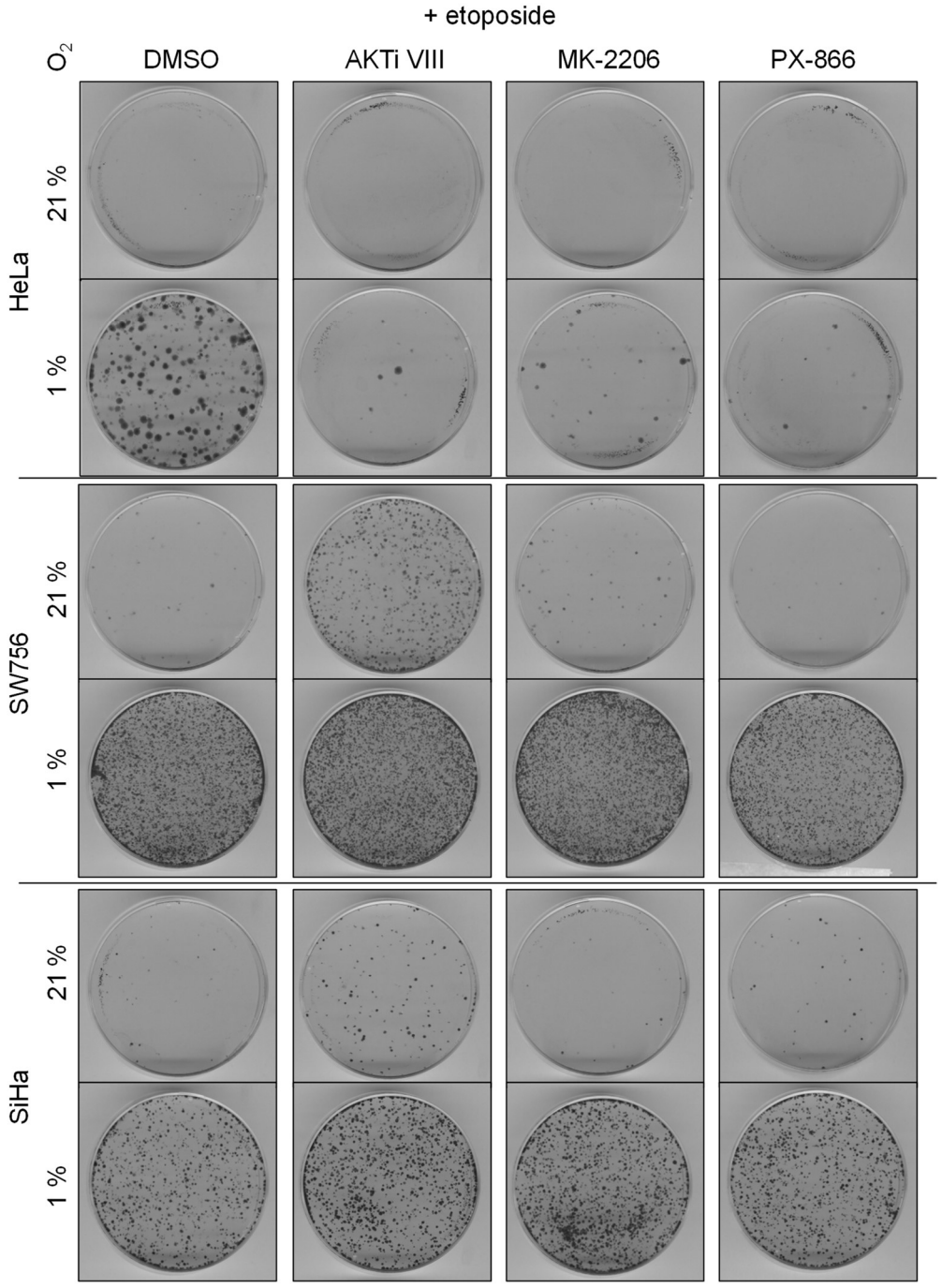

Fig. 28. PI3K/AKT inhibitors modulate etoposide-induced colony forming capacity under hypoxia in a cell line-dependent manner. Colony formation assay of hypoxic and normoxic HeLa, SW756 and SiHa cells accompanying to senescence assay from Fig. 27.

2.7.3 Knockdown of AKT modulates the response of hypoxic HeLa cells to etoposide

To further analyze a putative role of AKT in the effects caused by PI3K/AKT inhibitors in etoposide treated cells under hypoxia, etoposide treatment was applied to HeLa and SiHa cells transfected with siRNAs targeting AKT1 or AKT1 and AKT2 according to the schematic in Fig. 29A. Successful knockdown was verified by immunoblotting (Fig. 29B).

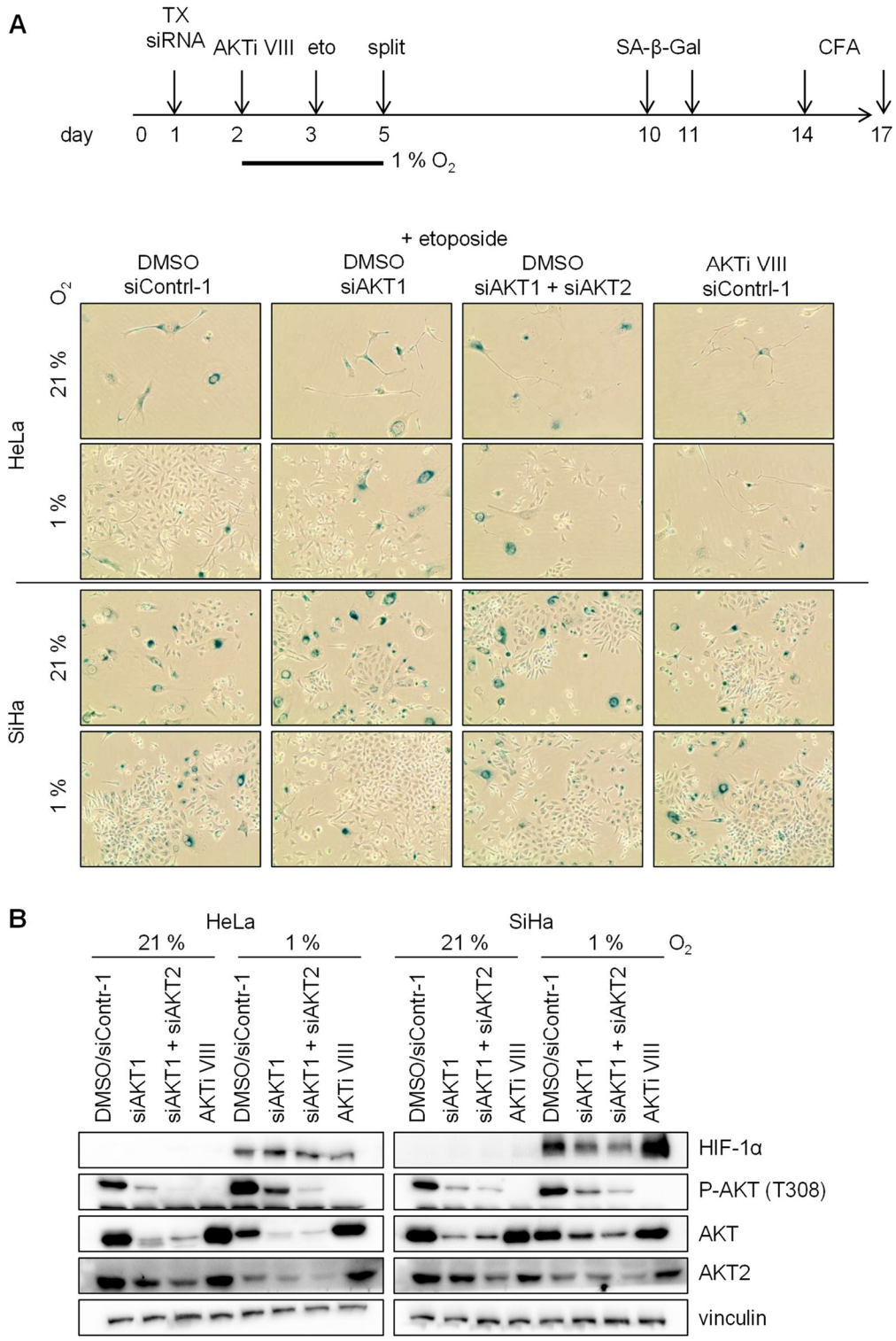

Fig. 29. AKT1/2 silencing modulates etoposide-induced senescence under hypoxia in a cell line-dependent manner. (A) Senescence assay after etoposide (10 µM) treatment of normoxic or hypoxic HeLa and SiHa cells either transfected with AKT1 and AKT2 targeting siRNAs (siAKT1, siAKT2) in the indicated combinations, or treated with 10 µM AKTi VIII. siContr-1 = control siRNA, DMSO = solvent control. Scheme on top: Treatment protocol, further specified in the text. TX = transfection. Eto = etoposide. SA-β-Gal = senescence associated β-galactosidase assay. CFA = colony formation assay. **(B)** Accompanying immunoblot showing protein expression of HIF-1α, P-AKT T308, AKT and AKT2. Vinculin = loading control.

Knockdown of AKT1 alone rendered hypoxic HeLa cells slightly more vulnerable to etoposide treatment as could be observed after subsequent cultivation under normoxia by a lower number of cells being able to avoid senescence induction (Fig. 29A) and by the outgrowth of fewer cells in colony formation assays (Fig. 30). This effect was further enhanced upon concomitant silencing of AKT1 and AKT2. Of note, treatment with AKTi VIII was however still more efficient in diminishing the colony forming capacity of etoposide treated hypoxic HeLa cells.

Analogue to the experiments performed with PI3K/AKT inhibitors, AKT knockdown did not affect the phenotypic response of hypoxic SiHa cells to etoposide, but an increased outgrowth of clones was observed in normoxic SiHa cells transfected with AKT1 or AKT1 and AKT2 targeting siRNAs (Fig. 29, Fig. 30).

Hence, silencing of AKT1 and AKT2 expression sensitized hypoxic HeLa, but not SiHa cells, towards etoposide treatment.

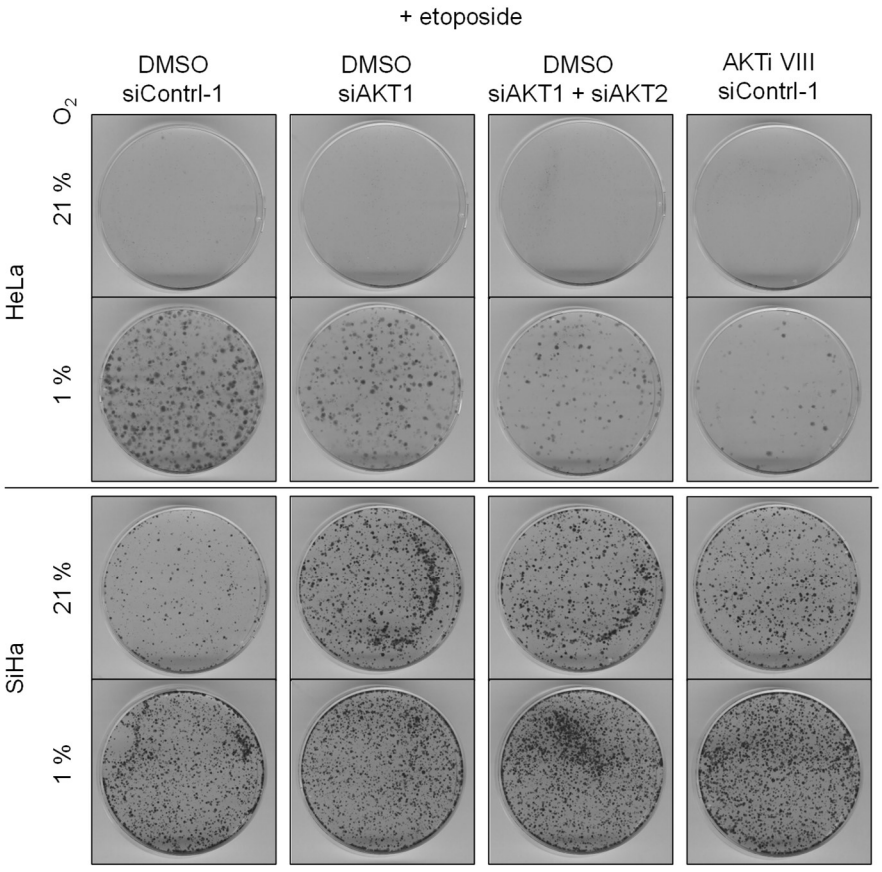

Fig. 30. AKT1/2 silencing modulates etoposide-induced colony forming capacity under hypoxia in a cell line-dependent manner. (A) Colony formation assay of Hela and SiHa cells accompanying to senescence assay from Fig. 29.

2.8 Proteome analysis of hypoxic HPV-positive cancer cells

In summary, the work of the present study revealed that HPV oncogene expression is repressed under hypoxia via the PI3K/AKT pathway in a glucose-dependent manner in that PI3K/AKT/mTORC2 inhibitors as well as high glucose levels counteract E6/E7 repression. To gain further insights into this process, mass spectrometry (MS)-based quantitative proteome analyses were performed, with the support of Prof. Dr. Jeroen Krijgsveld's group at DKFZ, using Thermo Scientific's tandem mass tag (TMT) isobaric labeling approach [164]. The cellular proteome of SiHa cells cultured under normoxia, under hypoxia, and under hypoxia treated with AKTi VIII or high glucose concentrations (25 mM) was assessed (illustrated in Fig. 31A). A representative immunoblot showed the expected E7 and P-AKT T308 expression under the investigated conditions (Fig. 31B).

To gain an impression about global alterations in the obtained data sets derived from 3 individual experiments, volcano plots were generated to visualize relative fold changes in relation to statistical significance (Fig. 31C). Comparison of the proteome (5967 measured proteins) of differentially treated hypoxic cells to normoxic cells showed that many alterations in protein expression were detected. However, significant changes ($p < 0.05$) with strong alterations in expression levels (log2 fold change < -1 or > 1) were limited (Fig. 31C, upper panel). Under hypoxia E6/E7 expression is shut down but reactivated again when cells are treated with AKTi VIII or with high glucose concentrations. Since high glucose blocks hypoxia-induced AKT phosphorylation, repression of E6/E7 could be counteracted by a common mechanism under both conditions. Hence, it is particularly interesting to compare these two conditions with untreated hypoxic cells, where E6/E7 is downregulated, to identify potentially common regulators of E6/E7 expression under hypoxia. Volcano plots of these comparisons showed that most of the significantly different expressed proteins were upregulated by the treatments relative to the hypoxia control, but some downregulated proteins were detected as well (Fig. 31C, lower panel).

In total, 46 proteins with significant differential expression (p-value < 0.05) between the hypoxia and normoxia DMSO-treated controls were detected. These are grouped into two main clusters, characterized by upregulation (9 proteins) or downregulation (37 proteins) as compared to the normoxia baseline. The alteration of protein expression caused by hypoxia was partially or fully reverted by the treatment with AKTi VIII and high glucose for many of the candidates (Fig. 32). Proteins with strong deregulation caused by hypoxia and a strong normalization effect of the treatments may be promising leads for future investigations of the mechanism behind E6/E7 reactivation through AKT inhibition and high glucose concentrations. Interesting candidates include, amongst others, metal responsive proteins like metallothionein 2A (MT2A) or proteins linked to the Wnt signaling pathway like Wnt5A or Dickkopf-related protein 1 (DKK1) (Fig. 32). A putative functional role of these proteins in

AKT-dependent repression of E6/E7 under hypoxia awaits further exploration in future studies.

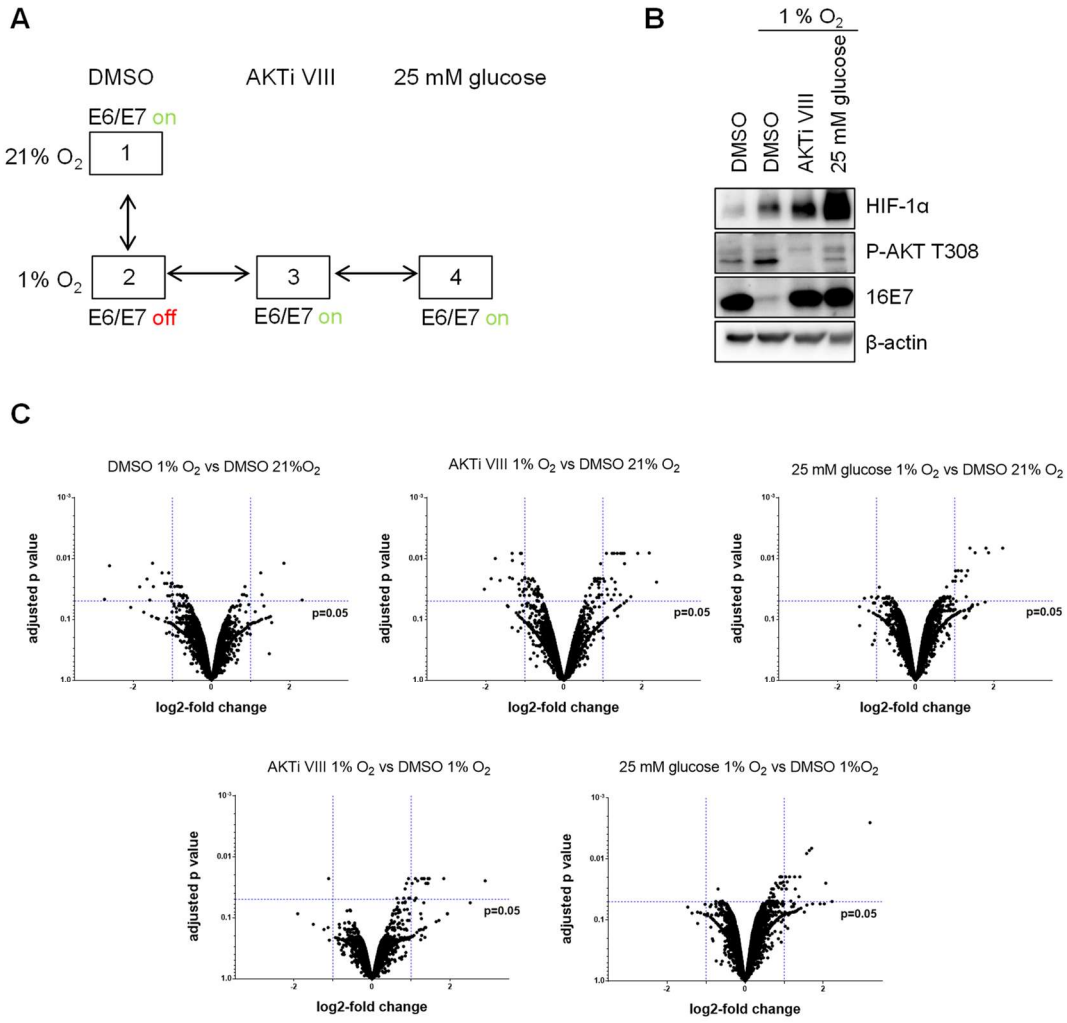

Fig. 31. Proteome analysis of hypoxic SiHa cells. TMT mass spectrometry analysis of SiHa cells treated with DMSO as solvent control, 10 µM AKTi VIII or kept in medium containing 25 mM glucose (instead of standard medium with 5.5 mM glucose) and cultured for 17 h under hypoxia or normoxia as indicated. **(A)** Scheme depicting the four analyzed treatment conditions. **(B)** Representative immunoblot showing protein expression of HIF-1α, P-AKT T308, HPV16 E7. β-actin = loading control. **(C)** Volcano plots depicting mean log2-fold change of protein expression versus adjusted p-value (n = 3). Upper graphs: Fold change of protein expression from hypoxic conditions (DMSO as solvent control, AKTi VIII, 25 mM glucose) relative to normoxic condition (DMSO treated). Lower graphs: Fold change of protein expression under hypoxia treated with AKTi VIII or cultured under hypoxia with 25 mM glucose relative to DMSO-treated hypoxic control. Proteome analyses were performed in collaboration with B. Kuhn and J. Krijgsveld (DKFZ).

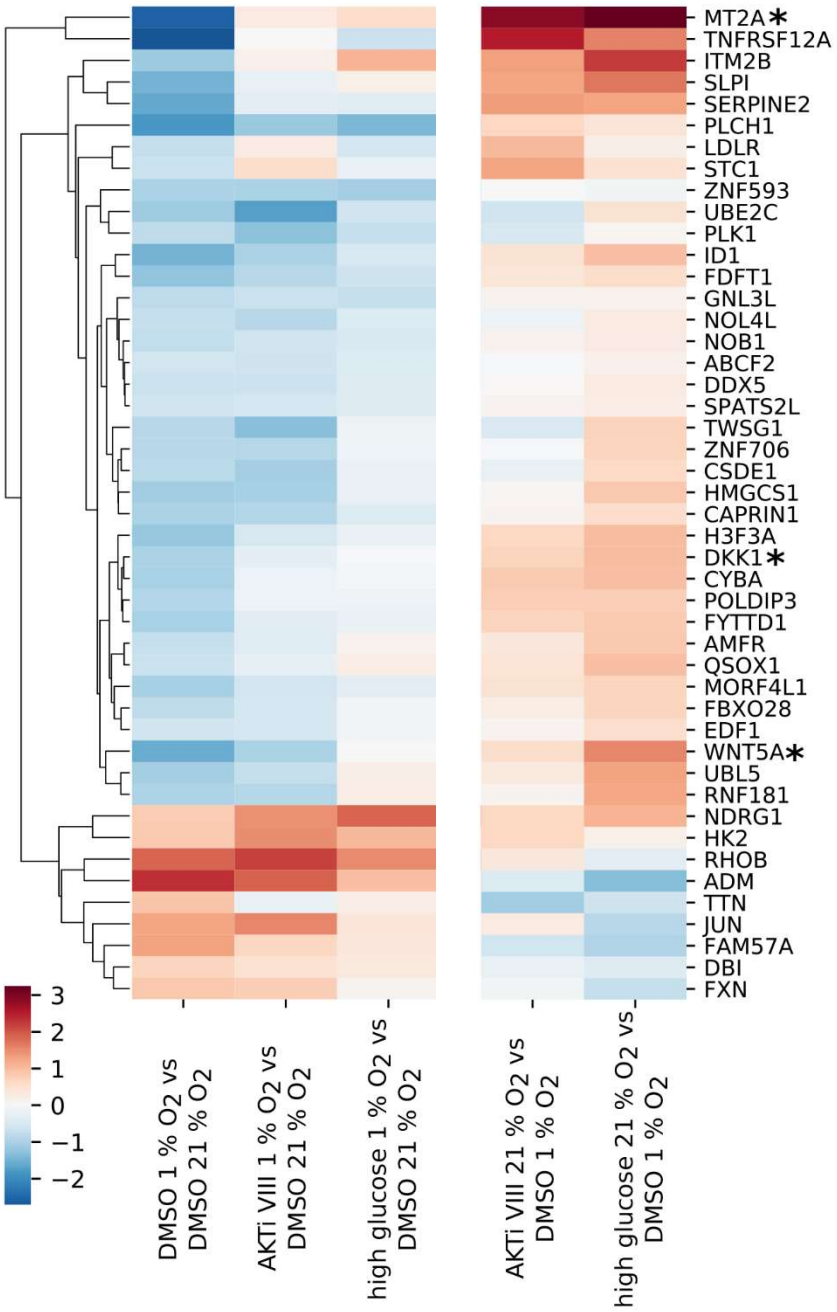

Fig. 32. Heatmap of differentially expressed proteins under hypoxia. Analysis of proteome data derived from TMT mass spectrometry described in Fig. 31. It was filtered for differential expression under hypoxia (DMSO-treated control) compared to normoxia ($p < 0.05$) and hierarchical clustering was performed. Left three columns: Comparisons of the different treatment conditions under hypoxia relative to normoxia. Right two columns: Comparisons of hypoxia treated with AKTi III or high glucose (25 mM) relative to DMSO-treated hypoxic control. Protein names are indicated on the right. Upregulation is shown in red, downregulation in blue (see color scheme at lower left). Proteins specifically mentioned in the text are marked with a star.

Chapter 3

Discussion

3. Discussion

Under normoxic conditions, HPV-positive cancer cells rely on sustained expression of the two viral oncogenes E6 and E7 and go into senescence when those are silenced. Contrarily, under hypoxia, a condition frequently found in subregions of solid tumors, they reversibly shut down E6 and E7 expression and enter a dormant state that potentially contributes to therapy resistance and tumor recurrences. This thesis aimed at elucidating the mechanism which underlies the repression of the HPV oncogenes under hypoxia. The results showed that hypoxic E6/E7 repression is regulated at the transcriptional level, but likely also at the level of protein and mRNA stability. Moreover, the critical signal cascade responsible for hypoxic E6/E7 downregulation was identified and functionally characterized, revealing that E6/E7 repression under hypoxia is dependent on the activity of the PI3K/AKT signaling pathway.

3.1 Level of E6/E7 repression under hypoxia

3.1.1 Transcriptional regulation contributes to repression of E6/E7 under hypoxia

Repression of E6/E7 mRNA expression under hypoxia is, at least partially, caused by inhibition of transcription as was demonstrated by reporter assays revealing that the activity of the HPV18 URR coding for E6/E7 transcripts was significantly reduced by approximately 50 % under hypoxia.

DNA methylation is unlikely to play a role in this context since no major alterations in methylation pattern at investigated (CpG-containing) sites in the HPV16 URR were detected and treatment with the demethylating agent 5-Aza did not prevent repression of E6/E7 under hypoxia. DNA methylation has previously been reported to be important for expression of E6/E7 in HPV-positive cancer cell lines since treatment with 5-Aza led to diminished E6/E7 mRNA and protein expression level [165]. This was only partially confirmed in the present studies where 5-Aza downregulated E6/E7 expression under normoxia in SiHa, but not in HeLa cells although higher concentrations of 5-Aza were applied compared to the aforementioned study. The suggested mechanism for downregulation of E6/E7 expression in SiHa cells upon DNA demethylation involves the microRNA miR-375. The promoter of miR-375 is methylated under normal conditions and treatment with 5-Aza reactivates miR-375 expression resulting in reduced levels of E6/E7 [165]. In HeLa cells, which were not included in the original study, this regulation was not observed, possibly due to cell line-dependent differential regulatory mechanisms. Hypoxia-induced reduction in DNA methylation at the L1 and L2 genes may be attributed to the observed downregulation of Dnmt1 expression, which was already previously reported for colorectal cancer cells [166].

Whereas the results indicate that DNA methylation plays no direct role in repression of E6/E7 under hypoxia, the data regarding the methylation status of histones was more complex. Total cellular levels of H3K4me3 and H3K27me3 were increasing under hypoxia, most likely due to diminished activity of O_2-dependent histone demethylases. Hypoxia-induced inhibition has for instance been reported for the H3K4me3 demethylase JARID1A or the H3K27me3 demethylase JMJD3 [84, 167]. This also goes in line with recent reports that describe increased bivalent epigenetic marking with H3K4me3 and H3K27me3 under hypoxia [85, 86]. Bivalently marked chromatin is characteristic, but not entirely exclusive, for embryonic stem cells. In many developmental genes the repressive mark H3K27me3 silences the gene, whereas the presence of H3K4me3 allows rapid activation when required [168]. In a comprehensive analysis, it was previously shown that although transcription is primarily determined by H3K4me3, the exact loci of the H3K4me3 and H3K27me3 marks is an additional decisive factor for transcriptional activity. For instance, increased H3K27me3 at the transcription start site (TSS) under hypoxia was closely associated with gene repression despite the presence of H3K4me3 [85]. Thus, increased enrichment of H3K27me3 (and H3K4me3) at the HPV16 URR in hypoxic SiHa cells may indicate transcriptional repression, especially since one of the applied primers (HPV16URR_2) spans a region close to the TSS of E6/E7. Primers for the hypoxia-activated genes VEGF and Glut1 were in regulatory regions more distant to the TSS. H3K4me3 and H3K27me3 detected at these sites may therefore rather be associated with transcriptional activation under hypoxia although an increase in both histone marks was detected here as well. Nevertheless, to adequately associate the detected chromatin marks with transcriptional activity of genes a better resolution (obtainable by ChIP-sequencing) would be required to gain information about the exact localization of H3K4me3 and H3K27me3 marks among the genome. Additionally, the data obtained in the present study cannot distinguish if enhanced signals from H3K4me3 and H3K27me3 at the same locus are caused by bivalent chromatin or by chromatin that harbors different epigenetic marks among the cell population. To gain information about putative co-localization of both histone marks, sequential ChIP assays would be required. Hence, the results obtained in the present work revealed alterations in histone marks at the HPV16 URR and raise the possibility that transcription of *E6/E7* is repressed by bivalent epigenetic marking with H3K4me3 and H3K27me3 but requires further detailed analyses to allow a final conclusion in this context.

Deletion analyses of the HPV18 URR revealed that hypoxic repression could be mediated by a 157 bp fragment of a 3'-portion of the HPV18 enhancer, even when fused to a heterologous promoter. Binding of YY1, a potential repressor of HPV transcription [169], was reported for this cis-regulatory element [128], leading to the recruitment of Brd4 to this site.

Yet, a role for YY1 in regulation of E6/E7 expression was not detected in the present studies -neither under normoxia nor hypoxia.

Interestingly however, treatment with the BET inhibitor JQ-1 led to downregulation of E6/E7 expression. JQ-1 binds to the bromodomain of BET family members, namely Brd2, Brd3, Brd4 and Brdt, and prevents their binding to acetylated histone lysines and the subsequent recruitment of transcriptional regulators [170]. BET inhibitors are currently undergoing clinical trials to investigate their anti-cancer activities and thus, are of substantial clinical significance [171]. In the context of YY1, Brd4 was described as negative regulator of E6/E7 expression [128]. In contrast, the JQ-1 induced repression of E6/E7 observed in the present experiments argues for an activating function of Brd4. However, since knockdown of Brd4 had no consequences on E6/E7 expression under the investigated conditions, this effect could also be attributable to the other Bet family members or be caused by a small amount of residual Brd4. JQ-1-dependent repression of HPV transcription has previously been reported, but only in the context of E2 [172], whose ORF gets disrupted upon integration of the viral DNA into the host cell genome in many cervical cancers including the here investigated HeLa, SW756 and SiHa cell lines [165, 173]. Thus, JQ-1 induced repression of E6/E7 can also occur independently of E2. During the course of this thesis, a paper was published describing an E2-independent mechanism of Brd4-mediated activation of *E6/E7* transcription that can be abolished by BET inhibitors such as JQ-1 [174]. More precisely, Brd4 was described to bind to super-enhancer-like-elements at tandemly integrated copies of the HPV genome that drive expression of *E6/E7* [174, 175]. In the present work, BET-inhibitor mediated downregulation of E6/E7 expression was observed in SiHa cells that are characterized by only 1-2 viral integrates [129]. Hence, BET family members may also activate E6/E7 transcription without the formation of super-enhancers at tandem repeats of viral DNA.

Remarkably, while JQ-1 treatment downregulated E6/E7 expression under normoxia, it counteracted repression of E7 under hypoxia in HeLa cells. JQ-1-mediated reactivation was not observed for E6 raising the possibility that differential regulation of protein stability of E6 and E7 or alternative splicing events are involved. However, since these phenomena were exclusively observed in HeLa cells, they are likely cell line-specific and were not further analyzed in the present work.

Apart from reported binding of YY1, binding sites for AP1, Oct1 and NF1 [36] have been described in the 157 bp fragment sufficient to mediate repression of transcriptional activity under hypoxia. Unpublished results from the group of Prof. Dr. Frank Rösl (DKFZ, Heidelberg) indicated that AP1, a major driver of HPV transcription [40], is probably not responsible for downregulation of E6/E7 under hypoxia (A. Hitschler et al., unpublished

data). A potential involvement of Oct1 or NF1 in hypoxic regulation of E6/E7 expression remains to be elucidated.

Taken together, transcription of the HPV *E6/E7* mRNA is reduced under hypoxia by a mechanism independent of DNA methylation but possibly influenced by alterations in H3K4me3 and H3K27me3. In addition, histone-binding BET proteins may play a direct or indirect role in hypoxic regulation of E6/E7 expression in a cell line dependent manner.

Notably, HPV promoter activity under hypoxia was reduced by half, whereas downregulation of *E6/E7* mRNA was more pronounced (80 % in HeLa cells, see [71]). Thus, effects observed in the reporter assays may only partially explain the repression of E6/E7 under hypoxia. This may be due to experimental limitations; in luciferase reporter assays the activity of the HPV URR was not assessed in the endogenous chromosomal context but with a transiently transfected episomal plasmid that may not be subject to all regulatory events occurring at the integrated viral promoter. Furthermore, effects on protein and mRNA stability of E6 and E7 under hypoxia could contribute to the downregulation.

3.1.2 Protein and mRNA stability of E6/E7 are reduced under hypoxia

In fact, E6 and E7 showed slightly reduced protein half-lives under hypoxia. Moreover, downregulation of E6/E7 under hypoxia was already detectable at the mRNA level and E6/E7 mRNA half-life was shortened under hypoxia. Measurements of both, mRNA and protein stability were subject to variations between individual experiments. This suggests that protein and mRNA half-lives are likely to be very sensitive to minor fluctuations in the experimental conditions such as slight variations in cell density that in turn affect, for instance, glucose concentrations in the cell culture medium. However, the detected tendencies consistently revealed a reduction of protein and mRNA half-lives. This data suggests that E6/E7 downregulation under hypoxia is mediated not only by the repression of the E6/E7 transcriptional promoter but also supported by a reduction of E6/E7 mRNA and protein half-lives.

3.2 Candidate transcription factors that are likely not involved in hypoxic repression of E6/E7

Since E6/E7 repression occurs to a substantial part at the transcriptional level and is glucose-sensitive, several strong candidates for hypoxic and glucose-dependent regulation of gene expression were investigated. In particular, HIF transcription factors are directly and indirectly involved in transcriptional regulation of many genes under hypoxia [77]. Although, as expected, a strong induction of HIF-1α and HIF-2α was observed under hypoxic conditions, E6/E7 repression was not prevented upon efficient knockdown of HIF-1α or

HIF-2α, alone or in combination. Work from our group additionally showed that induction of HIF-1α under normoxia using the HIF mimetics $CoCl_2$, mimosine and DMOG did not alter E7 expression [71]. Hence, HIF transcription factors likely neither directly nor indirectly affect E6/E7 expression indicating that repression of E6/E7 under hypoxia occurs via a HIF-independent mechanism.

Repression of E6/E7 under hypoxia was counteracted by high glucose concentrations raising the possibility that glucose-sensitive transcription factors are involved. The Mlx network emerged as a prime candidate involved in this regulation since it is an important coordinator of gene expression in response to glucose [137]. However, no experimental evidence linking Mlx to the regulation of E6/E7 expression was obtained. In specific, whereas the previously described Mlx-dependent upregulation of TXNIP by high glucose [139] was impaired upon silencing of Mlx and MondoA, neither the repression of E6/E7 nor the glucose-dependent reactivation of E6/E7 under hypoxia was affected under the same experimental conditions.

The c-Myc oncoprotein, which is part of a transcription factor network similar to the Mlx network, was found to be downregulated by hypoxia in a glucose-dependent manner thereby correlating with E6/E7 expression. This finding is corroborated by previous reports [141, 142]. Moreover, a positive correlation between E6/E7 and c-Myc expression has been described in that E6 is known to stabilize c-Myc [53, 54] and that silencing of E6/E7 expression in HeLa cells decreases c-Myc level [55, 56]. However, while E6/E7 are likely to positively regulate c-Myc expression under the conditions investigated in the present study, a reciprocal mechanism of c-Myc-dependent E6/E7 regulation was not detected since silencing of c-Myc had no impact on E6/E7 expression under hypoxia or normoxia.

Taken together, the cellular mechanism causing downregulation of viral oncogene expression under hypoxia appears to be independent of HIF transcription factors, the Mlx network and the c-Myc oncoprotein.

3.3 AKT-dependent repression of E6/E7 under hypoxia

However, evidence for a possible role for the AKT kinase in the process of hypoxic E6/E7 repression emerged in the present studies. Specifically, activating phosphorylation of AKT was induced under hypoxia in a glucose-dependent manner, thereby inversely correlating with E6/E7 expression. Moreover, time course experiments revealed that hypoxia-induced activation of AKT and reoxygenation-induced inactivation of AKT precede downregulation and reactivation of E6/E7 expression, respectively. These circumstantial evidences would be consistent with a role for AKT in hypoxic E6/E7 repression, but required experimental proof to demonstrate a functional connection.

3.3.1 Signaling via the PI3K/AKT pathway is required for repression of E6/E7 under hypoxia

In the PI3K/AKT pathway, PI3K is an upstream regulator being essential for activation of AKT and described to be important for activation of mTORC2 as well. mTORC2 phosphorylates AKT at S473, one of the two residues phosphorylated in fully activated AKT [95] (see also Fig. 5). Chemical inhibitors targeting AKT, PI3K or mTORC2 all counteracted repression of E6/E7 under hypoxia, providing strong experimental evidence that this signaling axis is crucial for downregulation of E6/E7 expression.

More detailed analyses revealed that PI3K and AKT inhibitors prevented phosphorylation of AKT at both amino acid residues (T308 and S473). Notably, blockade of S473 phosphorylation alone by targeting mTORC2 with KU-0063794 was sufficient to counteract repression of E6/E7 under hypoxia as well. A second mTOR inhibitor, rapamycin, did not block AKT S473 phosphorylation since it primarily targets mTORC1 [153], but not mTORC2 which is the responsible kinase for AKT S473 phosphorylation. Instead, treatment with rapamycin enhanced S473 phosphorylation since mTORC1-mediated feedback inhibition on mTORC2 was blocked. Phosphorylation of AKT at S473 by mTORC2 was described to facilitate T308 phosphorylation [104], which may explain the observation that T308 phosphorylation under hypoxia is reduced by high concentrations of KU-0063794 as well. Taken together, it was shown here that S473 phosphorylation of AKT is a prerequisite for repression of E6/E7 under hypoxia. Although unique blockade of T308 phosphorylation was not performed in the present work, results indicate that dual phosphorylation of AKT at T308 and S473 is required for hypoxia-induced downregulation of E6/E7 since AKT phosphorylated at S473 alone has no kinase activity [98]. Collectively, these results showed that E6/E7 repression under hypoxia is dependent on fully activated AKT, which is induced via PI3K and mTORC2.

AKT is a known activator of mTORC1 (see chapter 1.4.4). However, despite induction of AKT, phosphorylation of the mTORC1 targets p70S6K, S6 and 4E-BP1 was found to be downregulated in hypoxic cervical cancer cell lines, as was described before [71]. mTORC1, which induces protein synthesis and cell growth, can be inactivated by hypoxia in many cell types via multiple pathways [176]. One mechanism implicated in hypoxic mTORC1 regulation in cervical cancer cell lines involves the REDD1/TSC2 axis. Increased expression of REDD1, stimulated by hypoxia, reactivates TSC2, an inhibitor of mTORC1 [71, 177]. The reduced phosphorylation of mTORC1 targets in hypoxic cervical cancer cells indicates that this effect is dominant over AKT-induced inhibition of TSC2 and allows repression of growth promoting signals under hypoxic conditions.

Repression of E6/E7 under hypoxia was already detectable at the mRNA level and could be counteracted by PI3K/AKT/mTOR inhibitors at this level as well. Rapamycin also

counteracted *E6/E7* mRNA repression under hypoxia to some extent. While primarily targeting mTORC1, rapamycin can, upon prolonged treatment, also inhibit mTORC2 [178], which may explain the weak reactivation of hypoxic E6/E7 expression observed upon rapamycin treatment. Interestingly, *E6/E7* mRNA expression was induced by mTOR inhibitors and showed a tendency to slightly increase after treatment with AKT inhibitors under normoxia. At the protein level this could only be observed in some cell lines. This further corroborates a negative regulation of E6/E7 expression via the PI3K/mTORC2/AKT pathway, but also shows that AKT-mediated regulation of E6/E7 expression primarily occurs under hypoxic conditions whereas normoxic E6/E7 expression is only weakly influenced by inhibiting AKT activity.

Noteworthy, while E7 protein expression was efficiently reactivated under hypoxia by PI3K/AKT/mTORC2 inhibitors in all investigated cells lines, results for E6 were less coherent with reactivated E6 protein expression in HPV16-positive SiHa and MRI-H-186 being only weakly or not detectable. E6 and E7 are translated from alternatively spliced transcripts [21]. Thus, hypoxia-induced alterations in the relative abundance of the different transcript classes or effects of PI3K/AKT inhibitors on E6/E7 splicing events under hypoxia could represent a mechanism of differential regulation of E6 and E7 levels under hypoxia. Another, yet to be investigated potential explanation may be given by alterations of E6 protein stability in HPV16-positive cells under hypoxia that counteract PI3K/AKT-inhibitor induced reactivation of E6/E7 mRNA expression.

Notwithstanding some discrepancies in regulation of HPV16 E6, it was clearly shown that pharmacological inhibition of the AKT pathway counteracts repression of viral oncogene expression in hypoxic cervical cancer cell lines. Particularly the investigation of a series of inhibitors targeting different steps in the signaling cascade that all result in comparable output on E6/E7 expression argues for a specific effect of the PI3K/mTORC2/AKT axis in regulation of E6/E7 under hypoxia.

3.3.2 Regulation of E6/E7 in the context of Ca^{2+}, energy metabolism and AKT activation

Increased cytosolic Ca^{2+} concentrations are a characteristic feature of hypoxic cells [75]. Interestingly, it was demonstrated that repression of E6/E7 under hypoxia was dependent on Ca^{2+} since downregulation of E6/E7 was prevented by treatment with the Ca^{2+} chelator BAPTA-AM. In line with a possible role of Ca^{2+} in the regulation of HPV oncogene expression, treatment with the Ca^{2+} ionophore A23187 that increases intracellular Ca^{2+} levels led to downregulation of E6/E7 expression under normoxia. However, this effect was weaker in comparison to hypoxic downregulation of E6/E7 and furthermore, A23187-mediated downregulation of E7 in normoxic SiHa cells was not detected at all. This may indicate that Ca^{2+} is essential for repression of E6/E7 under hypoxia, but that further hypoxia-induced

cellular alterations are required for an efficient downregulation. However, it is also possible that increases in cytosolic Ca^{2+} induced by treatment with A23187 were not sufficiently high.

Another key characteristic of hypoxic cells is enhanced glycolysis and reduced OXPHOS to cope with limited O_2 supply [73]. Intriguingly, blockade of OXPHOS using inhibitors for complexes I or III of the mitochondrial electron transport chain repressed E6/E7 under normoxia in a glucose-dependent manner. This is interesting in the light of the finding of our group that high glucose concentrations also counteracted hypoxia-induced repression of E6/E7 [71]. Thus, under conditions of reduced OXPHOS, generated either by hypoxia or by inhibitor treatment, E6/E7 expression was strongly downregulated which could be prevented by an excess of glucose. Moreover, E6/E7 expression was reactivated by BAPTA-AM treatment in hypoxic and OXPHOS inhibitor-treated cells indicating that repression occurs in a related Ca^{2+}-dependent manner under both conditions.

However, not only inhibition of OXPHOS but also inhibition of glycolysis using 2-deoxyglucose (2-DG) can induce downregulation of E6/E7 expression as was previously reported [179]. Like glucose, 2-DG is phosphorylated by hexokinase, the first and rate-limiting glycolytic enzyme. This phosphorylated intermediate, 2-DG-6-phosphate, cannot be further metabolized, accumulates and as a feedback mechanism inhibits hexokinase [180]. 2-DG-mediated repression of E6/E7 was also found to be counteracted by the intracellular Ca^{2+} chelator TMB-8 [179] and by high glucose concentrations that compete with 2-DG (K. Hoppe-Seyler, unpublished data).

Taken together, these results showed that cells cultured under hypoxia or treated with OXPHOS or glycolysis inhibitors downregulate E6/E7 expression which is counteracted by high glucose levels and Ca^{2+} chelators. These cells are in a state of energy shortage due to impaired ATP production, which can be counteracted by high glucose levels that cells can use to fuel ATP synthesis. Hence, results indicate that E6/E7 is downregulated under energy deprived conditions in a Ca^{2+}-dependent manner. Notably however, work from our group has revealed that E6/E7 expression was not diminished upon treatment with 3-bromopyruvate (K. Hoppe-Seyler, S. Adrian, unpublished data). This alkylating agent leads to rapid depletion of cellular ATP and was reported to inhibit both, glycolysis and OXPHOS [181], indicating that downregulation of E6/E7 upon energy shortage is more complex and not exclusively triggered by low ATP levels.

Since activation of AKT by phosphorylation was established as being essential for repression of E6/E7 under hypoxia, it was of great interest whether phosphorylation of AKT was also associated with increases in intracellular Ca^{2+} or with OXPHOS inhibition. AKT activation has been described to be facilitated by Ca^{2+}-dependent CaMs [102]. However, since phosphorylation of AKT and regulation of E6/E7 expression was neither influenced by silencing of CaM1-3 nor by treatment with the CaM inhibitor W-7, AKT activation by hypoxia

is likely mediated via a different, CaM-independent, mechanism. Moreover, hypoxia-induced phosphorylation of AKT was abrogated by treatment with the Ca^{2+} chelator BAPTA-AM only in SiHa, but not in HeLa cells. Hence, BAPTA-AM induced reactivation of E6/E7 expression under hypoxia cannot generally be attributed to an inhibition of AKT activation. The here obtained results in HeLa cells are in contrast to publications reporting an inhibitory effect of BAPTA-AM on AKT phosphorylation [182, 183]. Since BAPTA-AM mediated attenuation of AKT phosphorylation was described to occur transiently [182], it may be possible that AKT phosphorylation in HeLa cells was only impaired at earlier time-points. However, analyses of earlier time-points also did not show reduced AKT activation upon BAPTA-AM treatment in hypoxic HeLa cells (data not shown). Hence, although it is still possible that the critical time-point of BAPTA-AM induced modulation of AKT phosphorylation was missed, it is more likely that the applied BAPTA-AM concentrations that are sufficient to reactivate E6/E7 expression under hypoxia in HeLa cells do not significantly repress AKT. This could mean that Ca^{2+}-dependent E6/E7 regulation does not occur upstream of AKT signaling but rather downstream or that these mechanisms act cooperatively in E6/E7 repression.

Furthermore, E6/E7 repression induced by treatment with OXPHOS inhibitors was not associated with an activation of AKT in all cases. Instead opposing regulation of P-AKT was partially detected. Rotenone, for instance, induced AKT phosphorylation in a glucose-dependent manner in HeLa cells but abolished AKT activation in SiHa cells. Consequently, E6/E7 repression mediated by OXPHOS inhibitors does not generally act via induction of AKT.

3.3.3 Repression of E6/E7 under hypoxia is mediated by AKT1 and AKT2

AKT has three isoforms (AKT1-3) that all can be activated via PI3K/mTORC2 [95] and that are all targeted by the AKT-specific inhibitors applied in the present study (AKTi VIII, MK-2206), albeit with decreasing affinity from AKT1 to AKT3. The present work revealed that AKT1 and AKT2 are involved in hypoxic regulation of E6/E7 expression. Expression of AKT3 was not detected in HeLa cells, which fits to the described rather restricted expression of AKT3 to neuronal cells or specific cancer types such as melanoma [95, 115]. A hypoxia-induced signal obtained with a polyclonal AKT3 antibody (CST) was identified by knockdown experiments as being likely not specific for AKT3. This notion is further supported by the observation that total AKT protein levels as determined with a pan-AKT antibody showed no increase under hypoxia, but rather declined when compared to cells cultured in parallel under normoxia.

Overexpression studies of AKT1 and AKT2 revealed that both isoforms can, in principle, repress E6/E7 expression under hypoxia. Their involvement in hypoxic E6/E7 repression was further corroborated by knockdown experiments of endogenous AKT1 and AKT2. More

precisely, it was shown that combined blockade of AKT1 and AKT2 was required to efficiently counteract repression of E6/E7 under hypoxia. Together with the finding that ectopically expressed constitutively-active AKT1 and AKT2 together did not further diminish AKTi VIII-mediated reactivation of hypoxic E6/E7 expression compared to individual overexpression of the two isoforms, this strongly indicates functional redundancy of AKT1 and AKT2 in hypoxic E6/E7 repression.

The levels of P-AKT showed no detectable alterations upon silencing of AKT2 and were only weakly diminished upon transient silencing of AKT1 but were strongly repressed when both isoforms are shut down. This suggests that AKT1 and AKT2, respectively, compensate for loss of the other isoform allowing constant high levels of active AKT under hypoxia as long as one of the isoforms is still expressed. Nonetheless, AKT1 is likely the most strongly expressed isoform in HeLa cells as can be concluded from signals derived from a pan-AKT antibody that were strongly downregulated upon silencing of AKT1 and not visibly affected by silencing of AKT2. In the AKT1 silenced single cell clones, phosphorylation of AKT at S473 was equally high under normoxic and hypoxic conditions. This may be caused by an upregulation of S473 phosphorylation of AKT2 already in normoxic cells to compensate for loss of AKT1 expression which was not detected in cells where AKT1 was only transiently silenced for a shorter time period. Since this effect was only observed for S473 but not for T308 phosphorylation, an overall induction of fully activated AKT under hypoxia can still be assumed.

Counteraction of hypoxic E6 repression was observed upon combined silencing of AKT1 and AKT2, although to a weaker extent than observed for E7. This indicates that, like E7 expression, E6 expression under hypoxia is repressed by AKT1/2 but also that reactivation of E6 upon blockade of AKT1/2 is likely to require more effective AKT1/2 inhibition. This is in line with results obtained by treatment with PI3K/AKT inhibitors where counteraction of E6 repression under hypoxia was not or only weakly detected in certain cell lines. The underlying mechanism resulting in partial differences in the dimension of AKT-dependent E6 and E7 regulation under hypoxia is still unclear.

Notably, under normoxia, knockdown of AKT1 and AKT2, alone or in combination, as well as AKT pathway inhibitors did not appreciably enhance E6/E7 expression. *Vice versa*, ectopic expression of constitutively-active AKT1 and AKT2 did not repress E6/E7 expression under normoxia. Collectively these results indicate that activation of AKT alone is not sufficient to significantly diminish E6/E7 expression levels but that additional cellular alterations that occur under hypoxia and that cooperate with AKT, are necessary for efficient repression of viral oncogene expression.

The PI3K/AKT cascade has the potential to regulate the activity of transcription factors [95] and to modulate the stability of mRNAs [184, 185]. It will be interesting for future studies to

identify the downstream factors linking hypoxic AKT1/2 activation to repression of E6/E7, which was found to be linked to inhibition of HPV transcription and reduction of the E6/E7 mRNA half-life.

3.3.4 Therapeutic implications of AKT inhibition in hypoxic cervical cancer cells

Aberrant activation of the PI3K/AKT pathway is a common feature of many tumors. This also applies to cervical cancer patients whose prognosis and response to conventional treatments is closely associated with the status of PI3K/AKT signaling [124]. In line with this, the most frequently mutated gene in cervical cancer patients is *PIK3CA* that encodes a subunit of PI3K. Apart from activating mutations, PIK3CA activity is also found to be enhanced in many cervical cancer cases due to genomic amplifications [123, 186]. Cervical cancer is therefore subject to trials using PI3K/AKT/mTOR inhibitors as therapeutic agents [125, 187]. Thus, the observation that clinically tested PI3K/AKT/mTORC2 inhibitors can reactivate viral oncogene expression in hypoxic cells is extremely interesting. The downregulation of E6/E7 in hypoxic cells likely serves as a protective mechanism for the tumor. The cells are not proliferating, do not express any viral antigens and are protected from therapeutic interventions such as chemotherapy [71]. This raised the question how these cells cope with the proliferative impulse induced by E6/E7 when reactivated by PI3K/AKT/mTORC2 inhibitors under oxygen-deprived conditions, which – as an undesired scenario – may lead to increased growth of tumor cells. Time-course experiments revealed, however, that hypoxic cells treated with PI3K/AKT inhibitors did not start to proliferate again despite E6/E7 expression. This indicates that the hypoxic state of the cell, which is often linked to inhibition of cell proliferation [67], and the anti-proliferative effects of AKT inhibition are dominant above the growth-promoting signals exerted by the re-induced viral oncogenes.

Hypoxic HPV-positive cancer cells are able to reactivate E6/E7 expression and resume proliferation when they are reoxygenated [71]. This observation could be of clinical relevance, for instance when hypoxic tumor cells regain improved access to O_2 after therapy-induced tumor shrinkage, which possibly could enable tumor recurrence [71]. Hence, in the present thesis it was also investigated how hypoxic HPV-positive cancer cells alter their response to chemotherapy when treated with PI3K/AKT inhibitors. Compared to normoxic cells, hypoxic cells were shown to be more protected from etoposide-induced senescence allowing the outgrowth of many cell clones during subsequent cultivation under normoxia. Additionally, it was observed that treatment with AKTi VIII or silencing of AKT1 and AKT2 allowed the outgrowth of a higher number of colonies after etoposide treatment of HPV-positive cancer cells under normoxia. The latter may be explained by the reduced proliferation induced by AKT inhibition since highly proliferating cells are more vulnerable to chemotherapeutic agents.

Interestingly, treatment with PI3K/AKT inhibitors sensitized hypoxic HeLa cells to etoposide-induced senescence induction. The specificity of the inhibitor-mediated effects was verified in knockdown experiments revealing that single knockdown of AKT1 weakly reduced the number of outgrowing cells and that combined silencing of AKT1 and AKT2 more strongly prevented the outgrowth of cells. This demonstrated that, apart from redundantly repressing E6/E7 expression under hypoxia, AKT1 and AKT2 also protect hypoxic HeLa cells from etoposide-induced senescence in a functionally redundant manner. Experiments with ectopic overexpression of E6/E7 under hypoxia would possibly yield further information whether the AKT-induced repression of E6/E7 is a contributing factor to AKT-mediated evasion from chemotherapy-induced senescence.

Reduced outgrowth of etoposide-treated cells after concomitant treatment with PI3K/AKT inhibitors under hypoxia was exclusively observed in HeLa, but not in SiHa or SW756 cells. In line with this, silencing of AKT1 and AKT2 did not influence chemotherapy response of hypoxic SiHa cells (SW756 cells were not investigated) indicating involvement of a cell type-dependent mechanism. Since HeLa has been established from a cervical adenocarcinoma, whereas all other cell lines were derived from squamous cell carcinomas [56], it will be interesting to extent further studies to other cell lines derived from cervical adenocarcinomas. Nonetheless, the ability of PI3K/AKT inhibitors to enhance the therapeutic effects of chemotherapy is not a peculiarity of hypoxic HeLa cells but is in line with AKT-associated increased therapy resistance and has also been described for other cancer cell types [121, 145, 188].

In conclusion, it was shown that while inhibition of the PI3K/AKT pathway counteracted repression of the HPV oncogenes under hypoxia in all investigated cell lines, it influenced the behavior of HPV-positive cells towards chemotherapy in a cell line dependent manner. Importantly, PI3K/AKT inhibitor-induced reactivation of viral oncogene expression in hypoxic cervical cancer cells did not induce proliferation and had either no or beneficial effects on the therapeutic outcome after etoposide treatment in hypoxic cells. Further detailed investigations regarding the effects of PI3K/AKT pathway inhibitors on hypoxic HPV-positive cancers are required to fully evaluate the clinical implications thereof. However, given the results of the present study it is plausible that reactivation of viral oncogene expression in hypoxic HPV-positive cancer cells has no detrimental effects on treatment outcome. It may even be possible that such cells would be more vulnerable to various therapeutic approaches and to the host’s immune system since they are no longer able to downregulate viral antigen expression.

3.4 Proteome analyses as starting point for future investigations

The cornerstones of the regulatory phenomena observed in the present studies are: (i) hypoxia blocks HPV oncogene expression, an effect that can be counteracted by (ii) AKT inhibition and by (iii) high glucose supply. To gain further insights into the underlying regulatory circuits and the resulting phenotypic consequences, proteome analyses were performed in SiHa cells by comparing normoxic and hypoxic conditions and assessing the response of hypoxic SiHa cells towards AKTi VIII and 25 mM glucose. These experiments provide information about cellular proteins and pathways that are regulated in parallel or inversely with HPV E6/E7. In principle, these pathways could underly a common regulation as E6/E7 expression or, alternatively, could themselves act as upstream regulators of E6/E7 under hypoxia or as downstream regulators which mediate E6/E7-dependent cellular effects in hypoxic cells. Thus, the proteomic analyses performed here should serve as an important experimental basis to address these issues in future studies.

Interestingly, two members of the Wnt signaling pathway, Wnt-5a and DKK1, were amongst the top hits of differentially expressed proteins under hypoxia. Both proteins were downregulated under hypoxia in an AKT- and glucose-dependent manner. Wnt signaling has important functions in embryonic development and adult stem cell biology, cell proliferation and migration. Deregulated Wnt signaling is therefore associated with cancer and metabolic diseases [189]. Wnt ligands induce cellular responses by binding to members of the Frizzled receptor family. Three different branches of the Wnt pathway have been identified so far: canonical Wnt signaling via β-catenin, the noncanonical planar cell polarity pathway and the noncanonical Wnt/Ca^{2+} pathway [190]. Wnt5a is characterized for activating noncanonical Wnt signaling but has also been implicated in antagonizing the canonical Wnt/β-catenin pathway [190-192]. DKK1, a member of the Dickkopf family, is an inhibitor of canonical Wnt signaling that binds to low-density lipoprotein receptor-related protein 6 (Lrp6), a coreceptor of Frizzled, and blocks signal transduction [193]. Hence, the results from the proteomics screen revealed the hypoxia-induced downregulation of two factors that negatively regulate canonical Wnt/β-catenin signaling which argues for an induction of this pathway under hypoxia. Since Wnt/β-catenin signaling has been linked to active PI3K/AKT signaling [194, 195], it will be interesting to investigate a functional role of this pathway as upstream regulator of AKT-dependent hypoxic repression of E6/E7.

A very prominently regulated protein identified in the proteome analyses is MT2A, which was downregulated under hypoxia and reinduced again under the treatment conditions that also counteracted hypoxic E6/E7 repression. MT2A belongs to the family of metallothioneins that bind heavy metals, have been reported to protect against oxidative stress and to be associated with cellular proliferation [196]. Apart from MT2A two additional metallothioneins were detected in the proteome screen (MT1X, MT1F) that showed a similar, only less

pronounced, pattern of regulation to what was observed for MT2A. Metallothionein expression has previously been described to be negatively regulated by the PI3K/AKT pathway in human hepatocellular carcinoma cells [197]. Thus, MT2A, MT1X and MT1F represent candidates that could be commonly regulated with E6/E7 or could also play a functional role in AKT-linked upstream regulation of E6/E7. Moreover, since metallothionein expression is associated with cellular proliferation another possible scenario would be that metallothioneins are downstream targets of E6/E7 that are involved in E6/E7-linked proliferation under normoxia.

The here described candidates represent examples for differentially regulated proteins linked to E6/E7 expression in hypoxic HPV-positive cells. Since the performed proteome analyses, at current, offer only circumstantial evidence, validation experiments addressing a functional role differentially expressed proteins, will hopefully provide additional insights into pathways involved in hypoxic E6/E7 repression and, moreover, could delineate novel downstream targets for the viral oncoproteins.

3.5 Conclusions and perspectives

Due to the disappointingly low vaccination rates as well as to the lengthy natural course of disease development, HPV-linked cancers are expected to remain an important medical challenge for many decades to come. It is therefore of high importance to improve the clinical management of these devastating tumors and to develop novel therapeutic strategies. To approach this goal from a rational basis, a better understanding of the crosstalk between oncogenic HPVs and their host cell is an important prerequisite.

Hypoxic tumor cells pose a major therapeutic problem also in HPV-positive cancers. Recently, it was found that hypoxic cells strongly repress HPV E6/E7 oncogene expression. This is linked to the induction of a reversible dormant state which could contribute to therapeutic resistance, immune evasion and tumor recurrence. The present work provides now first insights into the regulatory mechanisms of hypoxic repression of HPV oncogene expression.

Firstly, hypoxic inhibition of E6/E7 protein and mRNA expression is carried out by a combination of transcriptional repression and reduced mRNA and protein stabilities. *Secondly*, a series of factors were excluded as likely candidates mediating E6/E7 repression under hypoxia. These include YY-1, HIF-1/2α, the Mlx:MondoA transcription factor network and c-Myc. *Thirdly*, repression of E6/E7 expression is dependent on Ca^{2+} metabolism in that chelation of intracellular Ca^{2+} functions in a counteractive manner. *Fourthly*, the work identified the PI3K/AKT pathway as key mediator of hypoxic E6/E7 repression. Further functional analyses revealed that downregulation of the HPV oncogenes is redundantly mediated by AKT1 and AKT2 that are activated via PI3K and mTORC2 under hypoxia (see

model in Fig. 33). In this regard, pharmacological inhibitors of the PI3K/mTORC2/AKT pathway were shown to reactivate E6/E7 expression in hypoxic cells. However, this is not associated with viral oncogene-induced proliferation and moreover, can sensitize hypoxic cells to therapeutic effects of etoposide in a cell line-dependent manner. Under normoxia, activation of AKT1 and AKT2, alone or together, was not sufficient to repress E6/E7 but required the cellular background of hypoxic cells.

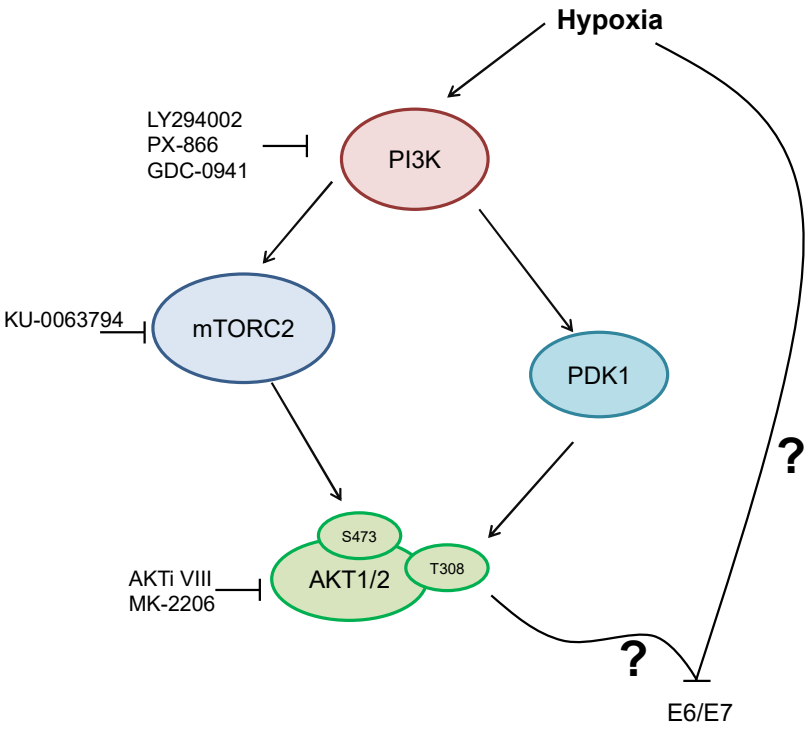

Fig. 33. Model of AKT-dependent E6/E7 regulation under hypoxia in HPV-positive cancer cells. AKT1 and AKT2 are activated under hypoxia. As an upstream regulator PI3K is required for activation of AKT, PDK1 and mTORC2. PDK1 and mTORC2 phosphorylate AKT at the residues S473 and T308, respectively, which leads to the repression of E6/E7 under hypoxia. Treatment with the indicated inhibitors interferes with AKT1/2 activation and counteracts hypoxic repression of E6/E7. The direct link between AKT and E6/E7 repression and potential further required hypoxic alterations are still unclear.

In conclusion, with the delineation of the AKT pathway as key regulator for hypoxic E6/E7 repression, interesting new insights into the crosstalk between virus and host cell have been gained. Considering the highly therapy resistant nature of hypoxic tumor cells, the present findings may create a basis for future studies addressing the development of novel treatment strategies. Ongoing work of our group and collaboration partners suggests that P-AKT is enriched in hypoxic tumor regions in biopsies derived from cervical cancer patients (immunofluorescence stainings, Arnulf Mayer, University Hospital Mainz, Germany) supporting the clinical relevance of the here obtained *in vitro* data. Mechanistically, the direct link between AKT activation and E6/E7 repression is still unclear. The proteome analyses

performed in this work provide a promising foundation to further investigate this issue and to identify relevant AKT-regulated downstream acting factors and additional cellular circuits modified under hypoxia in a glucose-dependent manner. Based on the proteome data, an important pathway which warrants further investigation is the Wnt signaling cascade which is hypoxia sensitive and functionally linked to AKT signaling [194, 195, 198]. It should also be noted that the present study focused on regulation of E6/E7 under chronic hypoxia. However, intermittent or acute hypoxia, mainly generated by defective tumor vessels, is likewise a key feature of solid tumors that has a high clinical impact [66]. Analyses of E6/E7 regulation under acute compared to chronic hypoxia are therefore also of great interest for the future.

Chapter 4

Materials and Methods

4. Materials and Methods

4.1 Reagents

Molecular biology grade reagents were applied where possible. All standard reagents for buffers and media were supplied by AppliChem (Darmstadt, Germany), BD Biosciences (Heidelberg, Germany), Bio-Rad (Munich, Germany), Carl Roth (Karlsruhe, Germany), Enzo Life Sciences (Lörrach, Germany), New England Biolabs (NEB, Frankfurt, Germany), Promega (Madison, WI, USA), Merck (Darmstadt, Germany), Sigma-Aldrich (St. Louis, M, USA) and Thermo Fisher Scientific (Waltham, MA, USA). Manufacturers of non-standard reagents are specified in the text.
All buffers and solutions were prepared with H_2O if not stated otherwise.

4.2 Cellular biology techniques

4.2.1 Cultivation of cell lines

HeLa, SiHa, SW756 and MeWo cells were cultured in Dulbecco's minimal essential medium (DMEM, Gibco, Thermo Fisher Scientific, USA). MRI-H-186 cells were cultured in RPMI 1640 medium (Gibco). The standard medium was supplemented with 10 % fetal calf serum (FCS, Gibco), 100 U/ml penicillin, 100 µg/ml streptomycin, 2mM L-glutamine (all from Sigma-Aldrich) and contained 1g/L (5.5 mM) glucose. For cell growth analyses, HeLa and SiHa cells that were transduced with a pMOWS hH2B mCherry expression vector to generate cells with red fluorescent histone H2B were provided (transduction was kindly performed by Dr. Joschka Willemsen, group of Dr. Marco Binder, DKFZ, Heidelberg). The stock cultures of the transduced HeLa mCherry H2B and SiHa mCherry H2B were kept under selection by using medium additionally supplemented with 1 µg/ml puromycin (Sigma-Aldrich). For experiments medium without puromycin was applied.
Standard cultivation of human cell lines was performed at 37 °C and 5 °CO_2 in a humidified incubator at 21 % O_2 (=normoxia). Incubation under hypoxia (= 1 % O_2, 5 % CO_2) was performed in a hypoxic incubator or in the Invivo$_2$ 400 physiological oxygen workstation (Ruskinn Technology Ltd, Bridgend, UK). To ensure a continuous adequate atmosphere, time course experiments were all performed in the Invivo$_2$ workstation.
For routine passage, cells were split every 3-4 days before reaching full confluency using 0.25 % Trypsin-EDTA solution (Gibco).
Prior to experiments number of viable cells was determined using the trypan blue method with the Countess™ Automated Cell Counter (Invitrogen, Carlsbad, CA, USA).

4.2.2 Cryopreservation and thawing of cells

For long-term storage of cells, cryopreservation was used. Cells were trypsinized, pelleted by centrifugation for 3 min at 800 g, resuspended in culture medium containing 30 % FCS and 10 % DMSO and aliquoted into cryotubes. The cryotyubes were transferred into an isopropanol-filled freezing container (Nalgene, Thermo Fisher Scientific) and kept for several days at -80 °C and finally stored in liquid nitrogen.
For thawing, cells were rapidly warmed to 37 °C in a water bath, resuspended in fresh culture medium and transferred into a new cell culture flask. Medium was removed and replenished the following day.

4.2.3 Treatment of cells with chemical compounds

Cells were treated with inhibitors or small molecule compounds (see Tab. 2) 1-2 days after seeding. The compounds were added directly into the medium and the appropriate volume of the solvent was applied to control cells.

Tab. 2. Chemical compounds.

Compound	Solvent	Final concentration	Supplier
5-Aza-2'-deoxycytidine (Decitabine)	DMSO	10 µM	Sigma-Aldrich
A23187	DMSO	5 µM	Enzo Life Science
AKT inhibitor VIII/ AKT1/2-inhibitor (AKTi VIII)	DMSO	5-10 µM	Sigma-Aldrich
Antimycin A	Ethanol	0.2-5 µM	Sigma-Aldrich
BAPTA-AM	DMSO	20-50 µM	Enzo Life Science
Etoposide	DMSO	10 µM	Enzo Life Science
GDC-0941	DMSO	5-10 µM	Selleck Chemicals (Houston, USA)
JQ1	DMSO	1-20 µM	Cayman Chemical (Ann Arbor, USA)
KU-0063794	DMSO	1-5 µM	Sigma-Aldrich
LY294002	DMSO	20 µM	Cayman Chemical
Metformin	DMEM	2.5 mM	Enzo Life Science
MK-2206	DMSO	1-10 µM	AdipoGen (San Diego, USA)
PX-866	DMSO	1-10 µM	Focus Biomolecules
Rapamycin	DMSO	50 nM	AdipoGen
Rotenone	DMSO	10-500 nM	Sigma-Aldrich
W-7	DMSO	10-50 µM	Cayman Chemical

4.2.4 Transfection of synthetic siRNAs

For transfection of synthetic siRNAs (Ambion, Thermo Fisher Scientific), cells were seeded in 6cm dishes and transfection was performed on the following day when cells had reached 30-40 % confluency. Prior to transfection, standard cell culture medium was replaced by 1.6 ml of cell culture medium lacking penicillin and streptomycin. For each dish 4 or 6 µl of the

transfection reagent DharmaFECT1, for HeLa or SiHa cells respectively, were pre-incubated in a final volume of 200 µl of reduced serum medium Opti-MEM I (Gibco) for 5 min at room temperature (RT). In parallel, 2-4 µl of the 10 µM siRNA stock solution were equally pre-incubated with Opti-MEM I in a final volume of 200 µl. Both solutions were then mixed and incubated for 20 min at RT. Subsequently, the 400 µl transfection mix was added dropwise to the cells to reach a final siRNA concentration of 10 or 20 nM as indicated in Tab. 3. The medium was replaced with standard cell culture medium 24 h after transfection. Harvesting of cells for downstream analyses was carried out 72 h after transfection.

Stock solutions of lyophilized synthetic siRNAs (10 µM) were prepared with nuclease-free H_2O. For transfection of AKT1- and AKT2-targeting siRNA, a pool of several siRNAs (referred to as siAKT1 and siAKT2) in equimolar concentrations was used. As a negative control, an siRNA that contains at least four mismatches to all known human genes was applied (siContr1).

Tab. 3. Synthetic siRNAs.

Target transcript	siRNA	siRNA sequence	Final concentration
AKT1	siAKT1 #1	5′-GCGUGACCAUGAACGAGUU-3’	20 nM
	siAKT1 #2	5′-CGGUAGCACUUGACCUUUU-3’	
AKT2	siAKT2 #1	5′-UGACUUCGACUAUCUCAAA-3’	20 nM
	siAKT2 #2	5′-CAACUUCUCCGUAGCAGAA-3’	
BRD4	siBrd4	5′-AGAUUGAAAUCGACUUUGA-3’	10 nM
-	siContr-1	5′-CAGUCGCGUUUGCGACUGG-3’	10-20 nM

4.2.5 Transfection of plasmid DNA and generation of single cell clones

Transfection of plasmid DNA was performed by means of the calcium phosphate coprecipitation technique according to Chen and Okayama [199]. In brief, cells were seeded in 6cm dishes in 3 ml of standard culture medium and DNA was transfected the next day when cells were 30 % confluent. Prior to transfection, plasmid DNA of interest was adjusted with pBluescript II vector (Stratagene, Heidelberg, Germany) to a final amount of 6 µg DNA per dish, if necessary. DNA was mixed with 150 µl of 0.25 M $CaCl_2$ and then with 150 µl 2x BES buffer (50 mM BES, 280 mM NaCl, 1.5 mM Na_2HPO_4, pH 6.95). The transfection mix was incubated for 10-20 min at RT and afterwards added dropwise to the cells. Cells were kept in a humidified incubator at 35 °C and 3 % CO_2 for 16-18 h. Medium was then removed, cells were washed once with medium and fresh medium was added for further incubation under standard conditions if not indicated otherwise. Harvesting of cells was usually performed 48 h after transfection or 72 h after transfection in the case of shRNA expressing pSuper plasmids.

Transfection of CRISPR plasmids was performed as described above. Standard culture medium was replaced 36 h after transfection with medium containing 1 µg/ml puromycin to select for successfully transfected cells. Cells were kept under selection medium for up to 5 days until all cells of a mock transfected plate were dead. Cells were then cultured in standard medium and either used directly as a pool for further experiments or seeded for generating single cell clones. To that end, cells were seeded in 96 well plates by performing serial dilution. Single cell clones were identified by eye using light microscopy and cultured until a sufficient number of cells were available. Efficiency of the knockdown was evaluated by detecting protein expression using immunoblot analyses.

4.2.6 Luciferase reporter assay

The activity of the HPV transcriptional control region, also designated upstream regulatory region (URR), under hypoxia was investigated by means of luciferase reporter assays with reporter plasmids that express firefly luciferase under the control of different elements of the HPV URR. All vectors for luciferase assays were kindly provided by Karin Hoppe-Seyler. All reactions were performed in duplicates for each individual experiment.

Transfection of plasmid DNA by the calcium phosphate coprecipitation technique was performed as described in chapter 4.2.5. The transfection mix for each sample contained additionally 0.2 µg pCMV-Gal plasmid as an internal standard to adjust for variations in the transfection efficiency by measuring β-galactosidase activity. Lysis of cells for luciferase and β-galactosidase activity measurements was carried out 48 h after transfection and 24 h after incubation under hypoxia. Cells were first washed with ice-cold PBS and then scraped in 200 µl triton lysis buffer (25 mM glycylglycine pH 7.8, 15 mM $MgSO_4$, 4 mM EGTA, 1 mM DTT, 10 % glycerol, 1 % Triton X-100). Samples were kept on ice during this procedure. Cellular debris was pelleted by centrifugation at 12,000 *g* and 4 °C for 5 min. For determination of luciferase activity, 30 µl of the supernatant were transferred into a 96 well plate. Measurement was carried out with a luminometer (LB943 Mithras^2, Berthold Technologies, Bad Wildbad, Germany). The luminometer injects 150 µl luciferase reaction buffer (25 mM glycylglycine pH 7.8, 15 mM $MgSO_4$, 5 mM ATP) and 50 µl luciferin solution (0.25 M luciferin in luciferase reaction buffer devoid of ATP) to each sample.

The luciferase that is expressed from the transfected reporter constructs catalyzes the ATP-dependent oxidation of luciferin to oxyluciferin and CO_2 whilst emitting light at 562 nm. The detected light is proportional to the expression of luciferase and thus allows to assess the transcriptional activity. To account for the transfection efficiency, luciferase values were normalized to the respective values of the β-galactosidase activity.

Tab. 4. Plasmids for Luciferase assays.

Vector designation	Comment	Source
pCMV-Gal	β-galactosidase expression	[200]
pBluescript II (pBL)	empty vector	Stratagene
HPV18URRL	luciferase reporter construct	[36]
p438/18L	luciferase reporter construct	[36]
p232/18L	luciferase reporter construct	[36]
pBtk*L	basis vector HSV TK promoter	[36]
p230s/tk*L	luciferase reporter construct	[36]
p116s/tk*L	luciferase reporter construct	[36]
pGAPDHLuc	luciferase reporter construct (1112 bp of the GAPDH promoter driving firefly luciferase)	[201]

4.2.7 β-galactosidase assay

To determine transfection efficiency of luciferase reporter assays, β-galactosidase activity was measured in parallel. 20-50 µl of the cell lysate were pipetted in a clear 96-well plate and 200 µl galactosidase reaction buffer (60 mM Na_2HP0_4, 40 mM NaH_2PO_4, 10 mM KCl, 1 mM $MgSO_4$, 1mg/ml ortho-nitrophenyl-β-galactoside (ONPG)) were added. Due to the hydrolysis of ONPG catalyzed by β-galactosidase, the yellow-coloured o-nitrophenol is produced and absorbance can be measured at 405 nm with an ELISA plate reader (Multiskan Ex, Thermo Electron, Karlsruhe, Germany). To account for unspecific absorbance, an additional measurement at 620 nm is performed and subtracted from values obtained at 405 nm.

4.2.8 Colony formation assay

A colony formation assay (CFA) is a landmark technique that was initially established to study the effects of radiation or chemotherapeutic drugs on the reproductive viability of cells by determining their clonogenic capabilities.

To investigate the effects of etoposide in combination with PI3K/AKT inhibitors under hypoxia and normoxia, cells were seeded in 6cm dishes and treated with PI3K/AKT inhibitors before incubation under normoxia or hypoxia as indicated. For CFAs of AKT1/2-silenced cells, cells were treated with DMSO or AKTi VIII 24 h after siRNA transfection and kept under hypoxia or normoxia. Etoposide (10 µM) was added 24 h after inhibitor treatment. For hypoxic cells, etoposide treatment was performed in the hypoxia workstation to ensure a constant oxygen concentration of 1 %. Cells were removed from the hypoxia workstation 48 h after etoposide treatment, split into new 6 cm dishes in ratios ranging from 1:2 to 1:200 and further kept in standard cell culture medium under normoxia.

The 1:2, 1:5 and 1:10 splits were used for senescence assays (SAs, see chapter 4.2.9)

Fixing and staining of the colonies was performed 9-12 days after splitting. For this purpose, medium was discarded, and cells were washed with phosphate-buffered saline (PBS 137 mM NaCl, 2.7 mM KCl, 4.3 mM Na_2HPO_4, 1.4 mM KH_2PO_4, pH 7.4). 350 µl of a

formaldehyde-crystal violet solution (12 mM crystal violet, 29 mM NaCl, 3.7 % formaldehyde, 22 % ethanol) were added per 6cm dish and incubated for 5 min. Dishes were then washed with H_2O and dried at 37 °C before taking images with the Epson Perfection 4990 Photo Scanner.

4.2.9 Senescence assay

To identify senescent cells, senescence associated β-galactosidase (SA-β-Gal) activity was detected. The enzymatic activity of SA-β-Gal is detectable at pH 6.0 using the chromogenic substrate X-Gal (5-bromo-4-chloro-3-indolyl β D-galactopyranoside) [202]. This enzymatic reaction eventually yields an insoluble blue product (5,5'-dibromo-4,4'-dichloro-indigo) that can be visualized by bright field microscopy.
For senescence assays (SAs) cells were treated and split as described for CFAs (see chapter 4.2.8) Staining of senescent cells was performed 5-6 days after splitting. First, cells were washed with PBS. Next, they were fixed in 1 ml fixation buffer (2 % formaldehyde, 0.2 % glutaraldehyde in PBS) per dish for 3 min at RT. After removing the fixation buffer and additional washing with PBS, 1.5 ml senescence assay buffer (40 mM citric acid, 150 mM NaCl, 2 mM $MgCl_2$, adjusted to pH 6.0 with Na_2HPO_4 and freshly supplemented with 5 mM $K_3[Fe(CN)_6]$, 5 mM $K_4[Fe(CN)_6]$ and 1 mg/ml X-Gal) were added and cells were incubated in a wet chamber for 16-24 h at 37 °C. Senescence assay buffer was then removed and PBS was added to the 6 cm dishes. Images of representative cells were taken with a brightfield microscope (EVOS XL Core Cell Imaging System, Life Technologies, Calsbad, CA, USA).

4.2.10 Cell growth analyses

Cell growth was assessed by staining with crystal violet. To this end, HeLa and SiHa cells were seeded in 96-well plates at a density of $3x10^3$ cells per well. One plate was used for each time point. 24 h after seeding, medium was replenished (100 µl per well) and cells were treated with inhibitors or solvent control and cultured under hypoxia or normoxia as indicated. All treatments were performed in quadruplicates. Cells were stained 0, 24, 48 and 72 h after treatment. For this purpose, medium was removed, cells were washed with 200 µl PBS and 30 µl formaldehyde-crystal violet solution (see chapter 4.2.8) were added per well. After 5 min of incubation, plates were washed with H_20, dried at 37 °C and stored in the dark at RT until further processing. For quantification of cells, 30 µl 33 % acetic acid per well were added to dilute cell-bound crystal violet. After 5 min incubation, absorbance was measured at 570 nm with a SPECTROstar Nano Absorbance Reader (BMG Labtech, Ortenberg, Germany).

Alternatively, cell growth was assessed using the IncuCyte® S3 Live-Cell Analysis System under normoxia or the IncuCyte® ZOOM Live-Cell Analysis System (both Essen BioScience, Ann Arbor, USA) under hypoxia. For IncuCyte® analyses, nuclei-labelled HeLa mCherry H2B and SiHa mCherry H2B cells were seeded in 96 well plates in triplicates and number of cells was determined as red object count.

4.3 Chromatin-based techniques

4.3.1 Methylated DNA immunoprecipitation (MeDIP)

Methylated DNA immunoprecipitation (MeDIP) was performed in cooperation with Dr. Thomas Günther and Prof. Dr. Adam Grundhoff (Heinrich-Pette Institute, Hamburg).
SiHa cells were seeded in 10 cm plates. 2 days after seeding medium was replenished and cells were incubated for 24 h under hypoxia or normoxia. Cells were washed once with PBS supplemented with 2 mM EDTA and afterwards lysed directly on the plate in 1 ml 3x DNA lysis buffer (70 mM Tris, 2.5 mM EDTA, 3 % sarcosyl) and 2 ml PBS plus EDTA. Lysate was transferred in a 15 ml falcon and 200 µg/ml proteinase K was added. To allow digestion of cellular proteins, lysate was incubated for 7 h at 55 °C in a water bath and then stored at 4 °C. Isolation of genomic DNA was performed by phenol extraction. To that end one volume of phenol:chloroform:isoamyl alcohol (25:24:1) was added per sample, incubated for 15 min while rotating and centrifuged for 10 min at 850 *g* at RT. Supernatant was transferred to a new tube and one volume of chloroform:isoamyl alcohol (24:1) was added. After incubation for 30 min while rotating, sample was centrifuged again and the supernatant was transferred to a new tube. To precipitate DNA, one volume of isopropanol and 0.1 volume of 3 M sodium acetate (pH 5.2) was added and DNA was pelleted by centrifugation for 1 h at 2000 *g* at 4 °C. DNA pellet was washed once with 70 % ethanol and air-dried before resuspending in 1 ml nuclease-free H_2O.
Immunoprecipitation of methylated DNA and following qPCRs were carried out by Dr. Thomas Günter (Heinrich-Pette Institute, Hamburg) as previously described [203]. Primer sequences are indicated in Tab. 5.

4.3.2 Chromatin immunoprecipitation (ChIP)

H3K4me3 and H3K27me3 at the HPV URR was assessed by chromatin immunoprecipitation (ChIP) in a cooperation with Dr. Thomas Günther and Prof. Dr. Adam Grundhoff (Heinrich-Pette Institute, Hamburg).
SiHa cells were seeded in 10 cm plates and 2 days later medium was replenished, and cells were incubated for 24 h under hypoxia or normoxia. Proteins were cross-linked with DNA by adding 1 % formaldehyde to the cell culture medium. Fixation was carried out for 10 min at

RT before reaction was stopped by applying 125 mM glycine solution for 5 min. Medium was then removed, cells were washed two times with ice-cold PBS, scraped from the plate in 2 ml ice-cold PBS and transferred to a 15 ml falcon tube. Cells were pelleted by centrifugation for 3 min at 200 *g* and 4 °C. Supernatant was removed and the cell pellet was stored at -80 °C until further use.

The following ChIP and qPCRs were performed by Dr. Thomas Günter (Heinrich-Pette Institute, Hamburg) according to a recently published protocol [204]. Primer sequences for qPCRs are given in Tab. 5

Tab. 5 Primer for MeDIP and histone ChIPs.

Genomic target region	Designation	Sequence of forward (for) and reverse (rev) primer	amplicon length
C1orf43	C1orf43	for: 5'-AGTGGGTGGAGAATGCAGAC -3'	89 bp
		rev: 5'-GAGATTACCCCACCCCATTC -3'	
Glut1 regulatory region	Glut1prom	for: 5'-CCCTAGTGCACCGAAGTCAC-3'	98 bp
		rev: 5'-GTACCCGGCTGTAAGGCAAG-3'	
HOXC13	HOXC13	for: 5'-GAGCCCGAGATTCACTCAAC-3'	90 bp
		rev: 5'-TTATGCCCAGTTTTGGGGTA-3'	
HPV16 L1	HPV16L1	for: 5'-GTCGTGGTCAGCCATTAGGT-3'	89 bp
		rev: 5'-TGCTGCATAAGCACTAGCATTT-3'	
HPV16 L2	HPV16L2	for: 5'-GCGGACGCACTGGGTATATT-3'	102 bp
		rev: 5'-AAGGGCCCACAGGATCTACT-3'	
HPV16 URR	HPV16URR_1	for: 5'-GTTGAACCGAAACCGGTTAGT-3'	70 bp
		rev: 5'-TCCTGAAACATTGCAGTTCTCTT-3'	
HPV16 URR	HPV16URR_2	for: 5'-ACTGCTTGCCAACCATTCCA-3'	107 bp
		rev: 5'-TAAGGCGTTGGCGCATAGTG-3'	
SHANK1 (CpG island)	CpG 4	for: 5'-GCTTTTCGAAGCTGTTGGAG-3'	71 bp
		rev: 5'-GGAAGATGGCGAATTCCTTT-3'	
tubulin alpha-1c chain	Tuba1C	for: 5'-TGGTAGTCTGTTAGTGGGAGATCCT-3'	62 bp
		rev: 5'-GGTCTGCGGCGGTGAA-3'	
VEGF regulatory region	VEGFprom	for: 5'-CTCTGGACAGAGTTTCCGGG-3'	79 bp
		rev: 5'-CAATGAAGGGGAAGCTCGAC-3'	

4.4 DNA-based techniques

4.4.1 Transformation of bacteria

Transformation of bacteria with plasmid DNA was performed according to the protocol of Hanahan [205].

Competent bacteria of the *E.coli* strain TG2 were used for transformation. They were generated by growing the bacteria overnight at 37 °C in Lysogeny Broth (LB) medium (1% Bacto trypton, 0.5% yeast extract, 170 mM NaCl, pH 7.0). Bacteria were then pelleted and resuspended in transformation buffer (10% polyethylene glycol 8000, 5% DMSO, 50 nM $MgCl_2$, 15% glycerol in LB medium, pH 6.5). Bacteria were frozen in liquid nitrogen and stored at -80 °C.

For transformation, competent TG2 bacteria were thawed on ice. 100 µl of bacteria suspension was mixed with 50-100 ng plasmid DNA and incubated for 30 min on ice. A heat-shock at 42 °C in a water bath was carried out for 45 sec, followed by incubation on ice for 3 min. 800 µl LB medium was added to the bacteria mixture and they were incubated at 37 °C while shaking for 45 min. The transformation reaction or a fraction thereof was then streaked on an LB agar plate (1.5 % agar agar for bacteriology (Gerbu, Heidelberg, Germany)) in LB medium and grown overnight at 37 °C. The LB agar plate was supplemented with the appropriate antibiotic (100 µg/ml ampicillin). Alternatively, the transformation mixture was used to inoculate an overnight culture of LB medium supplemented with ampicillin.

4.4.2 DNA preparation and enzymatic modification

Isolation of plasmid DNA

Cultures of transformed bacteria in LB medium supplemented with ampicillin, shaken at 37 °C overnight, were used for isolation of plasmid DNA. The PureLink™ Quick Plasmid Miniprep Kit (Invitrogen) or the PureLink™ HiPure Plasmid Filter Midiprep Kit (Invitrogen) were applied according to the manufacturer's protocol for the preparation of small and medium amounts of plasmid DNA.

The preparation of larger amounts of plasmid DNA was performed by the maxipreparation protocol based on Sambrook and Russell [206]. To that end, transformed bacteria were pelleted, resuspended in solution I (50 mM glucose, 25 mM Tris, 10 mM EDTA, pH 6.7), lysed in freshly prepared solution II (0.2 M NaOH, 1% SDS) and neutralized with solution III (3 M potassium acetate, 11.5% acetic acid). After briefly chilling on ice, lysate was centrifuged at 5,500 *g* and 4 °C for 10 min to pellet cellular debris. The plasmid-containing supernatant was transferred to a fresh tube and 20 ml isopropanol was added to precipitate DNA. After incubation for 30 min on ice, plasmid DNA was pelleted at 5,500 *g* and 4°C for 30 min. The pellet was resuspended in 4 ml TE buffer (10 mM Tris, 1 mM EDTA, pH 8.0) supplemented with 100 µl ethidium bromide solution (10 mg/ml). Samples were transferred to 6 ml PA Ultraclimp tubes (Sorvall, Asheville, NC, USA) and filled up with with CsCl solution (44 g CsCl, 41 ml TE, 1 ml ethidium bromide (10 mg/ml)). Ultracentrifugation was then carried out at 220000 *g* at 20 °C for 16 h in an OTD75B Sorvall Ultracentrifuge. The supercoiled plasmid DNA, visible through incorporation of ethidium bromide, was extracted and transferred to a 50 ml falcon tube. To remove ethidium bromide from plasmid DNA, extraction with water-saturated 1-butanol was performed several times. Precipitation of plasmid DNA was then carried out by adding 2 volumes of ethanol and incubating at -20 °C for 1 h. Following centrifugation at 5500 *g* and 4 °C for 30 min, DNA was resuspended in 4ml TE buffer supplemented with 160 µl of a 5 M NaCl solution. DNA was again precipitated with

ethanol and pelleted by centrifugation. Purified plasmid DNA was finally resuspended in 200--500 µl TE buffer and concentration was determined with the NanoDrop ND-100 spectrophotometer (Peqlab, Erlangen, Germany).

Restriction digestion

Restriction endonucleases from NEB or Fermentas were applied according to the manufacturer's protocol. For analytical digestion 0.5-1 µg of DNA was used in final volume of 20 µl and incubated for 1 h at 37 °C in a water bath. Preparative digestion was performed with 20 µg of plasmid DNA in a final volume of 50 µl and incubation for 2 h at 37 °C in a water bath. Preparative digestion of pLentiCRISPRempty with BsmBI was performed at 55 °C in a water bath for 1 h.

Dephosphorylation of 5' termini

The 5'-terminal phosphates of linearized plasmids were hydrolyzed to avoid recirculation. For this purpose, digested plasmid DNA was incubated with 5-30 units of calf intestinal alkaline phosphatase (CIP, NEB) in a final volume of 50 µl for 1 h at 37 °C in a water bath.

DNA precipitation with ethanol

To precipitate plasmid DNA from aqueous solutions, 2.5 volumes of ice-cold ethanol and 0.1 volume of 3 M sodium acetate (pH 5.2) were added and incubated at - 20 °C for 30-60 min. DNA was pelleted by centrifugation and washed once with 70 % ethanol. The pellet was then air-tried before dissolving in TE buffer.

Agarose gel electrophoresis and purification of DNA fragments

DNA fragments were separated according to their size by horizontal agarose gel electrophoresis. Dependent on the expected fragment size 1-2 % of agarose were dissolved by boiling in electrophoresis buffer (40 mM Tris, 5 mM sodium acetate, 1 mM EDTA, pH 7.8). PeqGREEN non-toxic DNA/RNA dye (Peqlab) was added at a dilution of 1:20,000 and the solution poured into a gel chamber (Peqlab). After allowing it to cool down, the gel was put into an electrophoresis chamber (Peqlab) that was filled with electrophoresis buffer. DNA samples were mixed with 6x DNA loading buffer (0.25 % bromphenol blue, 0.25 % xylencyanol, 30 % glycerol) and loaded on the gel. 5 µl of SmartLadder (Eurogentec, Seraing, Belgium) were applied as size marker. The gel was run at 80-100 V for 30-90 min. DNA was visualized via UV transillumination in a gel documentation system (Intas Science Imaging Instruments, Göttingen, Germany).

If DNA fragments were to be extracted from the agarose gel for cloning purposes, the QIAquick Gel Extraction Kit (Qiagen, Hilden, Germany) was applied according to the manufacturer's instructions.

Ligation

DNA fragments were inserted into linearized and 5'-dephosphorylated vectors. For the ligation procedure, 50-100 ng of vector were mixed with a 3-7 fold molar excess of the insert, 2 units of T4 DNA Ligase (Life Technologies) and the supplied reaction buffer in a final volume of 10-20 µl. The ligation reaction was incubated for 2 h at 21 °C or overnight at 16 °C. The T4 DNA ligase was then heat-inactivated for 10 min at 65 °C.

For amplification, TG2 bacteria were transformed with the ligation mixture as described. Success of cloning was confirmed by analytical digest followed by agarose gel electrophoresis and by sequencing. Sequencing services were provided by MWG-Biotech. Analysis of the sequences was performed using the Basic Local Alignment Search Tool provided by the National Center for Biotechnology Information.

4.4.3 Plasmids and cloning strategy

pSuper plasmids

shRNAs (short hairpin RNAs) were transcribed from pSuper (suppression of endogenous RNA) plasmids by the H1 RNA polymerase III promoter [207]. The pSuper transcript consists of a 19nt siRNA sequence directed against the target transcript in sense and antisense orientation separated by a hairpin that is processed to a functional siRNA upon expression in mammalian cells. The applied pSuper plasmids and their shRNA target sequences are listed in Tab. 6. The shRNA target sequences for Mlx were designed using an online tool provided by the Hannon lab (Cold Spring Harbor Laboratory, USA, http://cancan.cshl.edu/RNAi_central/RNAi.cgi?type=siRNA). All other target sequences are derived from the sources indicated in Tab. 6. All shRNAs were tested individually and then, if available, pooled at equimolar concentrations for further experiments.

To clone a specific shRNA into pSuper, the synthetic sense and antisense shRNA oligonucleotides (Eurofins Genomics, Ebersberg, Germany) were mixed and incubated for 5 min at 95 °C. To achieve annealing, the oligonucleotide mix was then incubated for 10 min at 70 °C in a water bath and slowly cooled down in the water bath until reaching 30 °C. Annealing of the oligonucleotides resulted in sticky ends required for. The 5'-termini of the double stranded oligonucleotides were phosphorylated using T4 polynucleotide kinase (PNK, NEB) in the supplied buffer supplemented with 1 mM ATP for 30 min at 37 °C followed by enzyme inactivation for 10 min at 70 °C in a water bath. The reaction was slowly cooled

down in the water bath to RT and subsequently ligated into Bgl II- and Hind III-digested and 5'-dephosphorylated pSuper.

Tab. 6. pSuper plasmids.

Vector	target transcript	shRNA target sequence	source for target sequence
pSuper shCalm1-1	*CALM1*	5′-AGGCAUUCCGAGUCUUUGA-3′	Ambion
pSuper shCalm1-2	*CALM1*	5′-GCCUUCUCCCUAUUUGAUA -3′	Ambion
pSuper shCalm2	*CALM2*	5′-GCACAAUUGACUUCCCUGA -3′	Ambion
pSuper shCalm3-1	*CALM3*	5′-AGAUGAUCAGGGAGGCUGA -3′	Ambion
pSuper shCalm3-2	*CALM3*	5′-GACUUCCCGGAGUCCUGA -3′	Ambion
pSuper shHif-1α-1	*HIF-1α*	5′-CUAACUGGACACAGUGUGU-3′	[208] *
pSuper shHif-1α-2	*HIF-1α*	5′-CUGAUGACCAGCAACUUGA-3′	[209] *
pSuper shHif-2α-1	*HIF-2α*	5′-GCGACAGCUGGAGUAUGAA-3′	[208] *
pSuper shHif-2α-2	*HIF-2α*	5′-CAGCAUCUUUGAUAGCAGU-3′	[210] *
pSuper shMlx-2	*MLX*	5′-UCAUGAAAGUGAACUAUGA-3′	online tool Hannon lab
pSuper shMlx-3	*MLX*	5′-CUGACCAGGUCAAGUUCAA-3′	online tool Hannon lab
pSuper shMondoA	*MONDOA*	5′-GAACAACUGCUCAGGGAAA-3′	[211]
pSuper shMyc	*c-MYC*	5′-CGAUGUUGUUUCUGUGGAA-3′	[212]
pSuper shYY1-1	*YY1*	5′-GCAAGAAGAGUUACCUCAG-3′	[213] *
pSuper shYY1-2	*YY1*	5′-GGCAGAAUUUGCUAGAAUG-3′	[213] *
pSuper	-	empty vector	[207]
pSuper shContr-1	-	5′-CAGUCGCGUUUGCGACUGG-3′	*
pSuper shNeg	-	5′-UACGACCGGUCUAUCGUAG-3′	*

* Plasmids were kindly provided by Karin Hoppe-Seyler & Claudia Lohrey

CRISPR plasmids

For generating AKT1 and AKT3 knockdown cells, the CRISPR/Cas9 (CRISPR = clustered regularly interspaced short palindromic repeats, Cas = CRISPR-associated) system was used. This technique is based on findings of an acquired defense mechanism of bacteria against phage infections [214]. To generate knockdowns in mammalian cell lines we exploit the type II CRISPR system [215]. In brief, a Cas9 endonuclease is guided to the target site in the gene of interest by an artificially designed guideRNA (gRNA), which combines features of the CRISPR RNA (crRNA) and the trans-activating RNA (tracrRNA). The gRNA contains a 20 nt sequence complementary to a sequence in the target gene that is located next to a so-called protospacer adjacent motif (PAM, 5'-NGG-3' for Cas9 from *Streptococcus pyogenes*). The Cas9 induces a DNA double-strand break at the target site and due to error-prone non-homologous end joining repair (NHEJ) small insertions or deletions (indels) are generated leading to a disruption of the reading frame.

The here applied vector LentiCRISPRv1 (Addgene, USA, plasmid #49535) contains an expression cassette for Cas9 and a second cassette for the gRNA. Single gRNAs were designed using the online tool E-CRISP (http://www.e-crisp.org/E-CRISP/, version 5.3)

provided by the Boutros lab (DKFZ, Heidelberg) or were taken from Doench et al. [216]. The 20 nt sequence was complemented with CACC at the 5'-termini of the sense strand and with AAAC at the 5'-termini of the reverse strand to create overhangs for the cloning site. Cloning of the gRNAs into the LentiCRISPRv1 was performed according to the protocol developed by the Zhang lab [217]. The single gRNAs were phosphorylated using T4 PNK in the supplied buffer supplemented with 1 mM ATP for 30 min at 37 °C, followed by 5 min at 95 °C. To anneal the single gRNAs, the reaction mix was cooled down to 25 °C in steps of 5 °C per min in the MJ Research PTC-200 thermal cycler (Global Medical Instrumentation, Ramsey, USA) LentiCRISPRv1 vector was linearized by digestion with BsmBI, cutting out a 1885 nt filler sequence. The linearized vector was then 5'-dephosphorylated and purified by agarose gel electrophoresis before the dimerized gRNA was ligated into it.

Tab. 7. CRISPR plasmids.

Vector	Target transcript	gRNA target sequence	Source for target sequence
LentiCRISPRv1	-	(no gRNA inserted)	
LentiCRISPRv1 AKT1 gRNA1	*AKT1*	5′-GACGTGGCTATTGTGAAGGA-3′	[216]
LentiCRISPRv1 AKT1 gRNA4	*AKT1*	5′-TGTCATGGAGTACGCCAACG-3′	[216]
LentiCRISPRv1 AKT3 gRNA1	*AKT3*	5′-GAGAATATATAAAAAACTGG-3′	www.e-crisp.org
LentiCRISPRv1 AKT3 gRNA2	*AKT3*	5′-GCCACTGAAAAGTTGTTGAG-3′	www.e-crisp.org
LentiCRISPRv1 AKT3 gRNA3	*AKT3*	5′-GTCGTTCTGTTTTCATTAAC-3′	www.e-crisp.org
LentiCRISPRv1 AKT3 gRNA4	*AKT3*	5′-ATTTCATGTAGATACTCCAG-3′	[216]

Protein expression vectors

Protein expression vectors were obtained from the sources indicated in Tab. 8. pLNCX1 basic vector was generated by cutting out the insert from the Addgene vectors #15989. This was performed by restriction digestion with Hind III/Cla I. Blunt ends were generated using T4 DNA polymerase (NEB) according to the manufacturer's instructions, followed by re-ligation of the linearized vector.

Tab. 8. Further protein expression vectors.

Vector designation	Designation in this thesis	Expressed protein	Source
pcDNA3	pcDNA3	-	Invitrogen
pcDNA3 YY1	pcDNA3 YY1	YY1	kindly provided by N. Lützner (Group of Prof. Dr. Frank Rösl, DKFZ, Heidelberg)
pLNCX1	pLNCX1	-	cloned from Addgene #15989
pLNCX1 myrAKT1 delta4-129	myrAKT1 deltaPH	myristoylated AKT1, deletion4-129 (HA tagged)	Addgene #15989 [218]
pLNCX1 myrAKT2 deltaPH	myrAKT2 deltaPH	myristoylated AKT2, deletion1-107 (HA tagged)	Addgene #27294 (kind gift from Morris Birnbaum)
pLNCX1 myr HA AKT1 K179M	AKT1 K179M	myristoylated AKT1, mutation K179M (HA tagged)	Addgene #9006 [219]

4.5 Protein-based techniques

4.5.1 Protein extraction from cells

To generate protein extracts for immunoblot analyses, cells were usually seeded in 6 cm dishes and treated according to the experimental setup. At the time point of harvesting, cells were washed with ice-cold PBS and 150 µl ice-cold CSK-1 lysis buffer (10 mM PIPES pH 6.8, 300 mM NaCl, 1mM EDTA, 300 mM sucrose, 1 mM $MgCl_2$, 0.5% Triton X-100) was added. The lysis buffer was freshly supplemented with 100 µl PhosSTOP phosphatase inhibitor cocktail (Roche Diagnostics, Risch-Rotkreuz, Switzerland), 25 µl Pefabloc (Merck, Darmstadt, Germany) and 10 µl P8340 protease inhibitor cocktail (Sigma-Aldrich) per 900 µl CSK-1 buffer. Cells were scrapped from the dish using a rubber cell scraper and transferred into a 1.5 ml tube.

For time course experiments, cells were washed and scraped in ice-cold PBS. The cell suspension was centrifuged for 10 s at 13000 *g* and the supernatant was removed. The cell pellet was stored at - 20 °C until all samples were collected. Sample preparation was then continued by lysing the pellets in an appropriate volume of CSK-1 buffer, freshly supplemented with phosphatase and protease inhibitors as described before.

Cell lysates (derived from frozen pellets or from directly lysed cells) were incubated for 30 min on ice to allow proper cell lysis before cellular debris was removed by centrifugation for 5 min at 13000 *g* and 4 °C. The supernatant was transferred to a fresh 1.5 ml tube. Protein concentration of the cell lysate was determined by the Bradford assay. To this end, 1-3 µl of the cell lysate was mixed with 1ml of the 1:5 diluted protein assay dye reagent concentrate (BioRad) in a disposable cuvette (BRAND® semi-micro disposable cuvettes, Sigma-Aldrich). After incubation for 5 min at RT, absorption at 595 nm was measured with a photometer (BioPhotometer D30, Eppendorf, Hamburg, Germany). Protein concentration was calculated by comparison to a BSA standard curve. Protein lysates were then adjusted to the desired concentration by diluting with 4x loading buffer (8 % SDS, 250 mM Tris-HCl, 20 % β-mercaptoethanol, 40 % glycerol, 0.008 % bromphenol blue). Samples were boiled for 5 min at 96 °C and further used for immunoblot analyses or kept at -80 °C for long-term storage.

4.5.2 SDS polyacrylamide gel electrophoresis (SDS-PAGE)

Protein lysates were separated according to their molecular weight by sodium dodecylsulfate-polyacrylamide gel electrophoresis (SDS-PAGE). Polyacrylamide gels were cast according to Tab. 9 using gel cassettes (NuPAGE empty gel cassettes mini, Life Technologies) or glass plates sealed with 1 % agarose.

Tab. 9. Recipe for SDS polyacrylamide gels.

Components for stacking gel	For 2 gels (5 %)	Components for resolving gel	For 2 gels (12.5 %)
H_20	3.5 ml	H_20	4.5 ml
30% Acrylamide/ bisacrylamide	830 µl	30% Acrylamide/ bisacrylamide	4.2 ml
0.47 M Tris-HCl (pH 6.7)	620 µl	3 M Tris-HCl (pH 8.9)	1.2 ml
10 % SDS	50 µl	10 % SDS	100 µl
10 % APS	100 µl	10 % APS	10 µl
TEMED	5 µl	TEMED	50 µl

Gels were installed into the XCell SureLockTM Mini-Cell Electrophoresis System (Life Technologies). Equal amounts of protein extract (15-30 µg) per lane were loaded on the gel. Additionally, 2 µl peqGOLD Protein-marker IV (PeqLab) was applied. Using tris-glycine SDS running buffer (2.5 mM Tris, 19.2 mM glycin, 0.1 % SDS), gels were run at 90-120 V for 1-2 h.

4.5.3 Western transfer and immunodetection of proteins

Proteins were transferred from the gel to Immobilon-P PVDF membrane (Millipore, Bedford, MA, USA) by semi-dry blotting procedure. For this purpose, the PVDF membrane that was activated in methanol and eight Whatman paper (GE Healthcare, Buckinghamshire, UK) per gel were soaked in Towbin transfer buffer (2.5 mM Tris, 19.2 mM glycine, 20 % methanol, pH 8.3). Then, a sandwich with four Whatman paper at the bottom (anode), then the membrane, the protein gel and four Whatman paper at the top (cathode) was assembled into a Trans-Blot® SD Semi-Dry Electrophoretic Transfer Cell (Bio-Rad). Routinely, 1 to 4 gels were assembled into one semi-dry transfer cell. Electrotransfer of proteins was performed for 1 h at 20 V.

After blotting, the membrane was incubated with Blocking solution (5 % skim milk powder, 1 % BSA, 0.2 % Tween-20 in PBS) for 1 h at RT to saturate unspecific binding sites. Next, the membrane was incubated with the primary antibody (Tab. 10) diluted in blocking solution overnight at 4 °C. Prior to incubation with the secondary antibody the membrane was washed three times for 10 min with PBS-T (0.2 % Tween-20 in PBS). Incubation with the appropriate secondary antibody, diluted in blocking solution, was carried out for 1 h at RT. Afterwards, the membrane was washed again three times for 10 min with PBS-T. Finally, signals were detected by means of enhanced chemiluminescence (ECL). To that end, ECL™ Prime Western Blotting Detection Reagent (GE Healthcare) or SuperSignal West Pico Luminol/Enhancer Solution (Thermo Fisher Scientific) was applied to the membrane

according to the manufacturer's instructions and images were acquired with the Fusion SL Detection System (Vilber Lourmat, Eberhardzell, Germany).

Tab. 10. Antibodies for immunoblotting.

Primary antibodies			
Specificity	**Source**	**Dilution**	**Supplier**
anti-4E-BP1	rabbit	1:1000	Cell Signaling Technology #9452
anti-4E-BP1 Phospho (S65)	rabbit	1:1000	Cell Signaling Technology #9451
anti-AKT	rabbit	1:1000	Cell Signaling Technology #9272
anti-AKT2 (F-7)	mouse	1:500	Santa Cruz sc-5270
anti-AKT3	rabbit	1:1000	Cell Signaling Technology #4059
anti-AKT3 (clone GMA104)	mouse	1:2000	EMD Millipore, Upstate 05-780
anti-AKT Phospho (S473)	rabbit	1:1000	Cell Signaling Technology #4058
anti-AKT Phospho (T308)	rabbit	1:1000	Cell Signaling Technology #9275
anti-Brd4 (EPR5150(2))	rabbit	1:500	Abcam ab128874
anti-c-Myc	mouse	1:250	BD Pharmingen #551102
anti-Dnmt1 (H-12)	mouse	1:500	Santa Cruz sc-271729
anti-GSK3-α/β Phospho (S21/S9)	rabbit	1:1000	Cell Signaling Technology #9331
anti-H3K4me3 (Tri-Methyl-Histone H3 Lys4 (C42D8))	rabbit	1:1000	Cell Signaling Technology #9751
anti-H3K27me3 (Tri-Methyl-Histone H3 Lys27 (C36B11))	rabbit	1:1000	Cell Signaling Technology #9733
anti-Hexokinase 2 (HK2)	goat	1:200	Santa Cruz sc-6521
anti-HIF-1α	mouse	1:500	BD Pharmingen #610959
anti-HIF-1β	rabbit	1:500	Novus Biologicals 100-122SS
anti-HPV16E6 (clone 849)	mouse	1: 3000	Arbor Vita Corporation (Sunnyvale, CA, USA)
anti-HPV16E7 (NM2)	mouse	1:1000	Kind gift of Dr. Müller, DKFZ, Heidelberg
anti-HPV18E6 (clone 399)	mouse	1: 2000	Arbor Vita Corporation
anti-HPV18E7	chicken	1:1000	Zentgraf, DKFZ, Heidelberg; ID: B (28) #47 31.10-11.11.95
anti-p70 S6 Kinase (p70S6K)	rabbit	1:1000	Cell Signaling Technology #9202
anti-p70 S6 Kinase Phospho (T389)	rabbit	1:1000	Cell Signaling Technology #9234
anti-PTEN	rabbit	1:2000	Cell Signaling Technology #9552
anti-S6 Phospho (S235/236)	rabbit	1:1000	Cell Signaling Technology #2211
anti-Vinculin	mouse	1:4000	Santa Cruz sc-73614
anti-YY1	mouse	1:500	Santa Cruz sc271134
anti-α-tubulin	mouse	1:5000	Merck CP06
anti-β-actin	mouse	1:50000	Sigma-Aldrich A2228

Secondary antibodies (HRP-coupled)		
Specificity	**Dilution**	**Supplier**
anti-chicken IgG	1:5000	Santa Cruz sc-2428
anti-goat IgG	1:5000	Santa Cruz sc-2020
anti-mouse IgG	1:5000	Santa Cruz sc-2005
anti-rabbit IgG	1:5000	Santa Cruz sc-2004

4.5.4 Determination of protein half-life

To compare the stability of proteins under hypoxia and normoxia, $4x10^5$ HeLa cells were seeded per 6 cm dish. Medium was replenished the following day and 2 days after seeding cells were pre-incubated for 4 h under hypoxia. To stop de novo protein translation, 10 µg/ml cycloheximide (CHX, Sigma-Aldrich) was added to the cells in the hypoxia workstation and cells were harvested for protein extraction at the indicated time-points after CHX treatment. Normoxic cells were kept in a standard incubator at 21 % O_2 and treated and harvested in parallel. Immunoblot analyses of protein lysates were performed and images were acquired. Band densities of E6 and E7 signals were quantified using Bio1D image analysis software (Vilber Lourmat) and normalized to the band densities of the respective loading control (β-actin, α-tubulin or vinculin). Half-life of E6 and E7 was calculated from an exponential decay curve that was generated by non-linear regression using SigmaPlot software.

4.5.5 Tandem mass tag (TMT) mass spectrometry (MS)

Mass spectrometry (MS)-based quantitative proteome analysis was performed in cooperation with Bianca Kuhn and Prof. Dr. Jeroen Krijgsveld (DKFZ, Heidelberg). For this purpose, an isobaric labeling approach using Thermo Fisher Scientific's tandem mass tags (TMTs) was applied. TMTs are isobaric tags, hence they share the same overall mass but differ in the distribution of heavy and light isotopes. They generally consist of an amine-reactive region, a mass normalization (balance) region and a reporter region. The light and heavy isotopes are distributed between the balance group and the reporter group yielding an overall identical mass but a unique reporter ion generated by the reporter region. Up to 10 samples (TMT 10plex) can be combined for analysis via liquid chromatography (LC)-MS/MS. By comparing the intensities of the unique reporter ions, a relative quantification of protein abundances can be performed. Thus, this multiplex technique allows the integrated analysis of up to 10 samples simultaneously [164].

For proteome analyses $1x10^6$ SiHa cells were seeded in 6 cm dishes. After two days, medium was replenished (5.5 mM or 25 mM glucose as indicated), cells were treated with 10 µM AKTi VIII or DMSO and cultured for 17 h under hypoxia or normoxia. For harvesting, cells were immediately put on ice, washed once with ice-cold PBS, scraped in 500 µl PBS and transferred in a 1.5 ml tube. Cells were pelleted by centrifugation, supernatant was removed and cell pellets were stored at -80 °C until further processing.

The following protocol describing sample preparation and mass spectrometry analysis was provided and the procedure performed by Bianca Kuhn (Group of Prof. Dr. Jeroen Krijgsveld, DKFZ, Heidelberg).

Cell pellets were resuspended in 70-300 µl 0.1 % (w/v) RapiGest SF Surfactant (Waters, Milford, USA) that was reconstituted in 100 mM triethylammonium buffer (TEAB). To

complete lysis and to share chromatin, sonication was performed at 4 °C using a Bioruptor Pico sonication device (Diagenode) with 30 sec on/off-pulses for 15-20 cycles. Determination of protein concentration was carried out using the Pierce™ BCA protein assay kit (Thermo Fisher Scientific) according to the manufacturer's protocol. 50 µg per sample was adjusted to 100 µl with 100 mM TEAB. Proteins were reduced by adding 5 mM dithiothreitol and incubation for 60 min at RT. To perform alkylation, 15 mM 2-chloroacetamide was added and samples were incubated for 30 min at RT. For proteolytic digestion modified trypsin (gold grade, Promega) was added in a 1:50 trypsin to protein ratio and incubated overnight at 37 °C while shaking. The next day, 1% trifluoroacetic acid (pH<2) was added to stop the reaction and break RapiGest SF. Samples were incubated at 37 °C for 30-45 min before centrifugation at 20000 *g* for 10 min. The supernatant was transferred to a new 1.5 ml tube and the sample was dried using a speed vacuum concentrator.

Isobaric labeling of the peptides was accomplished with 10plex TMT reagents (Thermo Fisher Scientific). 10 µg of each sample was dissolved in 100 mM TEAB buffer to obtain a concentration of 1 µg/µl, vortexed and incubated for 10 min at RT. TMT10plex reagents (0.8 mg) were dissolved in 41 µl of acetonitrile. 4.1 µL of one of the 10 TMT labels (TMT-126, TMT-127N, TMT-127C, TMT-128N, TMT-128C, TMT-129N, TMT-129C, TMT-130N, TMT-130C, and TMT-131) was combined with 10 µg of the corresponding peptide samples and incubated for 1 h at RT. The reaction was then quenched for 15 min by adding 8 µl of 5 % hydroxylamine. The labeled samples were pooled in equal amounts. The sample mix was vacuum dried and subsequently filled up to 90 µL with 0.1% formic acid in H_2O. For high pH LC fractionation, the sample mix was pwith ammonium formate (200 mM, pH 10) to reach a final concentration of 20 mM ammonium formate.

The sample mix was fractionated by high pH reverse-phase LC. Here, peptides were fractionated on a 1200 Infinity HPLC system (Agilent, Santa Clara, CA, USA) with a Gemini C18 column (3 µm, 110 Å, 100 × 1.0 mm; Phenomenex, Torrance, CA, USA) using a linear 60 min gradient from 0 % to 35 % (v/v) acetonitrile in 20 mM ammonium formate (pH 10) at a flow rate of 0.1 ml/min. Peptide elution was detected with a variable wavelength UV detector set to 254 nm. Sixty 1 min fractions were collected and pooled into 12 fractions. Fractions were then analyzed using LC-MS on an Orbitrap Fusion™ Tribrid™ (Thermo Fisher Scientific) mass spectrometer coupled to an Easy-nLC 1000 (Thermo Fisher Scientific) ultrahigh pressure liquid chromatography pump. Peptides were loaded onto an Acclaim PepMap™ 100 C18 Nano-Trap (100 µm x 2cm, nanoViper, C18, 5 µm 100Å pores) and separated over 50 cm Acclaim PepMapTM RSLC analytical columns (75 µm × 50 cm, nanoViper, C18, 2 µM, 100Å). For mobile phase Solvent A (0.1% formic acid in H_2O) and Solvent B (0.1 % formic acid in 80 % acetonitrile in H_2O) were used in the following gradient: 3–8 % B over 4 min, 8–10 % B over 2 min, 10-32 % over 68 min, 32–50 % B over 12 min

and 50-100 % B in 1 min, holding at 100 % B for 7 min. The gradient returned to 3 % B in 1 min and held there for 10 min to prepare for the next injection. The flow rate throughout the runs was 300 nl/min. Eluting samples were injected by electrospray ionization (ESI) using a 10 µm Picotip coated fused silica emitter and a nanospray-Flex ion source (Thermo Fisher Scientific) connected to an Orbitrap-Fusion. The Orbitrap Fusion mass spectrometer was operated in data-dependent mode using vendor supplied default setting for synchronous precursor selection (SPS) MS3 fragmentation.

Analysis of MS spectra was performed using Proteome Discoverer 2.1 (Thermo Fisher Scientific) and the proteins were identified using MASCOT search engine 2.3.2. (Matrix Science) against the Swissprot Homo sapiens proteome (21.06.2018). Percolator algorithm was used as the false discovery rate calculator, and all peptides were filtered at the strict target false discovery rate level of 0.01.

For the identification of the differentially expressed proteins under the described conditions, Linear Models for Microarray Data (limma, Version 3.36.2; RStudio, Version 1.1.456) were applied for all biological replicates. P-values were adjusted using Benjamini-Hochberg correction. Volcano plots were generated using GraphPad Prism software.

The heatmap of the proteins showing differential expression between hypoxia and normoxia was generated with support of Stephen Krämer (DKFZ, Heidelberg) using the pandas (0.23.3) and seaborn (0.9.0) python packages. Hierarchical clustering was performed using scikit-learn, using Euclidean distance and the average linkage method.

4.6 RNA-based techniques

4.6.1 RNA extraction from cells

To analyze mRNA expression under varying experimental conditions, RNA was usually harvested from 6 cm dishes. Cells were washed once with PBS and 600 µl RNA lysis buffer (Invitrogen, freshly supplemented with β-mercaptoethanol) per 6 cm dish was added to the cells. The lysate was resuspended, transferred to a 1.5 ml tube and either stored at -20 °C or directly further processed for RNA extraction. Isolation of total RNA was performed with the column-based PureLink RNA Mini Kit (Invitrogen) according to the manufacturer's instructions. To remove unwanted DNA from the sample PureLink DNase Set (Invitrogen) was applied. The purified RNA was diluted in 40-80 µl RNAse-free H_2O and concentration was determined with the NanoDrop ND-1000 spectrophotometer (Peqlab). Purified RNA was stored at -80 °C.

4.6.2 Reverse transcription (RT) and quantitative real-time PCR (qRT-PCR)

For cDNA synthesis the ProtoScript® II First Strand cDNA Synthesis Kit (NEB) was used. In brief, 500 ng of purified RNA was adjusted to a volume of 3 µl with RNAse-free H_2O and mixed with 1 µl of random primer. The mix of primer and RNA was denatured for 5 min at 70 °C and immediately put on ice. 5 µl of the 2x reaction mix and 1 µl of the 10x enzyme mix were added per sample. The 10 µl reaction mix was then incubated first for 5 min at 25 °C, followed by 1 h incubation at 42 °C and finally for 5 min at 80 °C in a thermal cycler. The cDNA product was stored at -20 °C.

Expression of mRNA was finally determined by quantitative real-time PCR (qPCR). Before using the cDNA for qRT-PCR, 40 µl of nuclease-free H_2O was added to the 10 µl cDNA reaction mix and then further diluted in a ratio of 1:10. For each primer pair that was to be analyzed, one reaction mix was prepared. The reaction mix for one sample was comprised of 10 µl SYBR™ Green PCR Master Mix (Applied Biosystems, USA), 0.4 µl forward primer, 0.4 µl reverse primer and 7.2 µl nuclease-free H_20 resulting in a final volume of 18 µl. The final concentration of the forward and reverse primers was 100 nM each for detection of mRNAs and 50 nM for detection of 18S rRNA. The reaction mix was pipetted in the well of a 96-well plate (MicroAmp™ Optical 96-Well Reaction Plate, Life Technologies) and 2 µl of the diluted cDNA was added. To control for contaminations a no template control containing 2 µl H_2O instead of cDNA was included for each reaction mix. All reactions were run as duplicates. The qRT-PCR was run on a 7300 Real Time PCR System (Applied Biosystems, Invitrogen) according to the following program.

Initiation:	50 °C	2 min	
Polymerase activation:	95 °C	10 min	
Denaturation:	95 °C	15 sec	40 cycles
Annealing and elongation:	60 °C	1 min	
Dissociation curves:	95 °C	15 sec	
	60 °C	1 min	
	95 °C	15 sec	
	60 °C	15 sec	

The generation of dissociation curves allowed detection of unspecific amplification artefacts. Calculation of mRNA expression was performed according to the comparative Ct ($2^{-\Delta\Delta Ct}$) method [220] with normalization to 18S rRNA as internal reference. Statistical analyses of fold change values were carried out after logarithmic transformation.

All primers were initially tested for sufficient efficiency (80-110 %) by generating a standard curve using serial dilutions.

Tab. 11. Primers for qRT-PCR.

Target RNA	Sequence of forward (for) and reverse (rev) primer	amplicon length
18 S rRNA	for: 5'-CATGGCCGTTCTTAGTTGGT-3'	66 bp
	rev: 5'-ATGCCAGAGTCTCGTTCGTT-3'	
BRD4	for: 5'-AACCTGGCGTTTCCACGGTA-3'	91 bp
	rev: 5'-GCCTGCACAGGAGGAGGATT-3'	
CALM1	for: 5'-TTGACTTCCCCGAATTTTTGACT-3'	81 bp
	rev: 5'-GGAATGCCTCACGGATTTCTT-3'	
CALM2	for: 5'-TTAGAGAAGCATTCCGTGTGTTTG-3'	81 bp
	rev: 5'-GGTTTGTCATCACATGGCGAA-3'	
CALM3	for: 5'-GACCATTGACTTCCCGGAGTT-3'	118 bp
	rev: 5'-GATGTAGCCATTCCCATCCTTG-3'	
HPV16 E6/E7	for: 5'-CAATGTTTCAGGACCCACAGG-3'	125 bp
	rev: 5'-CTCACGTCGCAGTAACTGTTG-3'	
HPV18 E6/E7	for: 5'-ATGCATGGACCTAAGGCAAC-3'	247 bp
	rev: 5'-AGGTCGTCTGCTGAGCTTTC-3'	
MLX	for: 5'-GGTCCGGTGGGTACAAGATG-3'	110 bp
	rev: 5'-ACTGTCCTCATCATCGGGGT-3'	
MONDOA	for: 5'-CAATCTCCCCAGAACAACTGC-3'	72 bp
	rev: 5'-CATCTGCCGGTTCTTTAGTGC-3'	
TXNIP	for: 5'-GGCGGGTGTCTGTCTCTGCT-3'	143 bp
	rev: 5'-GGCAAGGTAAGTGTGGCGGG-3'	

4.6.3 Determination of mRNA half-life

To assess E6/E7 mRNA stability under hypoxia and normoxia, HeLa cells were treated with the transcriptional inhibitor Actinomycin D (ActD, Sigma-Aldrich) 2 days after seeding at a density of $5x10^5$ cells per 6 cm dish. Prior to ActD treatment, cells were pre-incubated for 4.5 h under hypoxia. Treatment with 0.5 µg/ml ActD was carried out inside the hypoxia workstation. Harvesting for mRNA isolation was performed at the indicated time points after ActD treatment. Normoxic cells were treated and harvested in parallel. RNA extraction, cDNA synthesis and qRT-PCR with primers, detecting all three transcript classes coding for E6/E7, was performed. Based on the results from the qRT-PCR an exponential decay curve was generated by non-linear regression to calculate the mRNA half-life using SigmaPlot software.

4.7 Statistical analyses

All experiments were performed at least in three biological replicates, if not indicated otherwise. Mean values and standard deviations were calculated using Microsoft Excel (Microsoft Office 2010) or SigmaPlot software. Analyses of fold change values were carried out following logarithmic transformation. Statistical significance was determined by one-way ANOVA using SigmaPlot software. P-values of ≤0.05 (*), ≤0.01 (**), or ≤0.001 (***) were considered statistically significant.

Statistical analysis of MS-data is described in chapter 4.5.5.

Indexes

Indexes

List of figures

List of tables

Abbreviations

2-DG	2-deoxyglucose
4E-BP1	eukaryotic translation initiation factor 4E binding protein
5-Aza	5-aza-2'-deoxycytidine
ActD	actinomycin D
ANOVA	analysis of variance
AP1	activator protein 1
ARNT	aryl hydrocarbon receptor nuclear translocator
ATP	adenosine triphosphate
BET	bromodomain and extra-terminal
bp	base pairs
Brd	bromodomain-containing protein
BSA	bovine serum albumin
CaM	calmodulin
CFA	colony formation assay
ChIP	chromatin immunoprecipitation
CHX	cycloheximide
CIN	cervical intraepithelial neoplasia

CRISPR	clustered regularly interspaced short palindromic repeats
DKK1	Dickkopf-related protein 1
DMEM	Dulbecco’s minimal essential medium
DMOG	dimethyloxaloylglycine
DMSO	dimethyl sulfoxide
DNA	deoxyribonucleic acid
Dnmt1	DNA methyltransferase 1
e. g.	*exempli gratia*
E6-AP	E6-associated protein
ECL	enhanced chemiluminescence
et al.	*et alii*
FCS	fetal calf serum
Fig.	figure
FIH	factor-inhibiting HIF-1α
for	forward
Glut1	glucose transporter 1
GPCR	G protein-coupled receptor
gRNA	guide RNA
GSK3	glycogen synthase kinase 3
H3K4me3	trimethylation at lysine 4 of histone 3
H3K27me3	trimethylation at lysine 27 of histone 3
HAP	hypoxia-activated prodrug
HDAC	histone deacetylase
HIF	hypoxia-inducible factor
HK	hexokinase
HPV	human papillomavirus
HRE	hypoxia responsive element
HRP	horseradish peroxidase
HSV	herpes simplex virus
hTERT	human telomerase reverse transcriptase
JARID1A	jumonji/ARID domain-containing protein 1A
JMJD3	jumonji domain-containing protein 3
kDa	kilo dalton
LC	liquid chromatography
LCR	long control region
log2	binary logarithm
MeDIP	methylated DNA immunoprecipitation

Mlx	Max-like protein X
mRNA	messenger RNA
MS	mass spectrometry
MT2A	metallothionein 2A
mTOR	mechanistic target of rapamycin
mTORC1/mTORC2	mTOR complex 1/mTOR complex 2
myr	myristoylated
O_2	oxygen
ORF	open reading frame
OXPHOS	mitochondrial oxidative phosphorylation
p70S6K	p70 S6 kinase
PBS	phosphate-buffered saline
PCR	polymerase chain reaction
PDK1	phosphoinositide-dependent kinase-1
PDZ	post synaptic density protein (PSD95), Drosophila disc large tumor suppressor (Dlg1), zonula occludens-1 protein (zo-1)
PH	pleckstrin homology
PHD	prolyl hydroxylase
PHLPP	PH domain leucine-rich repeat protein phosphatase
PI3K	phosphoinositide 3-kinases
$PI3,4P_2$	phosphatidylinositol-3,4-bisphosphate
$PI4,5P_2$	phosphatidylinositol-4,5-bisphosphate
PIP_3	phosphatidylinositol-3,4,5-trisphosphate
PKB	protein kinase B
PPR	promoter proximal region
pRB	retinoblastoma protein
PTEN	phosphatase and tensin homologe
pVHL	von Hippel-Lindau protein
qPCR	quantitative real-time polymerase chain reaction
qRT-PCR	quantitative real-time reverse transcription-polymerase chain reaction
REDD1	protein regulated in development and DNA damage response 1
rev	reverse
RNA	ribonucleic acid
RNAi	RNA interference
rRNA	ribosomal RNA
ROS	reactive oxygen species
RT	room temperature

RTK	receptor tyrosine kinase
SA-β-Gal	senescence associated β-galactosidase
SC	squamocolumnar
SDS-PAGE	sodium dodecylsulfate-polyacrylamide gel electrophoresis
SerpinE2	serpin family E member 2
siRNA	small interfering RNA
SLPI	secretory leukocyte peptidase inhibitor
SP1	specificity protein 1
Tab.	table
TET	ten eleven translocation
TMT	tandem mass tag
TK	thymidine kinase
TSC2	tuberous sclerosis complex 2
TSS	transcription start site
Tx	transfection
TXNIP	thioredoxin interacting protein
URR	upstream regulatory region
VEGF	vascular endothelial growth factor
VLP	virus-like particle
YY1	yin yang 1

The one-letter code for amino acids and nucleotides was applied according to declarations by the International Union of Pure and Applied Chemistry (IUPAC).

Units

°C	degree Celsius
Da	Dalton
g	centrifugal acceleration
g	gram
h	hour
l	liter
M	molar
min	minute
sec	second
V	volt
%	percent

Prefixes

Symbol	Prefix	Factor
k	kilo	10^{3}
c	centi	10^{-2}
m	milli	10^{-3}
µ	micro	10^{-6}
n	nano	10^{-9}

References

1. Torre, L.A., et al., *Global cancer statistics, 2012.* CA Cancer J Clin, 2015. **65**(2): p. 87-108.
2. Vogelstein, B. and K.W. Kinzler, *The multistep nature of cancer.* Trends in Genetics, 1993. **9**(4): p. 138-141.
3. Hanahan, D. and R.A. Weinberg, *Hallmarks of cancer: the next generation.* Cell, 2011. **144**(5): p. 646-74.
4. Katzke, V.A., R. Kaaks, and T. Kuhn, *Lifestyle and cancer risk.* Cancer J, 2015. **21**(2): p. 104-10.
5. Peto, J., *Cancer epidemiology in the last century and the next decade.* Nature, 2001. **411**: p. 390.
6. Plummer, M., et al., *Global burden of cancers attributable to infections in 2012: a synthetic analysis.* The Lancet Global Health, 2016. **4**(9): p. e609-e616.
7. de Martel, C., et al., *Worldwide burden of cancer attributable to HPV by site, country and HPV type.* Int J Cancer, 2017. **141**(4): p. 664-670.
8. de Villiers, E.-M., *Cross-roads in the classification of papillomaviruses.* Virology, 2013. **445**(1): p. 2-10.
9. Doorbar, J., et al., *The biology and life-cycle of human papillomaviruses.* Vaccine, 2012. **30 Suppl 5**: p. F55-70.
10. Durst, M., et al., *A papillomavirus DNA from a cervical carcinoma and its prevalence in cancer biopsy samples from different geographic regions.* Proc Natl Acad Sci U S A, 1983. **80**(12): p. 3812-5.
11. Bouvard, V., et al., *A review of human carcinogens--Part B: biological agents.* Lancet Oncol, 2009. **10**(4): p. 321-2.
12. Smith, J.S., et al., *Human papillomavirus type distribution in invasive cervical cancer and high-grade cervical lesions: a meta-analysis update.* Int J Cancer, 2007. **121**(3): p. 621-32.
13. Vaccarella, S., et al., *Worldwide trends in cervical cancer incidence: impact of screening against changes in disease risk factors.* Eur J Cancer, 2013. **49**(15): p. 3262-73.
14. Lowy, D.R. and J.T. Schiller, *Preventing Cancer and Other Diseases Caused by Human Papillomavirus Infection: 2017 Lasker-DeBakey Clinical Research Award.* Jama, 2017. **318**(10): p. 901-902.
15. Schiffman, M., et al., *Carcinogenic human papillomavirus infection.* Nat Rev Dis Primers, 2016. **2**: p. 16086.
16. Castle, P.E. and M. Maza, *Prophylactic HPV vaccination: past, present, and future.* Epidemiol Infect, 2016. **144**(3): p. 449-68.

17. Lehtinen, M. and J. Dillner, *Clinical trials of human papillomavirus vaccines and beyond.* Nature Reviews Clinical Oncology, 2013. **10**: p. 400.
18. Bruni, L., et al., *Global estimates of human papillomavirus vaccination coverage by region and income level: a pooled analysis.* Lancet Glob Health, 2016. **4**(7): p. e453-63.
19. Schiller, J.T. and M. Muller, *Next generation prophylactic human papillomavirus vaccines.* Lancet Oncol, 2015. **16**(5): p. e217-25.
20. zur Hausen, H., *Papillomaviruses and cancer: from basic studies to clinical application.* Nat Rev Cancer, 2002. **2**(5): p. 342-50.
21. Doorbar, J., *Molecular biology of human papillomavirus infection and cervical cancer.* Clin Sci (Lond), 2006. **110**(5): p. 525-41.
22. Doorbar, J., *The E4 protein; structure, function and patterns of expression.* Virology, 2013. **445**(1-2): p. 80-98.
23. Doorbar, J., et al., *Human papillomavirus molecular biology and disease association.* Rev Med Virol, 2015. **25 Suppl 1**: p. 2-23.
24. DiMaio, D. and D. Mattoon, *Mechanisms of cell transformation by papillomavirus E5 proteins.* Oncogene, 2001. **20**: p. 7866.
25. Schiffman, M. and N. Wentzensen, *Human papillomavirus infection and the multistage carcinogenesis of cervical cancer.* Cancer Epidemiol Biomarkers Prev, 2013. **22**(4): p. 553-60.
26. Westrich, J.A., C.J. Warren, and D. Pyeon, *Evasion of host immune defenses by human papillomavirus.* Virus Res, 2017. **231**: p. 21-33.
27. Moody, C.A. and L.A. Laimins, *Human papillomavirus oncoproteins: pathways to transformation.* Nat Rev Cancer, 2010. **10**(8): p. 550-60.
28. Egawa, N., et al., *Human Papillomaviruses; Epithelial Tropisms, and the Development of Neoplasia.* Viruses, 2015. **7**(7): p. 3863-90.
29. Wentzensen, N., S. Vinokurova, and M. von Knebel Doeberitz, *Systematic review of genomic integration sites of human papillomavirus genomes in epithelial dysplasia and invasive cancer of the female lower genital tract.* Cancer Res, 2004. **64**(11): p. 3878-84.
30. Romanczuk, H. and P.M. Howley, *Disruption of either the E1 or the E2 regulatory gene of human papillomavirus type 16 increases viral immortalization capacity.* Proc Natl Acad Sci U S A, 1992. **89**(7): p. 3159-63.
31. Herfs, M., et al., *A discrete population of squamocolumnar junction cells implicated in the pathogenesis of cervical cancer.* Proc Natl Acad Sci U S A, 2012. **109**(26): p. 10516-21.
32. Hoppe-Seyler, K., et al., *The HPV E6/E7 Oncogenes: Key Factors for Viral Carcinogenesis and Therapeutic Targets.* Trends Microbiol, 2018. **26**(2): p. 158-168.
33. Goodwin, E.C., et al., *Rapid induction of senescence in human cervical carcinoma cells.* Proc Natl Acad Sci U S A, 2000. **97**(20): p. 10978-83.
34. Wells, S.I., et al., *Papillomavirus E2 induces senescence in HPV-positive cells via pRB- and p21(CIP)-dependent pathways.* Embo j, 2000. **19**(21): p. 5762-71.
35. Magaldi, T.G., et al., *Primary human cervical carcinoma cells require human papillomavirus E6 and E7 expression for ongoing proliferation.* Virology, 2012. **422**(1): p. 114-24.
36. Butz, K. and F. Hoppe-Seyler, *Transcriptional control of human papillomavirus (HPV) oncogene expression: composition of the HPV type 18 upstream regulatory region.* J Virol, 1993. **67**(11): p. 6476-86.
37. Bernard, H.U., *Regulatory elements in the viral genome.* Virology, 2013. **445**(1-2): p. 197-204.
38. McBride, A.A. and A. Warburton, *The role of integration in oncogenic progression of HPV-associated cancers.* PLoS Pathog, 2017. **13**(4): p. e1006211.
39. Hoppe-Seyler, F. and K. Butz, *Activation of human papillomavirus type 18 E6-E7 oncogene expression by transcription factor Sp1.* Nucleic Acids Res, 1992. **20**(24): p. 6701-6.

40. Thierry, F., et al., *Two AP1 sites binding JunB are essential for human papillomavirus type 18 transcription in keratinocytes.* J Virol, 1992. **66**(6): p. 3740-8.
41. Scheffner, M., et al., *The E6 oncoprotein encoded by human papillomavirus types 16 and 18 promotes the degradation of p53.* Cell, 1990. **63**(6): p. 1129-36.
42. Huibregtse, J.M., M. Scheffner, and P.M. Howley, *Cloning and expression of the cDNA for E6-AP, a protein that mediates the interaction of the human papillomavirus E6 oncoprotein with p53.* Mol Cell Biol, 1993. **13**(2): p. 775-84.
43. Scheffner, M., et al., *The HPV-16 E6 and E6-AP complex functions as a ubiquitin-protein ligase in the ubiquitination of p53.* Cell, 1993. **75**(3): p. 495-505.
44. Frolov, M.V. and N.J. Dyson, *Molecular mechanisms of E2F-dependent activation and pRB-mediated repression.* J Cell Sci, 2004. **117**(Pt 11): p. 2173-81.
45. Munger, K., et al., *Complex formation of human papillomavirus E7 proteins with the retinoblastoma tumor suppressor gene product.* Embo j, 1989. **8**(13): p. 4099-105.
46. Dyson, N., et al., *Homologous sequences in adenovirus E1A and human papillomavirus E7 proteins mediate interaction with the same set of cellular proteins.* J Virol, 1992. **66**(12): p. 6893-902.
47. Boyer, S.N., D.E. Wazer, and V. Band, *E7 protein of human papilloma virus-16 induces degradation of retinoblastoma protein through the ubiquitin-proteasome pathway.* Cancer Res, 1996. **56**(20): p. 4620-4.
48. Jones, D.L., D.A. Thompson, and K. Munger, *Destabilization of the RB tumor suppressor protein and stabilization of p53 contribute to HPV type 16 E7-induced apoptosis.* Virology, 1997. **239**(1): p. 97-107.
49. Hawley-Nelson, P., et al., *HPV16 E6 and E7 proteins cooperate to immortalize human foreskin keratinocytes.* Embo j, 1989. **8**(12): p. 3905-10.
50. Thomas, M., et al., *Human papillomaviruses, cervical cancer and cell polarity.* Oncogene, 2008. **27**(55): p. 7018-30.
51. Klingelhutz, A.J., S.A. Foster, and J.K. McDougall, *Telomerase activation by the E6 gene product of human papillomavirus type 16.* Nature, 1996. **380**: p. 79.
52. Veldman, T., et al., *Transcriptional activation of the telomerase hTERT gene by human papillomavirus type 16 E6 oncoprotein.* J Virol, 2001. **75**(9): p. 4467-72.
53. Veldman, T., et al., *Human papillomavirus E6 and Myc proteins associate in vivo and bind to and cooperatively activate the telomerase reverse transcriptase promoter.* Proc Natl Acad Sci U S A, 2003. **100**(14): p. 8211-6.
54. Zeng, Q., et al., *O-linked GlcNAcylation elevated by HPV E6 mediates viral oncogenesis.* Proc Natl Acad Sci U S A, 2016. **113**(33): p. 9333-8.
55. Kuner, R., et al., *Identification of cellular targets for the human papillomavirus E6 and E7 oncogenes by RNA interference and transcriptome analyses.* J Mol Med (Berl), 2007. **85**(11): p. 1253-62.
56. Hoppe-Seyler, K., et al., *Viral E6/E7 oncogene and cellular hexokinase 2 expression in HPV-positive cancer cell lines.* Oncotarget, 2017. **8**(63): p. 106342-106351.
57. Gewin, L. and D.A. Galloway, *E box-dependent activation of telomerase by human papillomavirus type 16 E6 does not require induction of c-myc.* J Virol, 2001. **75**(15): p. 7198-201.
58. Hwang, S.G., et al., *Human papillomavirus type 16 E7 binds to E2F1 and activates E2F1-driven transcription in a retinoblastoma protein-independent manner.* J Biol Chem, 2002. **277**(4): p. 2923-30.
59. Brehm, A., et al., *The E7 oncoprotein associates with Mi2 and histone deacetylase activity to promote cell growth.* Embo j, 1999. **18**(9): p. 2449-58.
60. Hurlin, P.J., et al., *Progression of human papillomavirus type 18-immortalized human keratinocytes to a malignant phenotype.* Proc Natl Acad Sci U S A, 1991. **88**(2): p. 570-4.
61. Smith, P.P., et al., *Cytogenetic analysis of eight human papillomavirus immortalized human keratinocyte cell lines.* Int J Cancer, 1989. **44**(6): p. 1124-31.
62. Duensing, S. and K. Munger, *Centrosomes, genomic instability, and cervical carcinogenesis.* Crit Rev Eukaryot Gene Expr, 2003. **13**(1): p. 9-23.

63. Klingelhutz, A.J. and A. Roman, *Cellular transformation by human papillomaviruses: lessons learned by comparing high- and low-risk viruses.* Virology, 2012. **424**(2): p. 77-98.
64. McKeown, S.R., *Defining normoxia, physoxia and hypoxia in tumours-implications for treatment response.* Br J Radiol, 2014. **87**(1035): p. 20130676.
65. Vaupel, P., M. Hockel, and A. Mayer, *Detection and characterization of tumor hypoxia using pO2 histography.* Antioxid Redox Signal, 2007. **9**(8): p. 1221-35.
66. Vaupel, P. and A. Mayer, *Hypoxia in cancer: significance and impact on clinical outcome.* Cancer Metastasis Rev, 2007. **26**(2): p. 225-39.
67. Brown, J.M., *Tumor Hypoxia in Cancer Therapy*, in *Methods in Enzymology*. 2007, Academic Press. p. 295-321.
68. Noman, M.Z., et al., *Hypoxia: a key player in antitumor immune response. A Review in the Theme: Cellular Responses to Hypoxia.* Am J Physiol Cell Physiol, 2015. **309**(9): p. C569-79.
69. Wilson, W.R. and M.P. Hay, *Targeting hypoxia in cancer therapy.* Nat Rev Cancer, 2011. **11**(6): p. 393-410.
70. Hunter, F.W., B.G. Wouters, and W.R. Wilson, *Hypoxia-activated prodrugs: paths forward in the era of personalised medicine.* Br J Cancer, 2016. **114**(10): p. 1071-7.
71. Hoppe-Seyler, K., et al., *Induction of dormancy in hypoxic human papillomavirus-positive cancer cells.* Proc Natl Acad Sci U S A, 2017. **114**(6): p. E990-e998.
72. Blagosklonny, M.V., *Geroconversion: irreversible step to cellular senescence.* Cell Cycle, 2014. **13**(23): p. 3628-35.
73. Bensaad, K. and A.L. Harris, *Hypoxia and metabolism in cancer.* Adv Exp Med Biol, 2014. **772**: p. 1-39.
74. Ullah, M.S., A.J. Davies, and A.P. Halestrap, *The plasma membrane lactate transporter MCT4, but not MCT1, is up-regulated by hypoxia through a HIF-1alpha-dependent mechanism.* J Biol Chem, 2006. **281**(14): p. 9030-7.
75. Toescu, E.C., *Hypoxia sensing and pathways of cytosolic Ca2+ increases.* Cell Calcium, 2004. **36**(3-4): p. 187-99.
76. Nakazawa, M.S., B. Keith, and M.C. Simon, *Oxygen availability and metabolic adaptations.* Nat Rev Cancer, 2016. **16**(10): p. 663-73.
77. Majmundar, A.J., W.J. Wong, and M.C. Simon, *Hypoxia-inducible factors and the response to hypoxic stress.* Mol Cell, 2010. **40**(2): p. 294-309.
78. Klimova, T. and N.S. Chandel, *Mitochondrial complex III regulates hypoxic activation of HIF.* Cell Death And Differentiation, 2008. **15**: p. 660.
79. Keith, B., R.S. Johnson, and M.C. Simon, *HIF1alpha and HIF2alpha: sibling rivalry in hypoxic tumour growth and progression.* Nat Rev Cancer, 2012. **12**(1): p. 9-22.
80. Duan, C., *Hypoxia-inducible factor 3 biology: complexities and emerging themes.* Am J Physiol Cell Physiol, 2016. **310**(4): p. C260-9.
81. Watson, J.A., et al., *Epigenetics, the epicenter of the hypoxic response.* Epigenetics, 2010. **5**(4): p. 293-6.
82. Johnson, A.B., N. Denko, and M.C. Barton, *Hypoxia induces a novel signature of chromatin modifications and global repression of transcription.* Mutat Res, 2008. **640**(1-2): p. 174-9.
83. Thienpont, B., et al., *Tumour hypoxia causes DNA hypermethylation by reducing TET activity.* Nature, 2016. **537**: p. 63.
84. Chang, S., et al., *Hypoxic reprograming of H3K27me3 and H3K4me3 at the INK4A locus.* FEBS Lett, 2016. **590**(19): p. 3407-3415.
85. Prickaerts, P., et al., *Hypoxia increases genome-wide bivalent epigenetic marking by specific gain of H3K27me3.* Epigenetics Chromatin, 2016. **9**: p. 46.
86. Adriaens, M.E., et al., *Quantitative analysis of ChIP-seq data uncovers dynamic and sustained H3K4me3 and H3K27me3 modulation in cancer cells under hypoxia.* Epigenetics Chromatin, 2016. **9**: p. 48.
87. Hajduch, E., G.J. Litherland, and H.S. Hundal, *Protein kinase B (PKB/Akt)--a key regulator of glucose transport?* FEBS Lett, 2001. **492**(3): p. 199-203.

88. von der Crone, S., et al., *Glucose deprivation induces Akt-dependent synthesis and incorporation of GLUT1, but not of GLUT4, into the plasma membrane of 3T3-L1 adipocytes.* Eur J Cell Biol, 2000. **79**(12): p. 943-9.
89. Roberts, H.R., et al., *Colon tumour cells increase PGE(2) by regulating COX-2 and 15-PGDH to promote survival during the microenvironmental stress of glucose deprivation.* Carcinogenesis, 2011. **32**(11): p. 1741-7.
90. Gao, M., et al., *Site-specific activation of AKT protects cells from death induced by glucose deprivation.* Oncogene, 2014. **33**(6): p. 745-55.
91. Zundel, W., et al., *Loss of PTEN facilitates HIF-1-mediated gene expression.* Genes Dev, 2000. **14**(4): p. 391-6.
92. Beitner-Johnson, D., et al., *Hypoxia activates Akt and induces phosphorylation of GSK-3 in PC12 cells.* Cell Signal, 2001. **13**(1): p. 23-7.
93. Stegeman, H., et al., *Activation of AKT by hypoxia: a potential target for hypoxic tumors of the head and neck.* BMC Cancer, 2012. **12**: p. 463.
94. Jiao, M. and K.J. Nan, *Activation of PI3 kinase/Akt/HIF-1alpha pathway contributes to hypoxia-induced epithelial-mesenchymal transition and chemoresistance in hepatocellular carcinoma.* Int J Oncol, 2012. **40**(2): p. 461-8.
95. Manning, B.D. and A. Toker, *AKT/PKB Signaling: Navigating the Network.* Cell, 2017. **169**(3): p. 381-405.
96. Bellacosa, A., et al., *Activation of AKT Kinases in Cancer: Implications for Therapeutic Targeting*, in *Advances in Cancer Research*. 2005, Academic Press. p. 29-86.
97. Osorio-Fuentealba, C. and A. Klip, *Dissecting signalling by individual Akt/PKB isoforms, three steps at once.* Biochem J, 2015. **470**(2): p. e13-6.
98. Alessi, D.R., et al., *Mechanism of activation of protein kinase B by insulin and IGF-1.* Embo j, 1996. **15**(23): p. 6541-51.
99. Facchinetti, V., et al., *The mammalian target of rapamycin complex 2 controls folding and stability of Akt and protein kinase C.* Embo j, 2008. **27**(14): p. 1932-43.
100. Vanhaesebroeck, B., et al., *The emerging mechanisms of isoform-specific PI3K signalling.* Nature Reviews Molecular Cell Biology, 2010. **11**: p. 329.
101. Calleja, V., et al., *Intramolecular and intermolecular interactions of protein kinase B define its activation in vivo.* PLoS Biol, 2007. **5**(4): p. e95.
102. Agamasu, C., et al., *The Interplay between Calmodulin and Membrane Interactions with the Pleckstrin Homology Domain of Akt.* J Biol Chem, 2017. **292**(1): p. 251-263.
103. Agamasu, C., R.H. Ghanam, and J.S. Saad, *Structural and Biophysical Characterization of the Interactions between Calmodulin and the Pleckstrin Homology Domain of Akt.* J Biol Chem, 2015. **290**(45): p. 27403-13.
104. Sarbassov, D.D., et al., *Phosphorylation and Regulation of Akt/PKB by the Rictor-mTOR Complex.* Science, 2005. **307**(5712): p. 1098-1101.
105. Bozulic, L., et al., *PKBalpha/Akt1 acts downstream of DNA-PK in the DNA double-strand break response and promotes survival.* Mol Cell, 2008. **30**(2): p. 203-13.
106. Chen, E.Y., et al., *Hypoxia activates a platelet-derived growth factor receptor/phosphatidylinositol 3-kinase/Akt pathway that results in glycogen synthase kinase-3 inactivation.* Cancer Res, 2001. **61**(6): p. 2429-33.
107. Zhang, J., et al., *Apelin/APJ signaling promotes hypoxia-induced proliferation of endothelial progenitor cells via phosphoinositide-3 kinase/Akt signaling.* Mol Med Rep, 2015. **12**(3): p. 3829-3834.
108. Guo, J., et al., *pVHL suppresses kinase activity of Akt in a proline-hydroxylation-dependent manner.* Science, 2016. **353**(6302): p. 929-32.
109. Manning, B.D. and L.C. Cantley, *AKT/PKB signaling: navigating downstream.* Cell, 2007. **129**(7): p. 1261-74.
110. Cross, D.A., et al., *Inhibition of glycogen synthase kinase-3 by insulin mediated by protein kinase B.* Nature, 1995. **378**(6559): p. 785-9.
111. Saxton, R.A. and D.M. Sabatini, *mTOR Signaling in Growth, Metabolism, and Disease.* Cell, 2017. **168**(6): p. 960-976.

112. Laplante, M. and D.M. Sabatini, *mTOR signaling in growth control and disease.* Cell, 2012. **149**(2): p. 274-93.
113. Nave, B.T., et al., *Mammalian target of rapamycin is a direct target for protein kinase B: identification of a convergence point for opposing effects of insulin and amino-acid deficiency on protein translation.* Biochem J, 1999. **344 Pt 2**: p. 427-31.
114. Elstrom, R.L., et al., *Akt stimulates aerobic glycolysis in cancer cells.* Cancer Res, 2004. **64**(11): p. 3892-9.
115. Madhunapantula, S.V. and G.P. Robertson, *Targeting protein kinase-b3 (akt3) signaling in melanoma.* Expert Opin Ther Targets, 2017. **21**(3): p. 273-290.
116. Cho, H., et al., *Akt1/PKBalpha is required for normal growth but dispensable for maintenance of glucose homeostasis in mice.* J Biol Chem, 2001. **276**(42): p. 38349-52.
117. Cho, H., et al., *Insulin resistance and a diabetes mellitus-like syndrome in mice lacking the protein kinase Akt2 (PKB beta).* Science, 2001. **292**(5522): p. 1728-31.
118. Tschopp, O., et al., *Essential role of protein kinase B gamma (PKB gamma/Akt3) in postnatal brain development but not in glucose homeostasis.* Development, 2005. **132**(13): p. 2943-54.
119. Peng, X.D., et al., *Dwarfism, impaired skin development, skeletal muscle atrophy, delayed bone development, and impeded adipogenesis in mice lacking Akt1 and Akt2.* Genes Dev, 2003. **17**(11): p. 1352-65.
120. Dummler, B., et al., *Life with a single isoform of Akt: mice lacking Akt2 and Akt3 are viable but display impaired glucose homeostasis and growth deficiencies.* Mol Cell Biol, 2006. **26**(21): p. 8042-51.
121. Mayer, I.A. and C.L. Arteaga, *The PI3K/AKT Pathway as a Target for Cancer Treatment.* Annu Rev Med, 2016. **67**: p. 11-28.
122. Lim, H.J., P. Crowe, and J.L. Yang, *Current clinical regulation of PI3K/PTEN/Akt/mTOR signalling in treatment of human cancer.* J Cancer Res Clin Oncol, 2015. **141**(4): p. 671-89.
123. Wright, A.A., et al., *Oncogenic mutations in cervical cancer: genomic differences between adenocarcinomas and squamous cell carcinomas of the cervix.* Cancer, 2013. **119**(21): p. 3776-83.
124. Schwarz, J.K., et al., *Pathway-specific analysis of gene expression data identifies the PI3K/Akt pathway as a novel therapeutic target in cervical cancer.* Clin Cancer Res, 2012. **18**(5): p. 1464-71.
125. Hou, M.M., et al., *Targeted PI3K/AKT/mTOR therapy for metastatic carcinomas of the cervix: A phase I clinical experience.* Oncotarget, 2014. **5**(22): p. 11168-79.
126. Zhong, H. and J.W. Simons, *Direct comparison of GAPDH, beta-actin, cyclophilin, and 28S rRNA as internal standards for quantifying RNA levels under hypoxia.* Biochem Biophys Res Commun, 1999. **259**(3): p. 523-6.
127. Cole, S.T. and O. Danos, *Nucleotide sequence and comparative analysis of the human papillomavirus type 18 genome. Phylogeny of papillomaviruses and repeated structure of the E6 and E7 gene products.* J Mol Biol, 1987. **193**(4): p. 599-608.
128. Jha, S., et al., *Destabilization of TIP60 by human papillomavirus E6 results in attenuation of TIP60-dependent transcriptional regulation and apoptotic pathway.* Mol Cell, 2010. **38**(5): p. 700-11.
129. Meissner, J.D., *Nucleotide sequences and further characterization of human papillomavirus DNA present in the CaSki, SiHa and HeLa cervical carcinoma cell lines.* J Gen Virol, 1999. **80 (Pt 7)**: p. 1725-33.
130. Kooistra, S.M. and K. Helin, *Molecular mechanisms and potential functions of histone demethylases.* Nat Rev Mol Cell Biol, 2012. **13**(5): p. 297-311.
131. Shweiki, D., et al., *Vascular endothelial growth factor induced by hypoxia may mediate hypoxia-initiated angiogenesis.* Nature, 1992. **359**(6398): p. 843-5.
132. Chen, C., et al., *Regulation of glut1 mRNA by hypoxia-inducible factor-1. Interaction between H-ras and hypoxia.* J Biol Chem, 2001. **276**(12): p. 9519-25.

133. Christman, J.K., *5-Azacytidine and 5-aza-2'-deoxycytidine as inhibitors of DNA methylation: mechanistic studies and their implications for cancer therapy.* Oncogene, 2002. **21**(35): p. 5483-95.
134. Ghoshal, K., et al., *5-Aza-deoxycytidine induces selective degradation of DNA methyltransferase 1 by a proteasomal pathway that requires the KEN box, bromo-adjacent homology domain, and nuclear localization signal.* Mol Cell Biol, 2005. **25**(11): p. 4727-41.
135. Park, I.S., et al., *Characterization of the methylation patterns in human papillomavirus type 16 viral DNA in head and neck cancers.* Cancer Prev Res (Phila), 2011. **4**(2): p. 207-17.
136. Semenza, G.L., *Oxygen sensing, hypoxia-inducible factors, and disease pathophysiology.* Annu Rev Pathol, 2014. **9**: p. 47-71.
137. Havula, E. and V. Hietakangas, *Sugar sensing by ChREBP/Mondo-Mlx-new insight into downstream regulatory networks and integration of nutrient-derived signals.* Curr Opin Cell Biol, 2017. **51**: p. 89-96.
138. Chai, T.F., et al., *Hypoxia-inducible factor independent down-regulation of thioredoxin-interacting protein in hypoxia.* FEBS Lett, 2011. **585**(3): p. 492-8.
139. Stoltzman, C.A., et al., *Glucose sensing by MondoA:Mlx complexes: a role for hexokinases and direct regulation of thioredoxin-interacting protein expression.* Proc Natl Acad Sci U S A, 2008. **105**(19): p. 6912-7.
140. Stine, Z.E., et al., *MYC, Metabolism, and Cancer.* Cancer Discov, 2015. **5**(10): p. 1024-39.
141. Wong, W.J., et al., *MYC degradation under low O2 tension promotes survival by evading hypoxia-induced cell death.* Mol Cell Biol, 2013. **33**(17): p. 3494-504.
142. Okuyama, H., et al., *Downregulation of c-MYC protein levels contributes to cancer cell survival under dual deficiency of oxygen and glucose.* Cancer Res, 2010. **70**(24): p. 10213-23.
143. Calleja, V., et al., *Role of a novel PH-kinase domain interface in PKB/Akt regulation: structural mechanism for allosteric inhibition.* PLoS Biol, 2009. **7**(1): p. e17.
144. Vlahos, C.J., et al., *A specific inhibitor of phosphatidylinositol 3-kinase, 2-(4-morpholinyl)-8-phenyl-4H-1-benzopyran-4-one (LY294002).* J Biol Chem, 1994. **269**(7): p. 5241-8.
145. Hirai, H., et al., *MK-2206, an allosteric Akt inhibitor, enhances antitumor efficacy by standard chemotherapeutic agents or molecular targeted drugs in vitro and in vivo.* Mol Cancer Ther, 2010. **9**(7): p. 1956-67.
146. Ihle, N.T., et al., *Molecular pharmacology and antitumor activity of PX-866, a novel inhibitor of phosphoinositide-3-kinase signaling.* Mol Cancer Ther, 2004. **3**(7): p. 763-72.
147. Brunn, G.J., et al., *Direct inhibition of the signaling functions of the mammalian target of rapamycin by the phosphoinositide 3-kinase inhibitors, wortmannin and LY294002.* Embo j, 1996. **15**(19): p. 5256-67.
148. Gharbi, S.I., et al., *Exploring the specificity of the PI3K family inhibitor LY294002.* Biochem J, 2007. **404**(1): p. 15-21.
149. Dittmann, A., et al., *The commonly used PI3-kinase probe LY294002 is an inhibitor of BET bromodomains.* ACS Chem Biol, 2014. **9**(2): p. 495-502.
150. Zask, A., et al., *Synthesis and structure-activity relationships of ring-opened 17-hydroxywortmannins: potent phosphoinositide 3-kinase inhibitors with improved properties and anticancer efficacy.* J Med Chem, 2008. **51**(5): p. 1319-23.
151. Sarbassov, D.D., et al., *Phosphorylation and regulation of Akt/PKB by the rictor-mTOR complex.* Science, 2005. **307**(5712): p. 1098-101.
152. Garcia-Martinez, J.M., et al., *Ku-0063794 is a specific inhibitor of the mammalian target of rapamycin (mTOR).* Biochem J, 2009. **421**(1): p. 29-42.
153. Sarbassov, D.D., et al., *Rictor, a novel binding partner of mTOR, defines a rapamycin-insensitive and raptor-independent pathway that regulates the cytoskeleton.* Curr Biol, 2004. **14**(14): p. 1296-302.

154. Choo, A.Y., et al., *Rapamycin differentially inhibits S6Ks and 4E-BP1 to mediate cell-type-specific repression of mRNA translation.* Proc Natl Acad Sci U S A, 2008. **105**(45): p. 17414-9.
155. Glancy, B. and R.S. Balaban, *Role of mitochondrial Ca2+ in the regulation of cellular energetics.* Biochemistry, 2012. **51**(14): p. 2959-73.
156. Chae, Y.C., et al., *Mitochondrial Akt Regulation of Hypoxic Tumor Reprogramming.* Cancer Cell, 2016. **30**(2): p. 257-272.
157. Osawa, M., et al., *Solution structure of calmodulin-W-7 complex: the basis of diversity in molecular recognition.* J Mol Biol, 1998. **276**(1): p. 165-76.
158. Collatz, M.B., R. Rudel, and H. Brinkmeier, *Intracellular calcium chelator BAPTA protects cells against toxic calcium overload but also alters physiological calcium responses.* Cell Calcium, 1997. **21**(6): p. 453-9.
159. Reed, P.W. and H.A. Lardy, *A23187: a divalent cation ionophore.* J Biol Chem, 1972. **247**(21): p. 6970-7.
160. Teeter, M.E., M.L. Baginsky, and Y. Hatefi, *Ectopic inhibition of the complexes of the electron transport system by rotenone, piericidin A, demerol and antimycin A.* Biochim Biophys Acta, 1969. **172**(2): p. 331-3.
161. Wheaton, W.W., et al., *Metformin inhibits mitochondrial complex I of cancer cells to reduce tumorigenesis.* Elife, 2014. **3**: p. e02242.
162. Gonzalez, E. and T.E. McGraw, *The Akt kinases: isoform specificity in metabolism and cancer.* Cell Cycle, 2009. **8**(16): p. 2502-8.
163. Kohn, A.D., F. Takeuchi, and R.A. Roth, *Akt, a pleckstrin homology domain containing kinase, is activated primarily by phosphorylation.* J Biol Chem, 1996. **271**(36): p. 21920-6.
164. Rauniyar, N. and J.R. Yates, 3rd, *Isobaric labeling-based relative quantification in shotgun proteomics.* J Proteome Res, 2014. **13**(12): p. 5293-309.
165. Stich, M., et al., *5-aza-2'-deoxycytidine (DAC) treatment downregulates the HPV E6 and E7 oncogene expression and blocks neoplastic growth of HPV-associated cancer cells.* Oncotarget, 2017. **8**(32): p. 52104-52117.
166. Skowronski, K., et al., *Ischemia dysregulates DNA methyltransferases and p16INK4a methylation in human colorectal cancer cells.* Epigenetics, 2010. **5**(6): p. 547-56.
167. Zhou, X., et al., *Hypoxia induces trimethylated H3 lysine 4 by inhibition of JARID1A demethylase.* Cancer Res, 2010. **70**(10): p. 4214-21.
168. Harikumar, A. and E. Meshorer, *Chromatin remodeling and bivalent histone modifications in embryonic stem cells.* EMBO Rep, 2015. **16**(12): p. 1609-19.
169. May, M., et al., *The E6/E7 promoter of extrachromosomal HPV16 DNA in cervical cancers escapes from cellular repression by mutation of target sequences for YY1.* Embo j, 1994. **13**(6): p. 1460-6.
170. Filippakopoulos, P., et al., *Selective inhibition of BET bromodomains.* Nature, 2010. **468**(7327): p. 1067-73.
171. Chaidos, A., V. Caputo, and A. Karadimitris, *Inhibition of bromodomain and extra-terminal proteins (BET) as a potential therapeutic approach in haematological malignancies: emerging preclinical and clinical evidence.* Ther Adv Hematol, 2015. **6**(3): p. 128-41.
172. Helfer, C.M., J. Yan, and J. You, *The cellular bromodomain protein Brd4 has multiple functions in E2-mediated papillomavirus transcription activation.* Viruses, 2014. **6**(8): p. 3228-49.
173. Schwarz, E., et al., *Structure and transcription of human papillomavirus sequences in cervical carcinoma cells.* Nature, 1985. **314**(6006): p. 111-4.
174. Dooley, K.E., A. Warburton, and A.A. McBride, *Tandemly Integrated HPV16 Can Form a Brd4-Dependent Super-Enhancer-Like Element That Drives Transcription of Viral Oncogenes.* MBio, 2016. **7**(5).
175. Warburton, A., et al., *HPV integration hijacks and multimerizes a cellular enhancer to generate a viral-cellular super-enhancer that drives high viral oncogene expression.* PLoS Genet, 2018. **14**(1): p. e1007179.

176. Wouters, B.G. and M. Koritzinsky, *Hypoxia signalling through mTOR and the unfolded protein response in cancer.* Nat Rev Cancer, 2008. **8**(11): p. 851-64.
177. Brugarolas, J., et al., *Regulation of mTOR function in response to hypoxia by REDD1 and the TSC1/TSC2 tumor suppressor complex.* Genes Dev, 2004. **18**(23): p. 2893-904.
178. Sarbassov, D.D., et al., *Prolonged Rapamycin Treatment Inhibits mTORC2 Assembly and Akt/PKB.* Molecular Cell, 2006. **22**(2): p. 159-168.
179. Maehama, T., et al., *Selective down-regulation of human papillomavirus transcription by 2-deoxyglucose.* Int J Cancer, 1998. **76**(5): p. 639-46.
180. Bost, F., et al., *Energy disruptors: rising stars in anticancer therapy?* Oncogenesis, 2016. **5**: p. e188.
181. Ko, Y.H., et al., *Advanced cancers: eradication in all cases using 3-bromopyruvate therapy to deplete ATP.* Biochem Biophys Res Commun, 2004. **324**(1): p. 269-75.
182. Divolis, G., et al., *Differential effects of calcium on PI3K-Akt and HIF-1alpha survival pathways.* Cell Biol Toxicol, 2016. **32**(5): p. 437-49.
183. Zhou, S., et al., *BAPTA-AM, an intracellular calcium chelator, inhibits RANKL-induced bone marrow macrophages differentiation through MEK/ERK, p38 MAPK and Akt, but not JNK pathways.* Cytokine, 2010. **52**(3): p. 210-4.
184. Monick, M.M., et al., *Phosphatidylinositol 3-kinase activity negatively regulates stability of cyclooxygenase 2 mRNA.* J Biol Chem, 2002. **277**(36): p. 32992-3000.
185. Marderosian, M., et al., *Tristetraprolin regulates Cyclin D1 and c-Myc mRNA stability in response to rapamycin in an Akt-dependent manner via p38 MAPK signaling.* Oncogene, 2006. **25**(47): p. 6277-90.
186. Ma, Y.Y., et al., *PIK3CA as an oncogene in cervical cancer.* Oncogene, 2000. **19**(23): p. 2739-44.
187. Janku, F., et al., *Assessing PIK3CA and PTEN in early-phase trials with PI3K/AKT/mTOR inhibitors.* Cell Rep, 2014. **6**(2): p. 377-87.
188. Narayan, R.S., et al., *The allosteric AKT inhibitor MK2206 shows a synergistic interaction with chemotherapy and radiotherapy in glioblastoma spheroid cultures.* BMC Cancer, 2017. **17**(1): p. 204.
189. Clevers, H. and R. Nusse, *Wnt/β-Catenin Signaling and Disease.* Cell, 2012. **149**(6): p. 1192-1205.
190. Buechling, T. and M. Boutros, *Chapter two - Wnt Signaling: Signaling at and Above the Receptor Level*, in *Current Topics in Developmental Biology*, C. Birchmeier, Editor. 2011, Academic Press. p. 21-53.
191. Roarty, K., et al., *Loss of TGF-beta or Wnt5a results in an increase in Wnt/beta-catenin activity and redirects mammary tumour phenotype.* Breast Cancer Res, 2009. **11**(2): p. R19.
192. Ying, J., et al., *WNT5A exhibits tumor-suppressive activity through antagonizing the Wnt/beta-catenin signaling, and is frequently methylated in colorectal cancer.* Clin Cancer Res, 2008. **14**(1): p. 55-61.
193. Niehrs, C., *Function and biological roles of the Dickkopf family of Wnt modulators.* Oncogene, 2006. **25**: p. 7469.
194. Lau, M.T., C. Klausen, and P.C. Leung, *E-cadherin inhibits tumor cell growth by suppressing PI3K/Akt signaling via beta-catenin-Egr1-mediated PTEN expression.* Oncogene, 2011. **30**(24): p. 2753-66.
195. Ormanns, S., et al., *WNT signaling and distant metastasis in colon cancer through transcriptional activity of nuclear beta-Catenin depend on active PI3K signaling.* Oncotarget, 2014. **5**(10): p. 2999-3011.
196. Miles, A.T., et al., *Induction, regulation, degradation, and biological significance of mammalian metallothioneins.* Crit Rev Biochem Mol Biol, 2000. **35**(1): p. 35-70.
197. Datta, J., et al., *Metallothionein expression is suppressed in primary human hepatocellular carcinomas and is mediated through inactivation of CCAAT/enhancer binding protein alpha by phosphatidylinositol 3-kinase signaling cascade.* Cancer Res, 2007. **67**(6): p. 2736-46.

198. Xu, W., et al., *Hypoxia activates Wnt/β-catenin signaling by regulating the expression of BCL9 in human hepatocellular carcinoma.* Scientific Reports, 2017. **7**: p. 40446.
199. Chen, C. and H. Okayama, *High-efficiency transformation of mammalian cells by plasmid DNA.* Mol Cell Biol, 1987. **7**(8): p. 2745-52.
200. Butz, K., et al., *Functional p53 protein in human papillomavirus-positive cancer cells.* Oncogene, 1995. **10**(5): p. 927-36.
201. Lu, S., et al., *Identification of an additional hypoxia responsive element in the glyceraldehyde-3-phosphate dehydrogenase gene promoter.* Biochim Biophys Acta, 2002. **1574**(2): p. 152-6.
202. Dimri, G.P., et al., *A biomarker that identifies senescent human cells in culture and in aging skin in vivo.* Proc Natl Acad Sci U S A, 1995. **92**(20): p. 9363-7.
203. Weber, M., et al., *Chromosome-wide and promoter-specific analyses identify sites of differential DNA methylation in normal and transformed human cells.* Nat Genet, 2005. **37**(8): p. 853-62.
204. Gunther, T., et al., *Investigation of Viral and Host Chromatin by ChIP-PCR or ChIP-Seq Analysis.* Curr Protoc Microbiol, 2016. **40**: p. 1e.10.1-21.
205. Hanahan, D., *Studies on transformation of Escherichia coli with plasmids.* J Mol Biol, 1983. **166**(4): p. 557-80.
206. Sambrook, J. and D.W. Russell, *Molecular Cloning: A Laboratory Manual* 2001, New York, NY, USA: Cold Spring Harbor Laboratory.
207. Brummelkamp, T.R., R. Bernards, and R. Agami, *A System for Stable Expression of Short Interfering RNAs in Mammalian Cells.* Science, 2002. **296**(5567): p. 550-553.
208. Pursiheimo, J.P., et al., *Hypoxia-activated autophagy accelerates degradation of SQSTM1/p62.* Oncogene, 2009. **28**(3): p. 334-44.
209. Chen, K.F., et al., *Transcriptional repression of human cad gene by hypoxia inducible factor-1alpha.* Nucleic Acids Res, 2005. **33**(16): p. 5190-8.
210. Jensen, K.S., et al., *FoxO3A promotes metabolic adaptation to hypoxia by antagonizing Myc function.* Embo j, 2011. **30**(22): p. 4554-70.
211. Yu, F.X., et al., *Adenosine-containing molecules amplify glucose signaling and enhance txnip expression.* Mol Endocrinol, 2009. **23**(6): p. 932-42.
212. Xu, M., et al., *An unbiased in vivo screen reveals multiple transcription factors that control HPV E6-regulated hTERT in keratinocytes.* Virology, 2013. **446**(1-2): p. 17-24.
213. Wu, S., et al., *Transcription factor YY1 contributes to tumor growth by stabilizing hypoxia factor HIF-1alpha in a p53-independent manner.* Cancer Res, 2013. **73**(6): p. 1787-99.
214. Horvath, P. and R. Barrangou, *CRISPR/Cas, the immune system of bacteria and archaea.* Science, 2010. **327**(5962): p. 167-70.
215. Jinek, M., et al., *A programmable dual-RNA-guided DNA endonuclease in adaptive bacterial immunity.* Science, 2012. **337**(6096): p. 816-21.
216. Doench, J.G., et al., *Optimized sgRNA design to maximize activity and minimize off-target effects of CRISPR-Cas9.* Nat Biotechnol, 2016. **34**(2): p. 184-191.
217. Sanjana, N.E., O. Shalem, and F. Zhang, *Improved vectors and genome-wide libraries for CRISPR screening.* Nat Methods, 2014. **11**(8): p. 783-784.
218. Tuttle, R.L., et al., *Regulation of pancreatic beta-cell growth and survival by the serine/threonine protein kinase Akt1/PKBalpha.* Nat Med, 2001. **7**(10): p. 1133-7.
219. Ramaswamy, S., et al., *Regulation of G1 progression by the PTEN tumor suppressor protein is linked to inhibition of the phosphatidylinositol 3-kinase/Akt pathway.* Proc Natl Acad Sci U S A, 1999. **96**(5): p. 2110-5.
220. Livak, K.J. and T.D. Schmittgen, *Analysis of relative gene expression data using real-time quantitative PCR and the 2(-Delta Delta C(T)) Method.* Methods, 2001. **25**(4): p. 402-8.